


Universita' degli Studi di Padova

Dipartimento ICEA di Ingegneria Civile, Edile, Ambientale
Corso di Laurea Magistrale in Ingegneria Civile

University of Aberdeen
School of Engineering

MASTER THESIS:

EFFECTS OF IN-STREAM VEGETATION ON HYDRAULIC RESISTANCE IN REGULATED RIVERS

Student: Valentina Boscolo

First Supervisor: Prof. Vladimir Nikora

Co-supervisor: Mr. Mario Savio

Second Supervisor: Prof. Andrea Marion

academic year 2014-2015

EFFECTS OF IN-STREAM VEGETATION ON HYDRAULIC RESISTANCE IN REGULATED RIVERS

VALENTINA BOSCOLO

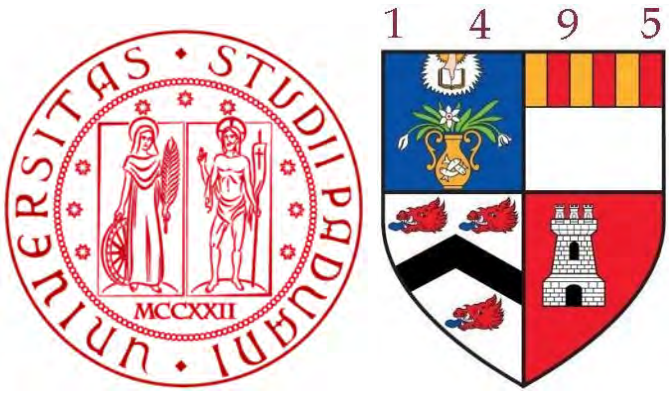

– July 2014–

Valentina Boscolo: *Effects of in-stream vegetation on hydraulic resistance in regulated rivers*, Università degli Studi di Padova, Corso di Laurea Magistrale in Ingegneria Civile © Aberdeen, July 2014

To my family and to Matteo

ABSTRACT

The aquatic vegetation covering the beds of natural streams plays an important role concerning physical, chemical and biological functions. Understand the hydraulic resistance in vegetated channels is important for a correct management of the rivers, to avoid floods and preserve the ecological functions of the plants at the same time.

This thesis is focused on hydraulic resistance over flexible submerged patchy vegetation. The main aim is to investigate different patterns of aquatic vegetation and to analyse the effects of the spatial variability of vegetation patches on hydraulic resistance. A laboratory study in an open-channel flume using patches of artificial grass-like vegetation was carried out in order to reach the project goal. The analysis of experimental data is presented in the form of Manning's n, Chezy's C and Darcy-Weisbach's friction factor f.

The analysis included also the assessment of existing hydraulic resistance models for channels with flexible submerged vegetation.

ACKNOWLEDGMENTS

I would like to express my gratitude to my co-supervisor Mario Savio for introducing me to the topic as well for the support on the way; for the useful comments, remarks, patience and time he spent with me through the learning and working process of this master thesis.

I would like to express my special appreciation and thanks to my supervisor Professor Vladimir Nikora for his direction, professionalism and reliability, for his enthusiasm and immense knowledge.

My gratefulness goes also to my home University supervisor Professor Andrea Marion which gave me the possibility to study at the University of Aberdeen.

I would like to thank all the Fluids Laboratory Staff for their help and availability during the experiments.

Furthermore I would like to thank my parents and my sister Giulia for their endless love and support and my grandmothers who raised me since childhood. A special thanks to my boyfriend Matteo for his love, kindness and support he has always shown, especially during these months away it has taken me to perform this thesis.

I would also like to thank my friends for a lifetime Marta and Laura and my friends in Padua University who have always supported me.

Thanks to all the people that I have always been close and that allowed me to reach this important goal.

CONTENTS

LIST OF FIGURES

LIST OF TABLES

A	= cross sectional area	R_e	= Reynolds number
A_v	= vegetation cross sectional area	S_b	= bed slope
A_w	= areal density	S_e	= energy slope
a	= frontal area per canopy volume	t	= stem thickness
B^X	= cross-sectional blockage factor	U	= cross-sec. mean velocity
B^{SA}	= surface-area blockage factor	u_*	= shear velocity
B^V	= volumetric blockage factor	w	= stem width
$\overline{B^X}$	= multi cross-sectional blockage factor	μ	= average
B^X	= cross-sectional blockage factor	σ	= stress
b	= flume width	τ	= shear stress
C	= Chezy's resistance coefficient	ν	= fluid viscosity
c_v	= coefficient of variation	$\overline{\sigma}$	= standard deviation
E	= Young modulus	ϵ	= strain
F	= function	ΔL	= extension
F	= applied force	Φ	= vegetation porosity
F_r	= Froude number		
f	= Darcy-Weisbach friction factor		
g	= gravity acceleration		
H	= flow depth		
$\overline{H}$	= mean flow depth		
H_v	= vegetation height		
h_v	= deflected vegetation height		
$\overline{h_v}$	= mean deflected vegetation height		
h	= water surface level		
H/h_v	= relative submergence		
h_v/H	= relative roughness		
I	= moment of inertia		
J	= stem flexural rigidity		
K_s	= Gauckler-Strickler resistance coefficient		
M_p	= plant density per unit bed area		
M_s	= stem density per unit bed area		
n	= Manning's roughness coefficient		
Q	= flow rate		
R	= hydraulic radius		

ITALIAN PREFACE

Viene fatto di seguito un breve riassunto in italiano delle informazioni contenute nei capitoli in cui si sviluppa la tesi, divise per capitolo.

CAPITOLO 1: INTRODUZIONE

Nel primo capitolo viene fatto un inquadramento generale del contesto, con particolare attenzione alle azioni reciproche che si attuano tra la vegetazione e il flusso dell'acqua. La vegetazione deprime le onde, stabilizza il fondo marino, migliora la qualità dell'acqua, altera la disponibilità di luce e la temperatura, regola l'ossigeno, il carbonio e la concentrazione di nutrienti, offre un habitat per molte specie animali. La capacità di portata di fiumi e torrenti dipende strettamente dalla presenza di vegetazione: le caratteristiche delle piante e la loro abbondanza influenzano la profondità del flusso, la capacità di trasporto dei sedimenti e altri importanti parametri idraulici. Sebbene la resistenza al flusso possa essere ridotta attraverso una rimozione completa o parziale della vegetazione, oltre ad essere un procedimento costoso, ciò può avere importanti implicazioni ecologiche. La rimozione completa della vegetazione, le cui radici legano la massa di terreno e la cui copertura vegetale protegge dall'azione erosiva della corrente, può comportare l'erosione del letto e delle sponde del fiume e la torbidità dell'acqua. D'altro canto una crescita illimitata della vegetazione può portare ad una perdita anche totale della capacità di convogliamento dell'acqua. La migliore soluzione è quella di avere un rivestimento vegetativo che eviti entrambe queste due condizioni.

CAPITOLO 2: BACKGROUND TEORICO

Nel secondo capitolo vengono illustrati dei concetti teorici di base sulla resistenza nei canali con vegetazione, i parametri della vegetazione che entrano in gioco, la differenza tra vegetazione rigida e flessibile, sommersa ed emersa.

Nei canali vegetati vi sono almeno due scale in cui la resistenza può operare, legate ai modi con cui si verificano le variazioni di velocità: la scala dello stelo e la scala della macchia. Alla scala dello stelo l'energia è persa a causa delle interazioni tra il flusso e le foglie delle piante, e la resistenza di forma è dominante. Alla scala della macchia vi è una perdita di energia dovuta al blocco prodotto dalla vegetazione, e la resistenza dovuta all'accelerazione locale è dominante. Solitamente entrambe le scale operano insieme. La scala della macchia è dominante in presenza di specie vegetative ad alta densità, viceversa nelle specie con struttura aperta la scala dello stelo ha un ruolo maggiore.

La prima caratteristica importante della vegetazione che influenza la resistenza al flusso è la tassonomia della specie: ramificazione, densità dei germogli, livello massimo di crescita che ciascuna specie può raggiungere nella sezione trasversale, presenza stagionale. La tassonomia della specie è molto importante per determinare

la resistenza idraulica a livello del singolo stelo, ma nella maggior parte dei casi la resistenza è principalmente alla scala della macchia perché i gambi operano insieme. E'più opportuno quindi classificare la vegetazione fluviale sulla base della forma funzionale piuttosto che sulla tassonomia generica: piante emergenti, piante galleggianti radicate, piante radicate sommerse e piante galleggianti. In aggiunta, vi è un parametro idraulico fondamentale che considera la dimensione della vegetazione in relazione alle condizioni del flusso, H/h_v, in cui h_v è l'altezza piegata della vegetazione e H la profondità dell'acqua che si instaura nel canale per date condizioni di moto. La configurazione piegata della vegetazione dipende dalla rigidità flessionale e dalla densità della vegetazione stessa. Il fattore di blocco è il parametro che misura la porzione del canale bloccata dalla vegetazione. Diversi tipi di fattori di blocco sono stati proposti in letteratura: fattore di blocco trasversale, superficiale e volumetrico. Il fattore di blocco superficiale non tiene conto della parte della profondità del canale occupata dalla vegetazione, quindi non è direttamente correlato alla resistenza. Green illustra una quarta versione del fattore di blocco, il fattore di bloco trasversale multi-sezione, che considera l'eterogeneità nella direzione verso valle oltre che in quella trasversale.

CAPITOLO 3: MODELLI IDRAULICI

Un approccio rigoroso per derivare le relazioni di resistenza idraulica si basa sull'integrazione doppia, mediata sia nel tempo sia nello spazio, delle equazioni di Navier-Stokes sul volume di fluido. Questo approccio richiede una conoscenza dettagliata della dinamica nella vegetazione, che ne rende molto difficile l'applicazione. In alternativa possono essere usati alcuni modelli semplificati. In questo capitolo sono riportate delle brevi linee guida circa l'integrazione delle equazioni di Navier-Stokes. Poi sono spiegati l'analisi semplificata di Petryk e Bosmaijan, effettuata per la vegetazione emergente o parzialmente emergente, e due metodi promettenti circa la vegetazione completamente sommersa. Si focalizza l'attenzione su questi due ultimi, che verranno presi in considerazione nell'analisi dei risultati.

Il primo riguarda il modello di Kouwen (1969), che ha condotto i primi esperimenti sui flussi al di sopra di un letto di vegetazione flessibile. L'equazione del profilo della velocità assume una velocità di scorrimento sulle punte delle piante e un profilo logaritmico al di sopra. Per le altezze che vanno dal fondo all'altezza deflessa della vegetazione, la velocità diventa molto bassa e assume quasi un valore costante. Pertanto, il profilo di velocità mostra un punto di flesso situato nella parte superiore della vegetazione, dove sono massimi i valori della turbolenza e degli sforzi tangenziali. Non è chiaro se tale modello possa essere applicato solo nel caso di copertura uniforme della vegetazione oppure anche quando la vegetazione è a chiazze come nei canali naturali.

Il secondo riguarda l'equazione di Carollo, Ferro, Termini (2005). Raccogliendo dei dati sperimentali utilizzando un canale artificiale e tre diverse concentrazioni di vegetazione, hanno indicato che l'applicazione del metodo di Kouwen produce una sovrastima sistematica della resistenza al flusso nei canali naurali con vegetazione flessibile, che è maggiore quando la concentrazione aumenta. Per ottenere un buon accordo con i dati sperimentali, si sono introdotti cinque termini adimensionali i cui

coefficienti sono stati valutati.

CAPITOLO 4: REVISIONE LETTERARIA

In questo capitolo è elencata una breve rassegna letteraria degli studi fatti sulla resistenza idraulica in presenza di vegetazione a macchie completamente sommersa, in cui questa tesi si concentra. Nelle applicazioni reali è infatti difficile trovare una copertura del fondo uniforme. Alcune specie di macrofite acquatiche possono crescere in modelli sparsi, costringendo il flusso a tessere sopra e intorno a loro in modo complesso. Si è mostrata la presenza di vortici orizzontali generati in questo confine e si è identificato l'effetto della vegetazione sulle correnti secondarie e la capacità delle piante nel deviare il corso del flusso. Poiché questi fattori causano perdite di energia, la distribuzione spaziale e la forma delle macchie della vegetazione all'interno del canale potrebbe influenzare la resistenza del canale. Vengono di seguito riassunti i risultati più importanti ottenuti a tal riguardo.

Li e Shen (1973) usando dei cilindri hanno studiato gli effetti di due configurazioni (elementi allineati e sfalsati) sulla resistenza al flusso. Hanno mostrato che la configurazione sfalsata era molto più efficace nel ridurre il flusso, plausibilmente perchè quando i cilindri sono disposti in file, gli effetti di ritardo erano limitati a quei gruppi, ma il flusso negli spazi tra le righe era relativamente privo di ostacoli; quando erano sfalsati, al contrario, gli effetti di ritardo erano più distribuiti. Fisher e Reeve (1994) hanno effettuato alcuni test con diverse configurazioni utilizzando pietre. Per la stessa percentuale di copertura, il modo sfalsato ha dato un valore di resistenza del 17% superiore.

Nikora (2008) ha condotto degli esperimenti sul campo con piante acquatiche sommerse (coprenti il $40 - 100\%$ del fondo) presenti su cinque fiumi in Nuova Zelanda, con una vasta gamma di vegetazione e configurazione. Ha suggerito dei semplici rapporti che utilizzano i parametri della vegetazione per prevedere gli effetti sulla resistenza. Quasi tutti i parametri della vegetazione hanno mostrato una buona correlazione con la resistenza. I modelli di Kouwen (1969) e Carollo (2005) sono stati testati per tali condizioni di vegetazione irregolare e hanno approssimato molto bene i dati qualora i parametri della vegetazione fossero spazialmente madiati. Non è stata trovata una dipendenza tra la resistenza e la disposizione della piante.

Bal (2011) ha studiato le prestazioni idrauliche di tre modelli con diversi tipi di macrofite con lo scopo di studiare l'effetto di diverse configurazioni di vegetazione sulla resistenza al flusso per verificare l'ipotesi di una rimozione parziale della vegetazione al fine di preservare il valore ecologico del fiume. Le piante usate sono state raccolte in due piccoli fiumi di pianura; ne sono state scelte diverse specie per valutare l'impatto della differente architettura sulla resistenza al flusso. Tre configurazioni di vegetazione, ricoprenti il 19% del fondo, sono state utilizzate. Si è visto come la resistenza idraulica dei modelli è stata significativamente influenzata dalle specie presenti e dalla distribuzione spaziale.

Nepf (2012) ha esaminato l'idrodinamica di un blocco circolare emergente poroso di vegetazione di diametro D. Dietro il blocco si forma una regione di ricircolo, seguita da un vortice di von Karman. La scia di ricircolo che si forma nel retro di un'ostruzione porosa è molto lunga a causa del flusso che entra attraverso il blocco

e ritarda la composizione del vortice.

CAPITOLO 5: OBIETTIVI

Le seguenti domande di ricerca sono state identificate:

1. Quali sono i parametri chiave che caratterizzano la resistenza idraulica in presenza di macchie di vegetazione?
2. Qual è il rapporto tra i parametri di resistenza e il fattore di blocco?
3. Quali sono gli effetti della variabilità spaziale delle macchie di vegetazione sulla resistenza idraulica?
4. Quale(i) modello(i) in letteratura è(sono) più adatto e robusto per prevedere la resistenza?

CAPITOLO 6: STRUMENTAZIONE

In questo capitolo viene illustrata la strumentazione che si è adoperata negli esperimenti, che consiste principalmente nella canaletta, l'erba artificiale e il velcro.

Tutti gli esperimenti sono stati condotti nella "canaletta blu" del laboratorio. La canaletta ha sezione rettangolare, è larga 40 cm, lunga 11 m, e ha un fondo con pendenza variabile fino a 1:50 controllata manualmente. L'acqua si riversa in un grande serbatoio di valle ed è ridistribuita a monte attraverso un tubo che permette il trasporto di portate fino a 20 l/s. Il controllo della portata viene effettuato da una valvola azionata a mano e la portata effettiva è indicata in un display digitale collegato ad un misuratore di portata elettromagnetico. Lungo la canaletta sono state prese dieci sezioni trasversali equamente distribuite in cui si trovano un'asta graduata incollata alla parete di vetro e una presa piezometrica nel fondo. I righelli sono utilizzati per misurare la profondità dell'acqua e l'altezza deflessa della vegetazione. Le prese piezometriche sono collegate ad un tabellone dove i livelli piezometrici possono essere facilmente letti. Alla fine della canaletta vi è un sistema di paratoie che può essere aperto/chiuso tramite una manovella. Aprendo o chiudendo le paratoie è possibile mantenere il flusso il più possibile uniforme durante gli esperimenti.

Le macchie di vegetazione utilizzate sono di erba sintetica sempreverde di polietilene. Questa scelta è stata dettata dalla necessità di ricavare degli elementi di dimensioni specifiche. Per fissare gli elementi di vegetazione nella posizione corretta sul fondo della canaletta è stato utilizzato un sistema di fissaggio di velcro. Esso si compone di due parti: uno strato di fissaggio utilizzato in combinazione con uno strato di velluto. La parte di fissaggio è stata tagliata della stessa dimensione del fondo della canaletta ed è stata incollata sopra di essa. La parte di velluto è stata cucita agli elementi di vegetazione. Con questo sistema si è permesso un veloce cambio di disposizione degli elementi, al fine di creare diverse configurazioni senza danneggiare il fondo di vetro della canaletta.

CAPITOLO 7: TEST PRELIMINARI

In questo capitolo vengono illustrati i procedimenti e i risultati dei test preliminari che sono stati condotti.

Gli elementi di vegetazione artificiale sono stati analizzati nella loro geometria misurando trenta piante selezionate in modo casuale. Le piante sono state tagliate il più vicino possibile alla base di polipropilene per ricavarne gli steli. Innanzitutto si è misurato per ogni pianta il numero di steli. In una fase successiva altezza, larghezza e spessore di ogni stelo sono stati misurati utilizzando un calibro digitale. E' stata quindi misurata la densità dell'erba in termini di piante e steli per metro quadrato.

Si sono quindi studiate le proprietà meccaniche dell'erba artificiale. Una prova di trazione è stata effettuata su cinque steli presi in modo casuale da cinque piante differenti, per un totale di 25 campioni. Gli steli sono stati tagliati il più vicino possibile al supporto e le loro dimensioni sono state misurate con un calibro digitale. Ogni fusto è stato posizionato tra le due ganasce della macchina, facendo attenzione al suo allineamento. Il morsetto superiore viene mosso con una velocità costante di 5 mm/minuto e la macchina registra i valori della forza F che corrispondono ai valori dell'estensione. Si sono quindi calcolati i momenti d'inerzia nelle due direzioni, il momento d'inerzia medio e la rigidezza flessionale dello stelo.

Dei test preliminari sono stati fatti per analizzare il comportamento idraulico della canaletta in condizioni di flusso uniforme con il proprio fondo di vetro e con lo strato di fissaggio di velcro incollato. Due pendenze sono state studiate per entrambi i casi: 1:500 e 1:1000, con circa 18-19 condizioni di flusso analizzate per ciascuna. Per ogni profondità, incrementata di volta in volta di un passo fisso, si è controllata la condizione di moto uniforme, si sono registrati i valori del tirante e dei livelli piezometrici in corrispondenza delle aste e si è registrato il valore della portata per 2 minuti ogni 10 secondi. Si son calcolati i parametri di resistenza di Darcy-Weisbach, Chezy, Manning e Gauckler-Strickler, poi analizzati in funzione del numero di Reynolds.

CAPITOLO 8: CONFIGURAZIONI E PROTOCOLLO DELLE MISURE

In questa sezione viene spiegata l'esecuzione degli esperimenti. Considerate le dimensioni della canaletta, si è deciso di utilizzare elementi quadrati di vegetazione di lato 10 cm. Gli elementi sono stati ottenuti tagliando i quadrati da un tappeto di erba artificiale. Il fondo della canaletta è stato coperto col velcro, dove i pezzi sono stati attaccati dopo aver cucito su di essi la parte di velluto. Per determinare l'influenza della densità di vegetazione, si sono studiate configurazioni con tre fattori di blocco superficiali: 10, 20 e 30%. Per vedere invece una possibile influenza della disposizione dei pezzi sulla resistenza si sono esaminate, a parità di fattore di blocco, due diverse configurazioni: elementi allineati ed elementi sfalsati.

Viene poi dettagliato il protocollo di misura che è stato seguito per ogni esperimento. Prima di procedere, è importante controllare la posizione dell'erba e la presenza di bolle d'aria all'interno dei piezometri. Dopo che la configurazione desiderata della vegetazione è stato posizionata sul fondo, si impostano la pendenza della canaletta e la portata. Dopo che il sisema si è aggiustato, la condizione di moto quasi uniforme, che può essere regolata aprendo o chiudendo le paratoie a valle, deve essere garantita. Si parte dalla portata minima che ricopre le punte della vegetazione a quella massima che è in grado di fornire la pompa. Ad ogni prova

successiva, la portata viene aumentata in modo che il livello salga di circa 5 mm. Inoltre, ogni configurazione è stata studiata con due pendenze: 1:500 e 1:1000. La condizione di flusso quasi uniforme è verificata controllando che la pendenza reale non differisca più del 3% da quella voluta. Completati tali passaggi, possono essere raccolti i dati nelle dieci sezioni trasversali: i tiranti, l'altezza deflessa della vegetazione, la quota piezometrica. Si sono registrati anche dodici valori della portata, presi ogni 10 secondi.

CAPITOLO 9: CALCOLO DEI PARAMETRI IDRAULICI

I dati raccolti sono stati utilizzati per il calcolo dei principali parametri idraulici. In questo capitolo è descritto come sono stati calcolati i parametri idraulici e quindi come sono stati utilizzati per calcolare i parametri presi in considerazione per analizzare la resistenza: i coefficienti di Manning n, Chezy C e Darcy-Weisbach f. Si sono clcolati il tirante medio e l'altezza deflessa media della vegetazione e la pendenza della linea dell'energia, il numero di Reynolds, il numero di Froude e la velocità d'attrito. E' interessante fare alcune considerazioni in merito alla velocità d'attrito. La velocità d'attrito è stata calcolata attraverso la classica formula che deriva dalla definizione dello sforzo tangenziale considerando sia il raggio idraulico sia il tirante, e attraverso la formula di Nikora (2001) che tiene in conto della porosità della vegetazione. Dal confronto delle due si vede come gli effetti delle pareti del canale sulla resistenza siano trascurabili rispetto agli effetti del fondo.

CAPITOLO 10: RISULTATI

In questo capitolo vengono illustrati i risultati ottenuti analizzando i dati raccolti in laboratorio. La prima parte del capitolo comprende l'analisi della resistenza idraulica: l'attenzione è focalizzata principalmente sulla resistenza idraulica in funzione del numero e della configurazione delle macchie. Nella seconda parte vengono studiati e valutati i modelli di resistenza idraulici. Non è stata fatta alcuna distinzione tra le due pendenze del fondo studiate per ogni configurazione, poiché la pendenza non ha influenzato la resistenza idraulica. I parametri di resistenza idraulica (Darcy-Weisbach, Chezy e Manning) sono stati graficati in funzione del numero di Reynolds. Si notano due trend differenti: le configurazioni allineate e sfalsate con un fattore di blocco del 10% presentano circa la stessa resistenza, mentre le configurazioni con il 20 e il 30% hanno due differenti resistenze, che sono maggiori per quelle sfalsate. Inoltre, i parametri di resistenza per le configurazioni 10% allineato, 10% sfalsato, 20% allineato e 30% allineato presentano la stessa tendenza, le configurazioni 20% sfalsato e 30% sfalsato sono anch'esse abbastanza simili, ma la loro resistenza è molto maggiore rispetto all'altro gruppo.

I parametri di resistenza sono poi stati diagrammati in funzione della scabrezza relativa. Le considerazioni fatte sono uguali a quelle precedenti. I parametri di resistenza sono stati quindi graficati in funzione dei fattori di blocco: il fattore di blocco trasversale massimo e il fattore di blocco trasversale mediato. Per quello massimo i dati sono stati interpolati con un fit lineare e esponenziale. A causa della diversa resistenza idraulica delle configurazioni, sono state necessarie due equazioni

differenti. Entrambi i fit hanno mostrato un buon indice di correlazione. Per quello medio è interessante distinguere i dati relativi ai tre fattori di blocco superficiali.

Vengono quindi testati i modelli di Kouwen (1969) e di Carollo (2005). I dati raccolti seguono l'equazione suggerita da Kouwen, di cui sono stati calibrati i coefficienti. Il modello di Carollo è stato applicato utilizzando i coefficienti proposti dagli autori, mostrando un povero accordo. Per correggere questa distorsione i parametri sono stati ricalibrati utilizzando un metodo di regressione lineare. Si è poi seguito l'approccio di Nikora (2001) per i canali con vegetazione irregolare per tenere in considerazione sia della sommersione relativa sia della dimensione relativa della macchia.

CAPITOLO 11: DISCUSSIONE DEI DATI

Si è visto come le configurazioni indagate hanno mostrato una diversa resistenza idraulica, in relazione al fattore di blocco superficiale e alla configurazione (allineato o sfalsato). Le configurazioni con fattore di blocco superficiale del 10% hanno mostrato circa la stessa resistenza idraulica per le configurazioni sfalsate e allineate. Le configurazioni allineate e sfalsate con fattore di blocco superficiale del 20% e del 30% hanno sperimentato una diversa resistenza idraulica, che era maggiore per la configurazione sfalsata. Inoltre, le configurazioni allineate del 20% e 30% hanno sperimentato la stessa resistenza idraulica che era simile a quella della configurazione allineato con il 10%. La resistenza idraulica causata dalla configurazione sfalsata con un fattore di blocco superficiale del 30% era leggermente maggiore di quella sfalsata con il 20%. Si è cercato di dare una spiegazione di questi risultati analizzando i vortici che la macchia di vegetazione provoca dietro di essa. Considerando un forte blocco a causa dell'alta densità della macchia di vegetazione, si è ottenuto che il vortice di von Karman si forma ad una distanza di circa 0,25 m dietro la macchia di vegetazione. Si è confrontato tale valore con le configurazioni indagate. Quando il fattore di blocco superficiale è del 10%, è probabile che la scia di von Karman venga generata ma il modello non influenza la resistenza idraulica poiché i pezzi sono molto lontani e il flusso può ritornare indisturbato ad una certa distanza dietro di essi. Quando il fattore di blocco è del 20% le macchie sono molto vicine nella configurazione allineata, e dal momento che la loro distanza è di 0,25 m, la scia di von Karman non ha spazio sufficiente per essere generata. Al contrario, nella configurazione sfalsata, la distanza viene aumentata (0,50 m) e il vortice di von Karman è in grado di generarsi, causando perdite di energia e turbolenze. La stessa situazione sopra descritta si verifica quando il fattore di blocco è del 30%. È interessante notare che, sulla base di questo modello ipotetico, le configurazioni allineate con il 20% e 30% presentano circa la stessa resistenza idraulica poiché si comportano come due strisce. La configurazione sfalsata con il fattore di blocco superficiale del 30% provoca una maggiore resistenza idraulica di quella sfalsata con il 20% a causa del numero maggiore di elementi che costringono il flusso a tessere tra di loro aumentando le perdite di turbolenza. Nella determinazione delle leggi di resistenza, le configurazioni sono state divise in due gruppi, in quanto la loro resistenza idraulica non differiva molto.

I parametri fisici fondamentali della vegetazione che sono stati presi in considerazione sono stati la scabrezza relativa, il fattore di blocco trasversale massimo

e il fattore di blocco trasversale medio. I coefficienti di Darcy-Weisbach, Manning e Chezy sono stati graficati in funzione di questi parametri. Le correlazioni tra i parametri di resistenza idraulici e i parametri della vegetazione erano alti ($R^2 > 0.9$). I tre parametri avevano lo stesso potere predittivo in questo studio, e le considerazioni che possono essere fatte per uno di loro sono le stesse per gli altri. Si è scelto di mostrare le relazioni tra i parametri di resistenza idraulica e il fattore di blocco trasversale massimo; relazioni che sono state interpolate con un fit sia lineare che esponenziale. Entrambe le equazioni mostrano un elevato coefficiente di correlazione per tutti e tre i parametri idraulici. I limiti dei parametri idraulici (caso di assenza di vegetazione) sono stati calcolati per i fit esponenziale e lineare. I risultati hanno mostrato che i valori ottenuti dalle equazioni esponenziali erano più simili a quelli calcolati per lo strato di fissaggio rispetto a quelli ottenuti dal fit lineare. Questo è in accordo con la teoria di Green (2005), suggerendo un aumento della resistenza verso un blocco completo. Il fit lineare ha avuto ugualmente un altissimo potere predittivo e questo può essere dovuto al basso valore del fattore di blocco della sezione trasversale che è stato indagato. Entrambi i modelli di Kouwen (1969) e Carollo (2005) hanno mostrato un buon accordo con i dati raccolti, che è coerente con la conclusione di Nikora (2001) che i modelli possono essere estesi alle condizioni di vegetazione irregolare se vengono usate delle misure della vegetazione mediate sul sito. Il modello di Carollo ha fornito un buon coefficiente di correlazione, ma i coefficienti della legge funzionale devono essere calibrati per la situazione specifica.

CAPITOLO 12: CONCLUSIONI

In questo capitolo viene fatto un riassunto di quanto è stato fatto e delle conclusioni che si sono ottenute.

CAPITOLO 13: LAVORI FUTURI

Un piano di indagine per rilevare il campo di velocità che utilizza l'UVP è già stato fatto. I dati saranno raccolti lungo entrambi gli assi della canaletta, per ottenere un profilo doppiamente mediato del campo di velocità. Ulteriori esperimenti sono in programma al fine di indagare la resistenza idraulica per configurazioni con elementi allineati e sfalsati con un fattore di blocco superficiale superiore. Lo scopo è quello di verificare se l'ipotesi fatta di una non-dipendenza tra la configurazione e la resistenza idraulica per i valori più elevati del fattore di blocco superficiale può essere corretta. I prossimi passi saranno poi quelli di indagare diverse forme della macchia per esprimere la resistenza idraulica non solo in funzione del modello della vegetazione, ma anche della sua forma e dimensione.

Part I

INDRODUCTION

1 INTRODUCTION

The vegetation covering the bed and the banks of rivers and streams has an important role concerning the hydrodynamic behaviour, the ecological equilibrium and the characteristics of the rivers themselves. Interactions between flow and vegetation are complex and depend on flow factors (e.g. mean velocity of flow, turbulence, water characteristics, channel morphology) and vegetation characteristics (type of plant, age and size).

Knowledge of interactions between flow and vegetation is important for both engineering and ecological applications.

Flow conditions can affect the role of plants as suspended sediment filters, sinks for dissolved nutrients and contaminants, habitat for other stream biota [35]. Seagrasses are essential primary producers and they are the basis for many food webs [11]. They also damp waves, stabilize the seabed, provide shelter for fish and enhance water quality by filtering nutrients. The uptake of nutrients by an individual stem depends on its boundary layer, as it happens for the capture of pollen [12, 19]. Aquatic vegetation is abundant also in lowland rivers, where it gives habitat, alter light availability and temperature, regulates oxygen, carbon and nutrients concentrations.

(a) (b)

Figure 1: (a) seagrasses and (b) aquatic vegetation in rivers.

Reciprocally, plant characteristics and abundance affect flow depth, flood conveyance, sediment transport capacity and other important hydraulic parameters. The discharge capacity of water in rivers and streams is strictly dependent on the presence of vegetation. The presence of numerous obstacles on the path of the flow can cause considerable turbulence: in these conditions the water flow is significantly delayed. The increased resistance can cause a higher water level with unfavourable floods and adverse consequences to agriculture due to an increase in the groundwater level [1].

Many researchers suggest that the submerge genus *Ranunculus spp.* is a very serious danger for floods due to the particularly dense stands it produces [33]. *Sparganium erectum* is a stiff emergent species that can resist bending. If the flow is slow

enough for emergent plants to penetrate into the center of the channel, it can become a significant flooding hazard [8]. The free-floating plant *Eichhornia crassipes* can collect against narrow-span bridges, causing backwater effects, or can cover the complete surface of the channel with a loss of up to 60% in water-carrying efficiency [10].

(a) *Ranunculus spp.*

(b) *Sparganium erectum.*

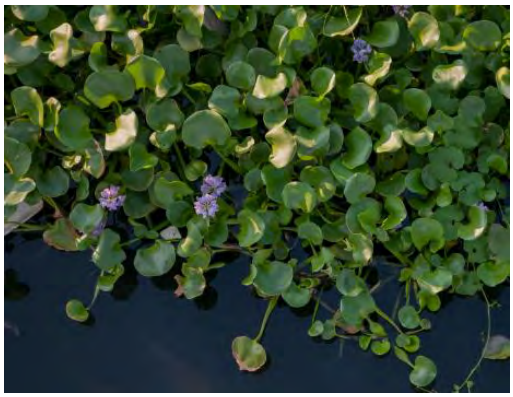

(c) *Eichhornia crassipes.*

Although resistance to flow can be reduced by a complete or partial removal of the vegetation, this is a costly procedure and can have ecological implications. A complete removal of the plants in a river can lead to erosion of the bed and the banks and turbidity of water. The roots of the vegetation bind the soil mass, and the vegetation cover protects the channel from the erosive action of flowing water and hinders the movement of soil particles from the bed of the channel. This protective action varies with the species of vegetation and with uniformity of coverage. For any individual type of vegetation it varies depending on the age and the condition of the plants and on the season of the year. But an unrestricted growth of vegetation, as mentioned before, can lead to a total loss of capacity to convey water. The best solution is to have a vegetative lining that avoids both these two conditions.

Developing knowledge about the hydrodynamics over vegetated beds is the main aim to understand the water flow conditions, to design flood protection and to plan a corrected mitigation management for natural rivers.

Part II

CHAPTERS

2

THEORETICAL BACKGROUND

In the following chapter, background information is given about the resistance in vegetated channels. Then, the importance of plant characteristics and the main parameters involved are discussed. The difference between rigid and flexible, submerged and emergent vegetation is explained too.

2.1 VEGETATED CHANNEL RESISTANCE

In 1965 Rouse classified flow resistance into four components: (1) surface or skin friction, (2) form resistance or drag, (3) wave resistance from free surface distortion and (4) resistance from local acceleration or flow unsteadiness.
In vegetated channels these components have a role depending on flow and vegetation characteristics.

It has been generally agreed that the presence of vegetation in rivers and streams (flexible low grass blades, dense bushes, firm trees) increases flow resistance, changes backwater profiles and sediment transport and deposition. In vegetated channels there are at least two scales at which vegetation resistance can operate, that are related to the scale at which velocity changes occur [5]: the stem scale and the stand scale. At the stem scale energy is lost due to interactions between the flow and the individual leaves, and the form resistance or drag is dominant. At the stand scale there is a loss of energy due to the block produced by the vegetation that causes a volume displacement of the flow, and the resistance from local acceleration is dominant. At the stem scale velocity variations occur in the vicinity of each stem, while at the stand scale there are larger-scale flow variations between the low velocities within the stand and the accelerated flow outside. Usually both scales operate together, and their relative importance depends on the discharge passing through the vegetation and the one going around the vegetation. The stand scale of resistance is dominant in the presence of high density species, conversely in open-structured species the stem scale has a major role.

Hydraulic resistance can be found in literature as [6]:

- Manning's equation: $V = \frac{1}{n} R^{2/3} S^{1/2}$
- Darcy-Weisbach's equation: $V = \sqrt{\frac{8g}{f}} \sqrt{RS}$
- Chezy's equation: $V = C\sqrt{RS}$

where R = hydraulic radius, g = gravitational acceleration and S = bed slope.

Manning's equation is the most widely used resistance measure among these, in particular with respect to vegetated channel. Although it expresses the resistance at the reach scale and reflects only the influence of the boundary shear on flow depth

and averaged velocity, Manning's coefficient n is often used as a lumped parameter accounting for all the various influences in a river reach. It is commonly estimated through experience from simple verbal or photograph descriptions of channels. A more advanced method is to split channel resistance into its component parts, and to determine the final value of Manning's n from knowledge of the separate, smaller scale contributing effects using tables (e.g. Dackombe and Gardiner, 1983).

Various methods have been suggested to synthesize a composite resistance coefficient.

In cases where resistance is due to surface roughness only (and it is possible a variation of the roughness across the channel cross section but not longitudinally), a formulation of an overall value of Manning's n has been proposed:

$$n = \left(\frac{\sum_{i=1}^{N} (K_i n_i^a)}{K} \right)^{1/a} \tag{1}$$

where i is a subscript that refers to the subsection associated with the local value n_i and $i = 1 \div N$, K is the weighting variable and a is the exponent. Pavlosky (1931) proposed $a = 2$ while Horton (1933) proposed $a = 3/2$.

To account for the interactions between subsection flows through transverse momentum exchange, that are not considered in Eq. 1, Wallingford (2004) suggested a lateral distribution model:

$$n_l = (n_{sur}^2 + n_{veg}^2 + n_{irr}^2)^{1/2} \tag{2}$$

where n_l is a local composite unit roughness, and n_{sur}, n_{veg}, n_{irr} account respectively surface, vegetation and irregularity roughness.

To account the variation of the roughness not only in the transverse direction, the United States Soil Conservation Service, based on a concept introduced by Cowen (1956), proposed the following equation (1963):

$$n = (n_b + n_1 + n_2 + n_3 + n_4)m \tag{3}$$

where n_b accounts for the channel surface, n_1 for surface irregularities, n_2 for shape variations in the cross-section sizes, n_3 for obstructions, n_4 for vegetation and m for sinuosity.

A simplified version of Eq. 3, that uses the squares of the resistance components, was used by Morin et al. (2000):

$$n^2 = n_b^2 + n_4^2 \tag{4}$$

Eq. 2 and 3 both include terms that account resistance from form and surface drag. Since these phenomena are very different and their effect strongly depends on

the water depth, James et al. (2008) proposed the following equation that combines form and bed shear resistance:

$$U = \sqrt{\frac{1}{C_S + C_D}}\sqrt{2glS} \tag{5}$$

where U = cross-sectional averaged velocity, g = acceleration due to gravity, $l = s^2/d$ where l = roughness length, s = space between the form roughness elements, d = width of the elements, C_D = drag coefficient and C_S = term that accounts for the bed shear resistance. The term C_S can be expressed as a function of local Darcy-Weisbach's f or Manning's n:

$$C_S = \frac{fl}{4H} = \frac{2gln^2}{H^{4/3}} \tag{6}$$

in which H = flow depth. The equation was originally developed to combined vegetation stem and bed resistance, but it can be applied also at the channel reach scale to consider large emergent roughness elements.

The use of look-up tables can be very subjective and the estimated n can be highly inaccurate (Hey, 1972), particularly when the additional factor of vegetation is introduced. The unreliability of resistance tables or photograph guides, combined with the heterogeneity of vegetation types and distributions, leads to develop most reliable methods to determine channel resistance in vegetated rivers.

2.2 MAIN VEGETATION PARAMETERS INVOLVED

There are many vegetation characteristics that affect the hydraulic resistance in vegetated channels, and they are discussed in this section.

2.2.1 *Geometrical characteristics of the plant*

The first important vegetation characteristic that affects the flow resistance is the geometry of the vegetation itself, concerning the taxonomy of the species as the branching index, the density of the shoots, the maximum level of growth that each species can reach in a cross section, the seasonal presence of the plant [5]. Vegetation has foliage and side-branches, which depend on the species and make describing the vegetation resistance even more complicated. These branches and leaves move from one part to the other as a result of flow interactions. The position and amount of side branches and leaves may be different even for the same type of plant, and it is variable depending on season, which makes describing the influence on the flow resistance very complex. The taxonomy of the species is very important to determine the flow retardance caused by a plant stem, but in most cases the resistance is mainly at the stand scale because the stems operate together. It seems more appropriate to classify plants on their functional form rather than on generic taxonomy. In Fig. 2 there are the four main types of riverine vegetation classified on their functional form: emergent plants, rooted floating plants, rooted submerge plants and floating plants [5].

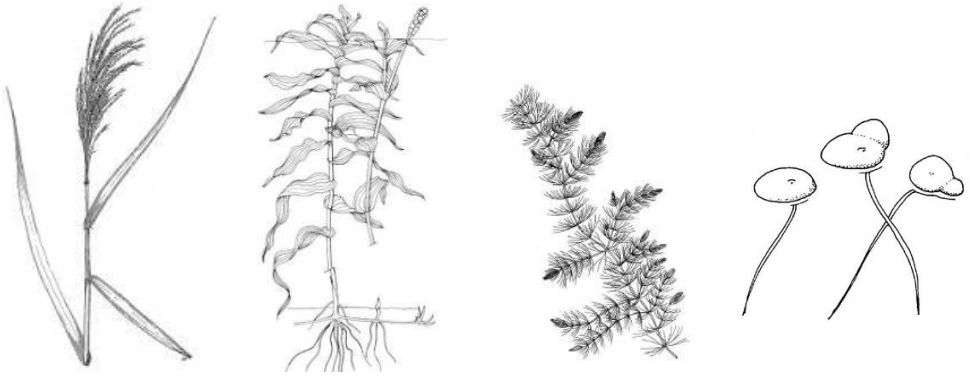

(a) *Phragmites sp.* (b) *Potemogeton sp.* (c) *Ceratophyllum sp.* (d) *Lemna sp.*

(a) *Emergent.* (b) *Rooted floating.* (c) *Rooted submerged.* (d) *Floating.*

Figure 2: Taxonomy and functional form of riverine vegetation.

In addition to this, there is a hydraulic parameter which considers the characteristic dimension of the vegetation in relation to flow conditions. The experimental results from the laboratory studies of Kouwen [30] showed that the friction factor in fully developed turbulent regime is a primary function of the relative roughness for the flow over flexible plastic elements. The parameter H/h_v, in which h_v is the deflected height of the vegetation and H the water depth that is established in the channel for given conditions of motion, is of fundamental importance. One of the main problems in vegetated channel is the determination of the vegetation height. This can be solved if the flexural and drag properties of the vegetation are known. This issue could be solved by comparing the bending characteristics of vegetation with unknown mechanical properties, to that of well-known flexible plastic strips [30, 23].

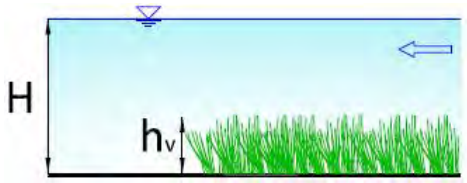

Figure 3: Relative roughness (water depth - vegetation deflected height).

2.2.2 *Mechanical characteristics of the plant*

Flow over flexible vegetation induces bends and reduces the height of the vegetation stems. As a result, the flow-vegetation interactions are reduced. The vegetation configuration depends on flexural rigidity and density of the vegetation itself. These characteristics depend essentially on the species. The flexural rigidity of the vegetation is expressed as $J = EI$, where E is the modulus of elasticity of the roughness element's material and I is the second increment of area of its cross section.

Kouwen and Unny [30] developed a method to estimate the roughness deflection for flow over submerged flexible vegetation as a function of the stiffness of the vegetation itself.

Kouwen and Unny suggested to establish the values of MEI, the aggregate stiffness, to define the deflected vegetation height and proposed as key dimensionless parameter the term $H_v/(\frac{MEI}{\rho {u_*}^2})^{1/4}$, where u_* is the shear velocity, H_v the vegetation height and M is the number of roughness elements per unit area of channel bed and thus represents the density. They carried out a series of experiments involving different configurations of plant density and different flexibility of the vegetation elements. These elements were obtained by cutting strips out of plastic sheets of different thickness.

The relationship obtained is:

$$\frac{h_v}{H_v} = \frac{3.57}{H_v}\left(\frac{MEI}{\rho u_*^2}\right)^{1/4} - 0.286 \tag{7}$$

where H_v is the vegetation height and h_v is the deflected vegetation height.

The use of the aggregate stiffness is based on the hypothesis that the concentration and the bending stiffness have a similar effect on flow resistance: an increase in the number of strips per unit area has the same effect of an increase of the single strips stiffness. However, the measure of MEI can be difficult in the field, and the flexibility of an individual stem is hard to determine and highly variable. Moreover, dense groups of blades may have different bending properties compared to a single blade. Even in a simplified form, it is very complicated to take the flexibility into account and to determine the deflected vegetation height.

2.2.3 *Blockage factor of vegetation*

The blockage factor B is the parameter that measures the portion of the channel blocked by vegetation, or equivalently the proportion of the channel containing vegetation [31]. Several types of blockage factors have been proposed in the literature. Kouwen [24] introduced the proportion of just a single cross-section that was blocked by vegetation, which is called *cross-sectional blockage factor* B^X.

Fisher [22] introduced the *surface-area blockage factor* B^{SA} which relates the plan surface area of the vegetation to the plan surface area of the channel.

Finally there is the *volumetric blockage factor* B^V (Fisher [22]) that relates the volume occupied by the vegetation to the volume of the channel.

The first two versions are two-dimensional measures, the third is three-dimensional.

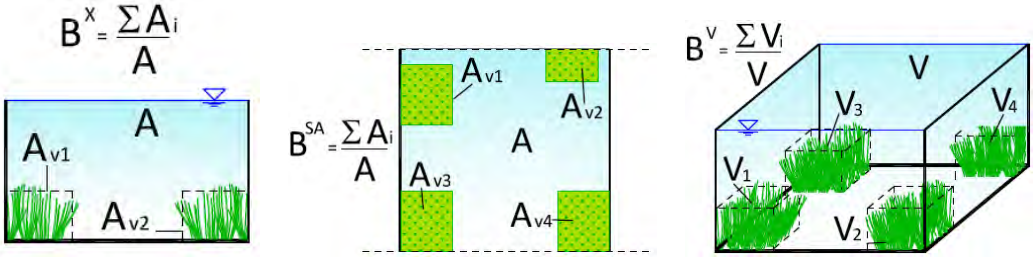

(a) *Cross-sectional.* (b) *Surface-area.* (c) *Volumetric.*

Figure 4: Types of blockage factor.

Fisher [22], studying a 40 m stretch of the Candover Brook (Hampshire, UK), related the surface-area blockage factor to Manning's n, finding the following best-fit relationship:

$$n = 0.0337 + 0.0239 \left(\frac{B^{SA}}{UR} \right) \tag{8}$$

She suggested using the surface-area blockage factor since it was easier to be measured. There is to say that the surface area does not take into account the proportion of channel depth occupied by plants, so it is not directly related to resistance. The cross-sectional and volumetric versions of the blockage factor are measures of relative roughness and thus should be directly proportional to the volume displacement component of channel resistance.

Green [4] introduced a fourth version of the blockage factor, the *multi-cross-sectional blockage factor* $\overline{B^X}$, to take into account two main problems that affect the other blockage factors. The first is that the cross-sectional blockage factor considers the vegetation distribution in the vertical axis, but it does not consider the heterogeneity in the downstream direction. The second is that the volumetric blockage factor biases in favour of the deeper sections if the depth is not uniform. The multi-cross-sectional blockage factor is a quasi-three-dimensional measure and it is built by averaging the proportion of vegetation in several cross-sections.

2.3 RIGID AND FLEXIBLE VEGETATION

Studies to understand the physics of flow in vegetated channels involve the use of rigid elements and flexible strips distributed on the channel bed. The distinction between rigid and flexible elements can take place in both cases of emerged or submerged vegetation (see Section 2.4). The resistance of rigid vegetation is less complex to describe than that caused by the flexible one because the drag coefficient of flexible vegetation decreases when the vegetation is bent. The behaviour of flexible vegetation depends on the flow conditions. As flow increases, several distinct regimes of flattening can be identified [5]:

1. vegetation is not deflected and it is stationary;

2. stems and leaves assume an orientation in the flow direction;
3. stiff vertical stems begin to vibrate, flexible stems move with a sinuous movement;
4. stiff stems are inclined, submerged plants are strongly orientated;
5. stems are prone and compacted;
6. damage of plants and loss of leaves or part of the stem.

These regimes can be summarized in three different configurations [24, 28, 14]: erect elements, elements that are subjected to a waving motion and elements that assume permanently a prone position.

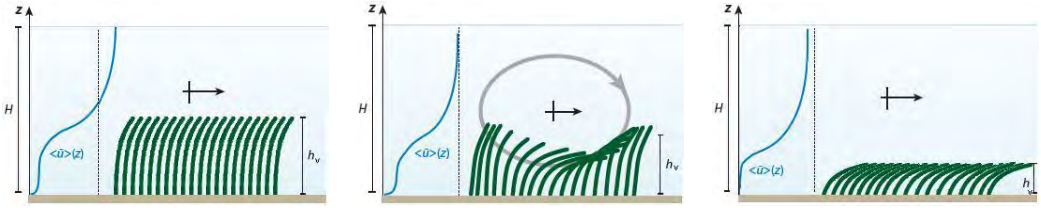

(a) *Erect.* (b) *Waving motion.* (c) *Prone position.*

Figure 5: Main regimes of flattening for submerged vegetation (adopted from [20]).

As the velocity increases the bending of the vegetation is higher. Kouwen [23] introduced the concept of critical shear velocity $u_{*,cr}$ to describe the prone configuration. Vegetation can be regarded as prone if the share velocity u_* is higher than the critical value. The critical value can be defined using Eq. 9 for flexible vegetation and using Eq. 10 for long, stiff vegetation.

$$u_{*,cr} = 0.028 + 6.33(MEI)^2 \tag{9}$$

$$u_{*,cr} = 0.23(MEI)^{0.106} \tag{10}$$

The introduction of two different expressions of the critical shear velocity is justified by Carollo [14] by the two different observed deformation behaviours of the vegetation. For strongly deformable vegetation elements, the inflected elements show an elastic behaviour and the deformation is reversible. For high values of MEI, indeed, the inflection of the elements produces a plastic deformation and the stems remain in a bent configuration.

2.4 EMERGENT AND SUBMERGENT VEGETATION

Studying the hydraulic resistance due to the presence of vegetation, as mentioned in Section 2.2.1, the height of the vegetation with respect to the water level is important and it influences the velocity profile. As far as flow resistance is concerned, the vegetation can be roughly classified into three different categories [15]:

1. *Fully submerged vegetation:* $h_v/H < 1$

   The equivalent resistance due to vegetation presence can be described as a wall shear stress and the related roughness coefficient can be express as a function of h_v and the biomechanical characteristics of the vegetation [24, 26]. Universal velocity distribution laws such as the logarithmic profile may prevail in the upper part of the water depth. The vegetation is considered *deeply submerged or unconfined* if $h_v/H < 10$ and *shallow submerged* if $5 < h_v/H < 1$. In this case, there is a two-layer flow [23]: the lower layer in which the flow passes through the vegetation and the upper layer in which the flow above vegetation is accelerated. Usually, the flow in the lower part is not negligible compared to that in the upper part, and it has much lower velocity than that in the surface-flow layer. The velocity profile is influenced by the density of the vegetation [23, 15]. The distinction of these two regions is more and more evident with increasing vegetation concentration because a reduction of the momentum exchange between these two regions occurs.

2. *Partially emergent vegetation*: $h_v/H = 1$

   The hight of the vegetation is of the same magnitude of the water depth.

3. *Emergent vegetation*: $h_v/H > 1$

   The resistance is the effect of the hydrodynamic drag of the single plants [32].

Once the difference between emergent and submergent vegetation and rigid and flexible vegetation is clarified, it is said that this thesis focuses on flexible fully submerged vegetation. Thus, the next chapters will deal in more detail with the studies done on this type of vegetation.

3

MATHEMATICAL FRAMEWORK

A rigorous approach for deriving hydraulic resistance relationships is based on the integration of the double-averaged, both in time and space, Navier-Stokes equations over stream reach fluid volume. This approach requires detailed knowledge of dynamic vegetation geometry, which makes it very difficult to apply. Some simplified alternatives can be used.

In this chapter are given some outlines about the double averaged Navier-Stokes equations approach. Then, a simplified analysis conducted for emergent or partially emergent vegetation and two promising methods about fully submerged vegetation are explained.

3.1 DOUBLE AVERAGED NAVIER-STOKES EQUATIONS APPROACH

The double averaging procedure on the classical Navier-Stokes equations, where the classical time-averaged Reynolds equations is supplemented by a spatial-averaging procedure in the plane (x, y) parallel to the average bed, has been applied to canopy problem (Wilson and Shaw, 1977) and also to rough bed (Nikora, 2001) [26].

Fully submerged vegetation acts on the flow field as a relative submergence roughness. In this case a two-layer flow takes place, as mentioned in Section 2.4. Fully submerged vegetation is considered as a 2D, steady flow in the (x, z) plane, as Fig. 6 shows.

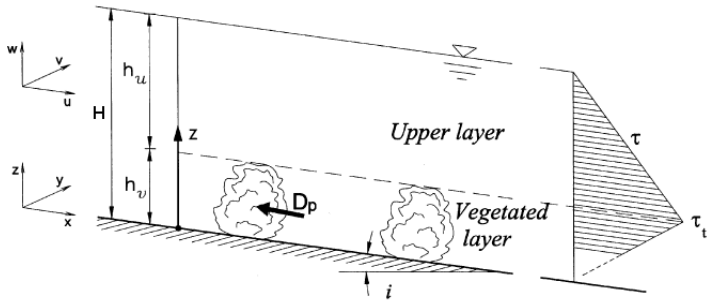

Figure 6: Coordinate axes for Double averaged Navier-Stokes equations approach (adopted from [26]).

Applying the double-averaged Navier-Stokes equations approach, and considering the viscous term negligible, we obtain four differential equations, two for the upper-layer (Eq. 11 and Eq. 12) and two for the vegetated-lower-layer (Eq. 13 and Eq. 14) [26]:

$$gi - \frac{\partial \langle \overline{u'w'} \rangle}{\partial z} - \frac{\partial \langle \widetilde{u}\widetilde{w} \rangle}{\partial z} = 0 \tag{11}$$

$$g - \frac{1}{\rho}\frac{\partial\langle\overline{p}\rangle}{\partial z} + \frac{\partial\langle\overline{w'2}\rangle}{\partial z} + \frac{\partial\langle\widetilde{u}^2\rangle}{\partial z} = 0 \tag{12}$$

$$gi - \left\langle\frac{\partial\widetilde{p}}{\partial x}\right\rangle - \frac{1}{A}\frac{\partial A\langle\overline{u'w'}\rangle}{\partial z} - \frac{1}{A}\frac{\partial A\langle\widetilde{u}\widetilde{w}\rangle}{\partial z} = 0 \tag{13}$$

$$g + \frac{1}{\rho}\frac{\partial\langle\overline{p}\rangle}{\partial z} + \frac{1}{\rho}\left\langle\frac{\partial\widetilde{p}}{\partial z}\right\rangle + \frac{1}{A}\frac{\partial A\langle\overline{w'2}\rangle}{\partial z} + \frac{1}{A}\frac{\partial A\langle\widetilde{w}^2\rangle}{\partial z} = 0 \tag{14}$$

where the brackets $\langle\rangle$ refer to spatial averaging along (x, y) plane, the linear overbar symbol refers to the time-averaging, the wave overbar refers to the Reynolds decomposition, i = bed slope, A = ratio between the fluid area and the plane (x, y) area at level z.

By integration of Eq. 12 and 14 from the free surface to the generic value z of the vertical axis, we get the total stress distribution, which is expressed by Eq. 15 for the upper layer and by Eq. 16 for the lower vegetated layer:

$$\frac{\langle\tau\rangle}{\rho} = gi[H - z] = -\langle\overline{u'w'}\rangle - \langle\widetilde{u}\widetilde{w}\rangle \tag{15}$$

$$\frac{\langle\tau\rangle}{\rho} = gi\left\{H - h_v + \int_z^{h_v} A(z)dz\right\} = -A\langle\overline{u'w'}\rangle - A\langle\widetilde{u}\widetilde{w}\rangle + \int_z^{h_v}\left[\frac{A(z)}{\rho}\left\langle\frac{\partial\widetilde{p}}{\partial x}\right\rangle\right]dz \tag{16}$$

3.2 SIMPLIFIED APPROACH

3.2.1 *Petryk and Bosmaijan's model for emergent vegetation (1975)*

Petryk and Bosmajian [32] developed a theoretical model that expresses the vegetation resistance based on the drag forces that plants exert. The assumptions are: (1) $h_v > H$; (2) the velocity is slow enough so that the bending of the plants does not occur; (3) there is not a large velocity gradient along the depth and (4) the flow is steady or at most gradually varied. Thus, this model can be applied only to emergent or floating-leafed species where the leaf scale is dominant [5].

The drag force per bed surface can be expressed as [26]:

$$F_D = nC_D A_{pi}\rho\frac{U^2}{2} \tag{17}$$

where n = number of plants per bed surface; A_{pi} = area of the i-th plant projected in the streamwise direction; ρ = water density; C_D = drag coefficient; and U = mean flow velocity. By means of a momentum balance in the streamwise direction applied

to a volume of length L, we obtain the resistance coefficient which is expressed in Eq. 18 in terms of Gauckler-Strickler's equivalent coefficient $K_{s,eq}$:

$$K_{s,eq} = \frac{1}{\sqrt{R^{4/3}\left(\frac{C_d \sum A_{pi}}{2gA_cL} + \frac{1}{K_{sb}^2 R^{4/3}}\right)}} \tag{18}$$

where R = hydraulic radius; A_c = cross sectional area of the flow; g = acceleration due to gravity; and K_{sb} = Strickler coefficient due to bed roughness.

The term C_D is highly variable with different factors (e.g. species of vegetation, density of the plant, plant configuration, reference velocity U) and must be determined experimentally. It is probably the most uncertain parameter of Eq. 18.

3.2.2 *Kouwen's logarithmic resistance law (1969)*

Kouwen et al. [24] conducted the earlier experiments of flexible vegetated open-channel flows. Ree and Palmer [37] developed a graphical method to determine the Manning's coefficient n as a function of the product UR, where U = mean velocity and R = hydraulic radius. The $n - UR$ method is based on the finding that n is uniquely related to the product UR for a particular vegetation. The effect of the bed slope and the relative roughness is not directly indicated in these graphs. Kouwen et al. [24] found that for wide channels with flexible artificial vegetation elements, n is mainly a function of the relative submergence H/h_v where H is the water depth and h_v is the deflected height of the vegetation, in accordance with Rouse studies (1965). Thus, the representation of n as a function of UR is not satisfactory. They derived a quasi-theoretical formula for flexible vegetated open-channel flows. Kouwen's experiments were conducted in a laboratory flume (0.61 m wide, 0.46 m deep and 12 m long) using artificial flexible elements of styrene, 0.3 mm thick, 0.5 cm wide and 10 cm height, which were glued to the bottom of the channel. He conducted different experiments with various range of density and bed slope.

The equation found integrating the velocity profile upon the vegetation layer is:

$$\frac{U}{u_*} = C_1 + C_2 ln\left(\frac{H}{h_v}\right) \tag{19}$$

in which U = mean velocity; u_* = shear velocity; C_1 and C_2 = constants which depend on the density of the vegetation and on the stiffness of the vegetation respectively; H = water depth and h_v = deflected vegetation height.

Eq. 19 assumes a slip velocity at the tips of the plants and that the velocity profile is logarithmic above the vegetation. The general shape of the velocity profile obtained by means of a pitot tube follows Prandtl's universal logarithmic law, and it is shown in Fig. 7.

The logarithmic profile was found valid in the case of flow over a flexible plastic cover as in the case studied by Rouse of rough surface. For height from the bottom to the deflected vegetation height, the local velocity becomes very low and assumes almost a constant value [28]. Near the top of the vegetation both the local velocity and its gradient progressively increase, producing a vertical profile concave

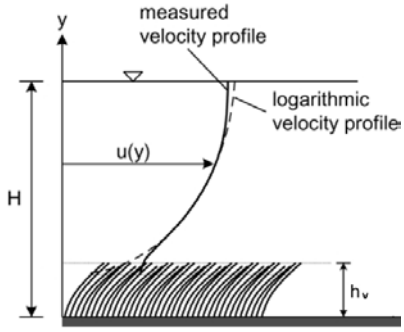

Figure 7: Vertical velocity profile above aquatic vegetation. Adopted from [34].

downward. Upon the vegetation, the velocity gradients decrease with the vertical y and the velocity profile is concave upward. Thus, the velocity profile shows an inflection point located at the top of vegetation, where the maxima values of both the turbulent shear stress and the turbulence intensity appear [14].

The advantage of using Eq. 19 is that h_v can be directly measured. This allows a general approach which includes all the different regimes of flow: (1) erect vegetation, (2) waving motion, (3) prone vegetation.

Kouwen et al. suggested replacing the ratio H/h_v with A/A_v where A = cross sectional area of the channel and A_v = cross sectional area of the channel blocked by vegetation. Eq. 20:

$$\frac{U}{u_*} = C_1 + C_2 ln\left(\frac{A}{A_v}\right) \tag{20}$$

is thus an approximation of Eq. 19, considering that it may not be legitimate to assume that the values of C_1 and C_2 are identical in these two equations.

This replacement can be justified if the boundary is completely uniform; in fact the distribution of the vegetation in Kouwen's experiments was uniform. Moreover, since Eq. 19 and 20 are based on logarithmic velocity profile above the canopy, it could be that they are applicable only in cases of fully submerged grass-like uniform vegetation, and not in patches [5]. It is not clear if such a method is applicable to natural channels.

3.2.3 *Carollo, Ferro and Termini's power hydraulic resistance law (2005)*

Carollo et al. [14] collected experimental data using a straight flume (0.60 m wide and 14.4 m long) having a bed covered by natural grass-like vegetation. They pointed out that the application of Kouwen's method produces a systematical overestimation of flow resistance in natural flexible vegetation flow which is greater as the vegetation concentration increase. To obtain good agreement with experimental data, the coefficients appearing in the log-law type flow resistance were re-estimated.

Experiments were carried out for three vegetation concentrations (M = 280-310-440 $stems/dm^2$). Carollo et al. evidenced an uncertainty of Kouwen's results: they observed that for the examined configurations, an increase in M produced a decrease

of the resistance. This implies that the quasi-smooth flow regime, for which there is an invariance of the friction factor with the element concentration, occurs. The overestimation of the flow resistances is due to the circumstance that Kouwen's method is based on the hypothesis that the U/u_* decreases for increasing values of the concentration.

Using the Π-theorem (Barenblatt, 1979) Carollo introduced the following resistance law, using five dimensionless terms:

$$\frac{U}{u_*} = A_0(M) \cdot \left(\frac{H}{h_v}\right)^{a_1} \cdot \left(\frac{u_* h_v}{\nu}\right)^{a_2} \cdot \left(\frac{H_v}{h_v}\right)^{a_3} \tag{21}$$

where a_1, a_2, a_3 are numerical coefficients calibrated using the available measurements; and A_0 is an unknown function of M that assumes, for a given vegetation concentration, a constant value.

The values of the coefficients introduced by Carollo are listed in Tab. 1:

$M[stems/dm^2]$	A_0	a_1	a_2	a_3
$M \leq 50$	$43.4M^{-1.0521}$	1.168	0	-0.861
$M \geq 280$	$0.0275M^{2.3701}$	1.168	-1.023	-0.861

Table 1: Carollo's coefficients A_0, a_1, a_2, a_3.

The comparison between the experimental values of U/u_* and the calculated values using Eq. 21 with Kouwen's results showed a poor agreement of Kouwen's experimental data. It can be attributed to the dependence on the term $(u_* h_v/\nu)$ which was not considered by Kouwen. The fitting of Eq. 21 to Kouwen experimental data was obtained by $a_2 = 0.086$. The term a_2 is almost equal to zero, confirming the substantial nondependence of Kouwen's data on this dimensionless term. It has to be considered in the flow resistance law only when high value of density of aquatic vegetation occurs ($50<M<280$ $stems/dm^2$). This result can be justified taking into account that the velocity of flow inside the vegetated layer can be deduced from the shear velocity [28, 30]. The dimensionless term $(u_* h_v/\nu)$ represents the Reynolds number of the flow inside the vegetated layer of thickness equal to h_v. Since an increase of M produces an appreciable decreasing in flow velocity inside the vegetated layer, the study of the dissipative phenomena has to take into account the shear Reynolds number.

4

LITERATURE REVIEW

In this chapter there is a brief literature review of studies made on flow resistance in the presence of fully submerged vegetation patches, on which this thesis focuses.

4.1 PATCHY VEGETATION

In real applications it is difficult to find uniform bed coverage of vegetation. Several species of submergent aquatic macrophytes can grow in scattered patterns across the channel, forcing the flow to weave over and around them in a complex way. As a result, there is often an extensive boundary between the slow flow inside the canopy stand and the faster flow in the free stream. Nezu and Onitsuka (2001) have suggested that horizontal vortices are generated at this boundary and have identified the effect of vegetation on secondary currents. Bennett et al. (2002) have shown the ability of plants to divert the course of the flow. As these factors cause energy losses, the spatial distribution and the shape of vegetation patches within the channel could influence the channel resistance [22].

Figure 8: Vegetation patches in natural streams. (adopted from [5])

4.1.1 *Tests on staggered configurations: Li and Shen (1973), Fisher and Reeve (1994)*

Li and Shen in 1973 used cylinders to simulate trees on a flood plain. They studied effects of tall nonsubmerged vegetation on flow resistance by investigating the wake caused by various cylinder set-ups. They used two main different configurations, whit aligned and staggered elements, and they showed that the staggered configuration was much more effective in reducing flow rates. A credible reason of this result is that when the cylinders were placed in rows, the retardation effects were

restricted to those bands, but the flow in the spaces between the rows was relatively unhindered. When placed alternately, on the contrary, the retardation effects were more evenly distributed, and the flow was stopped in accelerating. This is shown in Fig. 9. Moreover, Fisher and Reeve in 1994 carried out some tests with different configurations using stones. For the same percentage cover, the staggered pattern gave a resistance value 17% higher than aligned.

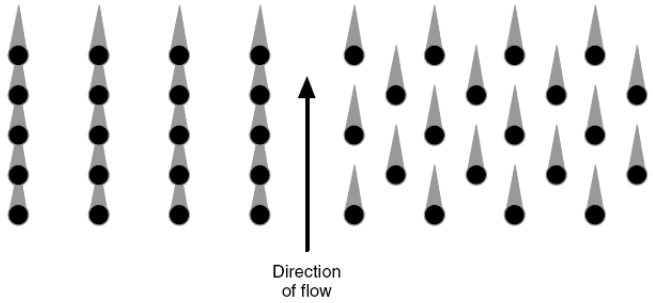

Figure 9: Planform view of the configurations studied by Li and Shen (1973). Black circle = cylinder; shaded triangle = wake zone behind cylinder (adopted from [5]).

4.1.2 *Green's empirical relationship (2005)*

Green [4] presented a regression equation between the weighted median of several cross-sectional blockage factor and n_4, the vegetation component of resistance, for sites containing the macrophyte *Ranunculus*. The equation determined was linear:

$$n_4 = 0.0043 B_{WM} - 0.0497 \tag{22}$$

where $n_4 = n_{tot} - n_b$ in which n_{tot} = total value of Manning's n and n_b = base value of n for a straight uniform smooth channel. Eq. 22 gave good results, but there is to say that it only accounts for the most significant factor affecting resistance (i.e. the volume displacement caused by the vegetation and the exclusion of most of the flow from within macrophyte stands). Since other studies suggested that the spatial location of the plants also affects flow resistance, Green [18] developed an empirical model to account for both the variation in macrophyte distribution between cross-sections and within cross-sections. He used hydraulic and vegetation data collected at 35 river sites in southern England containing the submergent macrophyte *Ranunculus*.

To take into account the spatial variability of the vegetation between cross-sections, hydraulic resistance was expressed as a function of the cross-sectional blockage factor percentile B_{69}, which gave the highest R^2 value (74.4%). The result demonstrated that cross-sections with higher than the median vegetation blockage are the best predictors of vegetation resistance. The following exponential equation was found:

$$n_4 = 0.0432 e^{0.0281 B_{69}} - 0.05 \tag{23}$$

The model was then improved by adding an additional parameter T relating the length of the vegetated/solid boundary in contact with the open channel to the

length of the wetted perimeter, acting as a pseudo-measure of the energy losses generated within the unvegetated stream by the macrohytes:

$$T = \frac{WP_e}{WP} \tag{24}$$

where T is the vegetation cross-sectional spatial-variability parameter (dimensionless); WP is the length of the solid boundary of the cross-section and WP_e is the effective wetted perimeter defined as the sum of the vegetation and solid boundaries. Fig. 10 explains better the concept.

(a) *Wetted perimeter* WP (b) *Effective wetted perimeter* WP_e

Figure 10: Definition of vegetation cross-sectional spatial-variability parameter T (adopted from [18]).

Residuals r between the predicted and calculated values of n_4 were calculated, and the regression equation ($R^2 = 0.5316$):

$$r = -0.1361T_{16} + 0.155 \tag{25}$$

was significant at the 0.01 level and thus able to account for some of the variation in the residuals. Combining Eq. 23 with 25, the following equation for the vegetation component of Manning's n was found:

$$n_4 = 0.0432e^{0.0281B_{69}} + 0.1361T_{16} - 0.205 \tag{26}$$

The model was also tested on three additional sites dominated by other species and whose values of channel resistance were outside the calibration range of the model.

4.1.3 *Nikora et al.'s field study (2008)*

Nikora et al. [35] examined the effects of aquatic vegetation on hydraulic resistance in a range of vegetation types and patch patterns. They suggested simple qualitative relationships to predict these effects using the vegetation parameters. They conducted field experiments with naturally occurring submerged aquatic plants in five streams in New Zealand. The aquatic plants at the selected stream reaches formed elongated patches that covered $40 - 100\%$ of the bed. At each site, five measurements campaigns were conducted over 6 months, which included measurements of a number of hydraulic and vegetation parameters. The vegetation parameters (e.g. height of the vegetation canopy, plant length, areal and volumetric biomass density, vegetation porosity) were patch-averaged and site-averaged, and were used

to explore the effects of vegetation on flow resistance factors: Manning's n, Chezy's C and Darcy-Weisbach friction factor f. The key physical parameters influencing the hydraulic resistance investigated were the patch-averaged relative roughness h_v/H, the plant inclination factor H_v/h_v, the areal vegetation cover b_v/b and the site-averaged relative roughness $(h_v/H)(b_v/b)$. All the terms are indicated in Fig. 11.

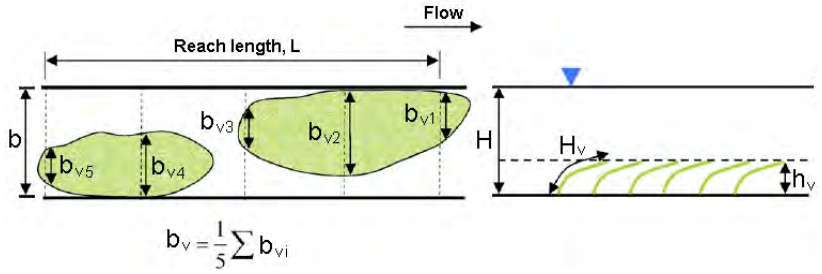

Figure 11: Symbology of vegetation characteristics (adopted from [35]).

All the vegetation parameters showed good correlation ($r^2 > 0.80$) with the resistance coefficients, except for the ratio H_v/h_v ($r^2 = 0.15 - 0.33$) and the areal and volumetric biomass densities ($r^2 = 0.5$ and 0.25 respectively). The little explanatory power of the term H_v/h_v was attributed to the interplay between the increasing stiffness during the plant growth and the drag force, which made this term almost constant. The site-averaged relative roughness, instead, had the highest predictive power, as it accounts for both the relative submergence and the relative patch size. Exponential functions provided the best fit for the relationships between the site-averaged relative roughness and the flow resistance factors, suggesting that a non-linear combination of bed and vegetative resistance could be more suitable.

Both Kouwen et al.'s [24] and Carollo et al.'s [14] models were tested and they approximated data very well. In Fig. 12 there are the relationships $U/u_* = F(Hb/h_v b_v)$ and $U/u_* = F(Hb/H_v b_v)$ found.

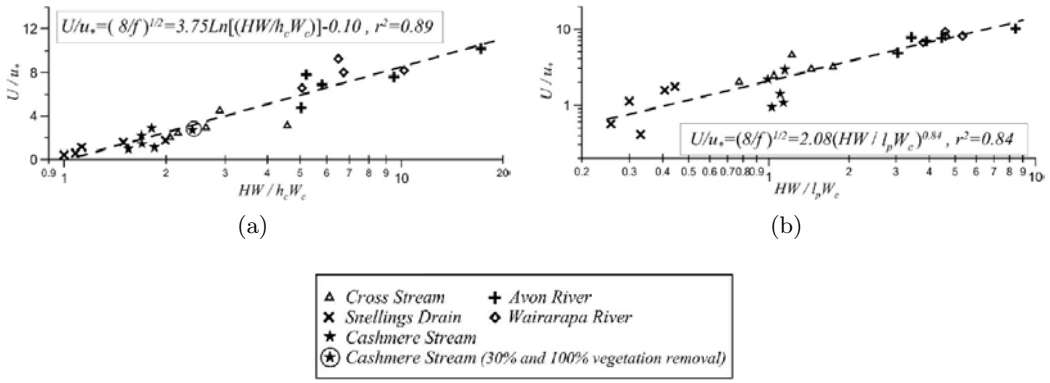

Figure 12: Relationships (a) $U/u_* = F(Hb/h_v b_v)$ and (b) $U/u_* = F(Hb/H_v b_v)$ found in Nikora's et al. field study (2008), (adopted from [35]).

Fig. 12 shows two important facts: (1) Kouwen et al.'s and Carollo et al.'s models were found to be extended for conditions of patchy vegetation if site-averaged vegetation measured are considered and (2) no dependence on dominant plant species and their patch mosaic patterns was shown.

Effects of individual plant species and their characteristic patch patterns were not significant in Nikora et al.'s field study.

4.1.4 *Combination of local resistance effects: James and Jordanova's tests on distributed roughness (2010)*

James and Jordanova [7] used results from experiments made by other authors on different distributed roughness in channels to test formulations for combining local resistance effects.

They used Bhembe and Pandey's investigation (2006) on patterns of surface roughness. Elements were created in Bhembe and Pandey's experiments by gluing fine gravel particles ($d_{50} = 6.7\ mm$) to a square steel panel of size 0.5 m, and were arranged in different configurations that are shown in Fig. 13. Experiments were carried out in a flume 12 m long and 2 m wide on a slope of 0.05%. Each configuration was tested with a single discharge.

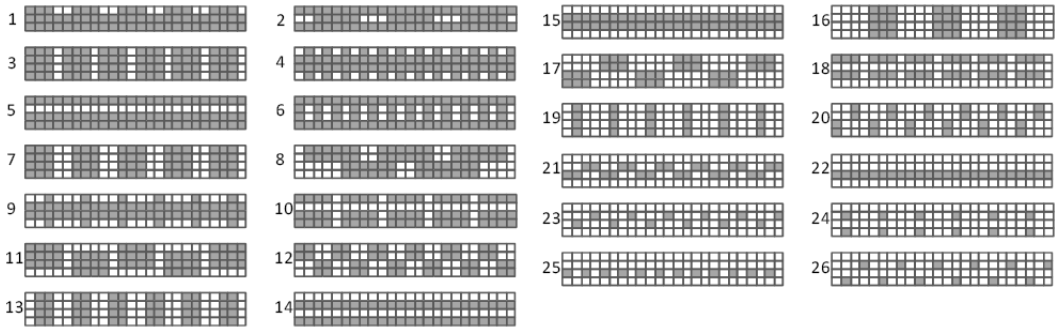

Figure 13: Patterns tested by Bhembe and Pandey, 2006 (adopted from [7]).

The overall Manning's value was calculating using Eq. 1 with $K = A$, the surface area, and with three different values of a (2, 3/2, 1). All of them gave good results, with $a = 1$ performing slightly better than the others. The average absolute errors in predicting n were respectively: 0.0013, 0.0011 and 0.00093. The greatest errors were made in all the three cases for the longitudinal patterns.

Fisher (1993) carried out experiments similar to those of Bhembe and Pandey using roughness elements of different shapes and patterns, formed by a single layer of 10 mm gravel. The configurations tested are showed in Fig. 14.

James and Jordanova, using Fisher's data, calculated the overall Manning's n for the discharge value of 0.05 m^3/s as indicated in Eq. 1 with $a = 2, 3/2, 1$. Predictions were more accurate for pattern B, C and F, suggesting an influence of the pattern shape on resistance.

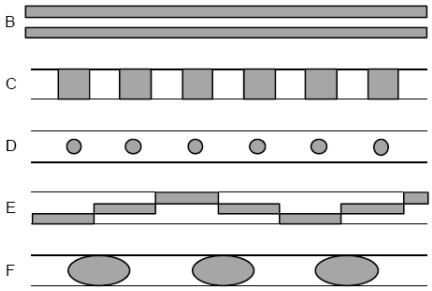

Figure 14: Patterns tested by Fisher, 1993 (adopted from [7]).

James and Jordanova tested James et al.'s data (2001) on spatially distributed patterns of emergent vegetation. Vegetation was made with 5 mm diameter circular rods placed in a staggered arrangement with a space distance of 25 mm. The patch patterns investigated are shown in Fig. 15.

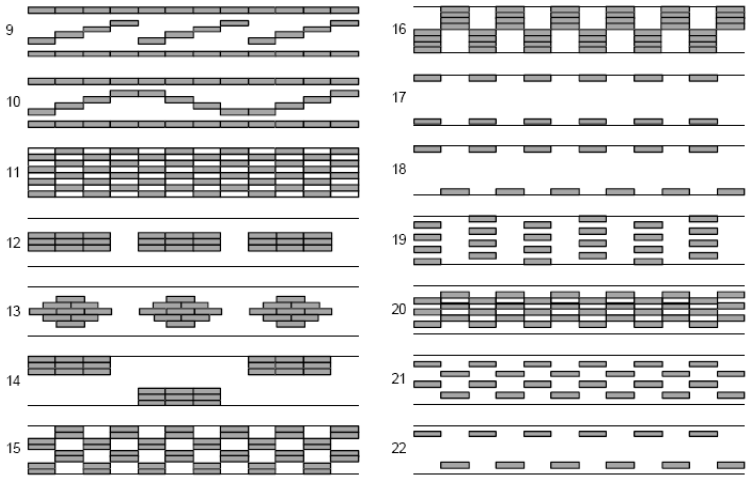

Figure 15: Patterns investigated by James et al., 2001 (adopted from [7]).

They applied Eq. 1 with $K = A$, the surface area, and $a = 2, 3/2, 1$ to account for the overall vegetation coverage, as well as Eq. 3 with $C_D = 1$ to determine the local vegetative resistance with different water depths. The values predicted with $a = 1$ were significantly better than that with the other two values. There was a strong difference between the different patterns of vegetation. The best fit was for evenly distributed, small patches. This showed that in this case the overall resistance was not a simple superposition of independent contributions in proportion of their preponderance, but included an emergent effect associated with the pattern.

James and Jordanova applied Eq. 3 to Nkosi's data (2007) on relative sparse, large form roughness elements. Nkosi studied 0.11 m diameter circular cylinders placed in a staggered configuration in the same flume described for Bhembe and Pandey's experiments with four different values of areal coverage (0.5-1-2-4 %). Patterns were studied with a smooth bed and with a gravel bed. The value of C_D was selected to minimize the average absolute error in predicted discharge. The model gave good results.

They concluded that the effective resistance of a channel with different roughness surface areas (e.g. vegetation that is completely submerged) can be well described by a combination of Manning's resistance coefficient for the different surfaces, weighted by their surface area (e.g. Eq. 1 with $a = 1, 2, 3/2$ equivalently). Eq. 1 gave also good results with $a = 1$ for patches of emergent vegetation, but accuracy decreased as patches became larger and less uniformly distributed. Resistance originating from both form and surface drag was not properly combined in such a way, and a rational combination equation (e.g. Eq. 3) was more effective.

4.1.5 *Bal's laboratory study on patterns of macrophytes (2011)*

Bal et al. [21] studied the hydraulic performance of three vegetation patterns with different types of macrophytes. The aim of their analysis was to study the effect of different patterns of vegetation on flow resistance to test the hypothesis of a partial removal of the vegetation (instead of a total removal) in order to preserve the ecological value of the river.

Laboratory experiments were carried out in a 25 m long and 3 m wide brick walled flume with a horizontal bed. Flume walls were covered with a foil to smoothen the surface. Plants were collected in two small lowland rivers. The used plant species were *Potamogeton natans L.*, *Stuckenia pectinata L.*, *Callitriche platycarpa Kütz.*, *Ranunculus penicillatus (Dum.) Bab.* and *Sparganium erectum L.*. These species were chosen to evaluate the impact of architectural differences on flow resistance.

Three vegetation patterns, covering the 19% of the surface area, were used. Configurations are shown in Fig. 16.

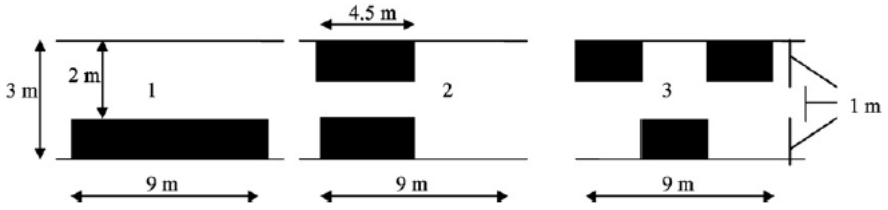

Figure 16: Patterns investigated by Bal et al., 2011 (adopted from [21]).

Compared with the empty situation, the different distribution patterns increased resistance between 14 and 23%. Hydraulic resistance of these patterns was significantly influenced by (1) the species present in the vegetation patches and (2) the spatial distribution of the patches.

Within the used species, three groups with similar resistance were detected, reflecting their architectural structure. This finding confirms the fact that at the stand scale friction is classified in functional plant groups (emergents, submergents, surface floating leaves and free floating leaves). *S. erectum*, a typical emergent species with open canopy, was shown to have significantly smaller friction values than all other species. *P. natans* and *S. pectinata* formed a group with similar friction values. The lower resistance values of this group compared with the submerged species (*C. platycarpa* and *R. penicillatus*) is in concordance with the conclusions of Guscio et al. (1965) whom suggested that floating vegetation reduces flow less than submerged

vegetation.

Spatial distribution patterns significantly influenced channel friction. Pattern 2 had higher friction values than pattern 1. Meanwhile, pattern 3 did not differ significantly from pattern 1 with more aligned vegetation blocs. They explained this fact saying that, since the amount of water diverted around macrophyte patches depends on biomass, shape and orientation of the plant towards flow direction and flow rate and those factors were for both patterns identical the same, the result was not unexpected.

4.1.6 *Studies on patch-scale turbulence*

Vegetative drag occurs at different scales: the blade scale, the patch scale and the reach scale, which are interconnected.

For a submerged canopy, there are three limits of behaviour, depending on the relative importance of the bed shear and the canopy drag [15].

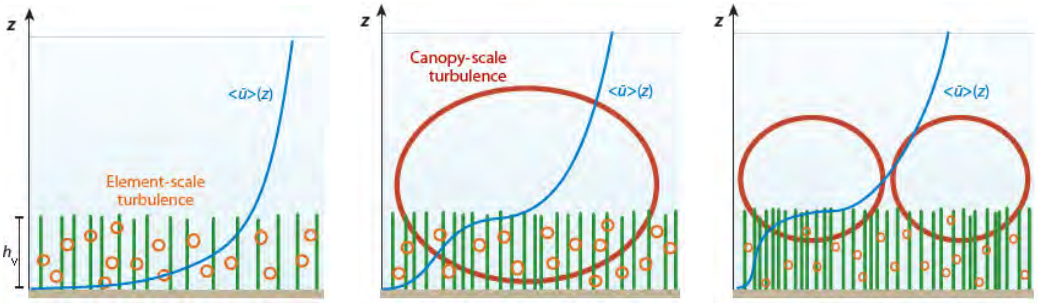

(a) *Sparse canopy.* (b) *Transitional canopy.* (c) *Dense canopy.*

Figure 17: Mean velocity profiles and turbulence scales for submerged vegetation of increasing roughness density (adopted from [15]).

Near sparse submerged canopies (Fig. 17(a)), the bed roughness and the near-bed turbulence are enhanced, but the velocity profile remains logarithmic. The turbulence is at the stem scale within the canopy. At the blade scale, the hydrodynamic response is dominated by the boundary layer formed on the plant surface.

If the canopy drag is large compared to the bed stress, the drag discontinuity at the top of the canopy generates a shear layer (Fig. 17(c)) where there are Kelvin-Helmholtz vortices at the canopy-scale that control the exchange of mass and momentum between the canopy and the overflow. The velocity profile has an inflection point near the top of the canopy. The canopy-scale vortices can induce a waving motion in flexible blades, causing a local depression in the canopy, called monami.

Canopy-scale turbulence differs from the much-larger boundary-layer turbulence which may form above the submerged canopy (Fig. 17(b)). If the vegetation is deeply submerged the canopy-scale vortices interact with the larger boundary-layer turbulence, and become three dimensional, enhancing secondary instabilities.

In Fig. 17 the longitudinal velocity profiles and the dominant turbulence scales for (a) *sparse canopy* ($ah_v \ll 0.1$), (b) *transitional canopy* ($ah_v \simeq 0.1$) and (c) *dense*

canopy ($ah_v \gg 0.1$) are shown. The term h_v is the deflected height of vegetation and a is the frontal area per canopy volume, $a = w/\Delta S^2$, where w is the characteristic width of the elements and ΔS is the average spacing between elements.

At the reach scale, flow resistance is connected mainly on the patch-scale vegetation distribution, described for example by the blockage factor.

Attention is here mainly placed on the patch-scale turbulence.

Nepf [16] examined the hydrodynamics of a circular patch of vegetation with diameter D. The patch was emergent, so that the flow field could be seen as 2D. The patch was porous, so it allowed flow to pass through it, altering the wake structure relative to that of a solid body (see Fig. 18).

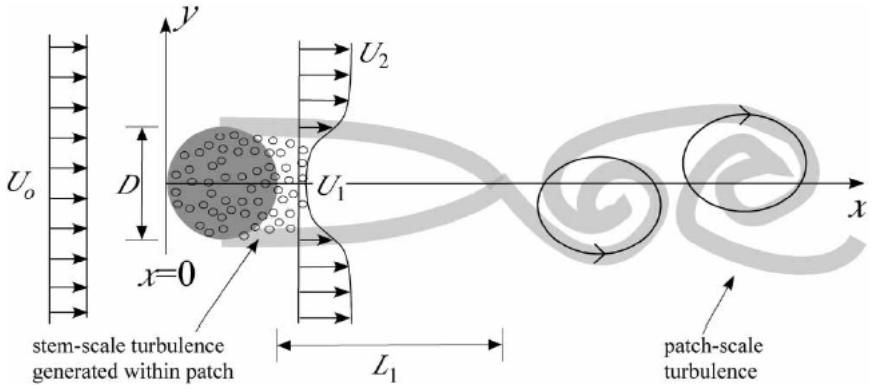

Figure 18: Circular patch of emergent vegetation and the von Karman vortex street (adopted from [16]).

Behind the patch there is a region of recirculation with velocity U_1, followed by a von Karman vortex street. The wake behind a porous obstruction is very long due to the flow that enters the wake through the patch and delays the composition of the von Karman vortex street at a distance L_1 behind the patch. The von Karman vortex was visualized using traces of dye. Both the terms U_1 and L_1 depend on the diameter of the patch and on the drag length scale, which can be considered in the dimensionless parameter called the flow blockage, $C_D aD$ (Chen et al., 2012). The wake transition described above has implications for the characterization of drag contributed. For low flow blockage patches, there is sufficient flow through the patch and the stem-scale drag dominates the flow resistance. For high flow-blockage patches, there is negligible flow through the patch, and the flow response is essentially identical to that of a solid body of the same patch frontal area, A_p. Thus, the flow resistance provided by the patch should in this case be represented by the patch-scale geometry $C_D A_p U^2$, where U is the channel velocity.

5

KNOWLEDGE GAPS AND PROJECT OBJECTIVES

As a result of studies explained in Chapters 3 and 4, many theoretical and conceptual approaches have been proposed and are in use to describe the hydraulic resistance in the presence of submerged flexible vegetation. Even if there is a general agreement that resistance coefficients depend on parameters of flow, vegetation characteristics and patchiness, the quantitative form of this dependence and the relative contributions of those factors to the overall resistance remain to be better understood today. Moreover, there is no agreement on a most suitable approach for general application, and the majority of resistance equations have been derived for channels with uniform plant distribution. Thus, our ability to model flows in vegetated channels is still lacking, particularly with scattered blocks of plants. In order to develop knowledge about the hydrodynamics over beds with vegetation patches, experiments were carried out using an open-channel laboratory flume. The experimental method is a good way to create an open channel flow condition [30]: it is possible to control accurately the bed slope, the flow rate and the uniformity of the flow. The main parameters (e.g. blockage factor, spatial variability, relative roughness) were studied in different hydraulic conditions including different ranges of relative submergence, bed slopes and flow rates, and in different patterns of artificial grass-like vegetation.

5.1 OBJECTIVES AND RESEARCH QUESTIONS

Based on the problem description, the objectives of this research and research questions are formulated. The aim of this thesis is to develop knowledge about the hydrodynamics in channels with vegetation patches and to identify the practical suitability of different existing vegetation resistance models. To reach the goal, the following research questions are identified:

1. What are the key parameters that characterize the hydraulic resistance due to the presence of vegetation patches?
2. What is the relation between resistance parameters and the blockage factor?
3. What are the effects of the spatial variability of vegetation patches on hydraulic resistance?
4. Which model(s) found in literature is(are) most suitable and robust to predict vegetation resistance?

6

EQUIPMENT

All experiments were carried out in the University of Aberdeen's Fluid Mechanics Laboratory. It houses excellent research facilities, including a large range of flumes and open channels. The facilities are supported by state-of-the-art instrumentation for measuring flow rate, flow velocities, bed profiles, sediment concentrations, transport and sizing. To learn more, visit the Laboratory's website [2].

6.1 LABORATORY FACILITIES

6.1.1 *Open channel and sediment re-circulation flume*

All the experiments were carried out in the rectangular flume called "*Blue flume*".

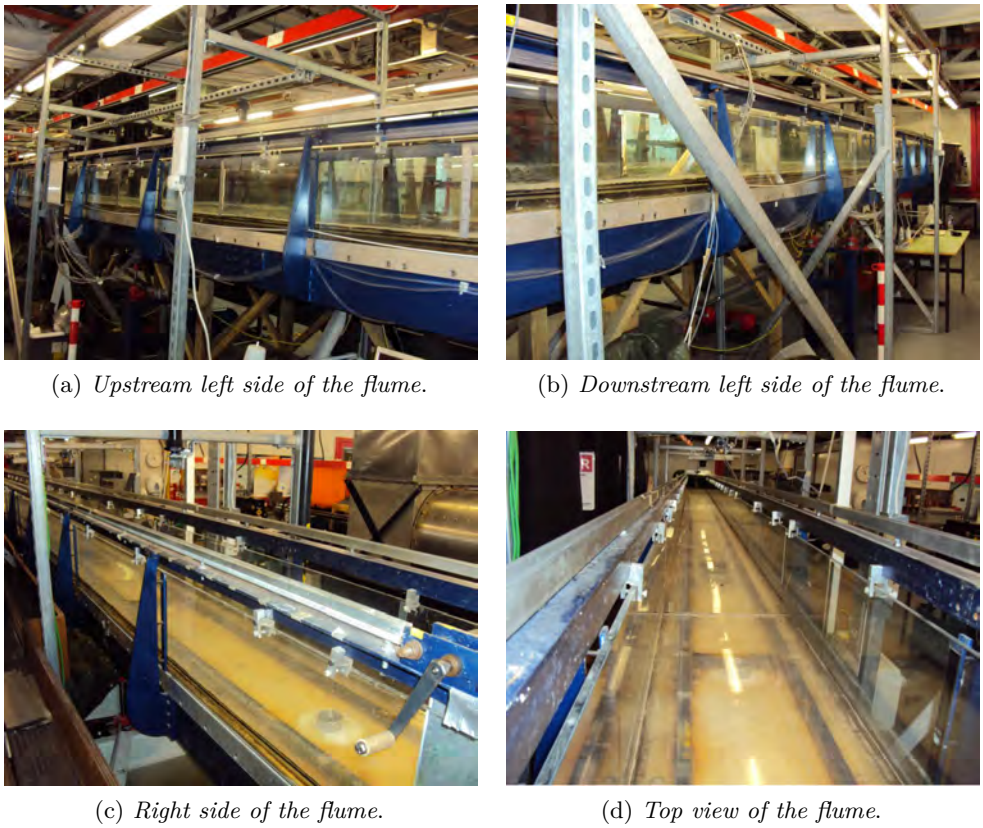

(a) *Upstream left side of the flume.* (b) *Downstream left side of the flume.*

(c) *Right side of the flume.* (d) *Top view of the flume.*

Figure 19: Pictures of the Open channel and sediment re-circulation flume.

This is one of the Lab's large open channel flow facilities and has the special facility of being able to re-circulate sediment that is transported to the downstream outlet. The flume was built specifically to investigate the transport of riverbed material under uniform flow conditions. The flume has a straight, rectangular section,

11 m long and 400 mm wide and a variable bed slope up to 1 in 50 which is manually controlled by a crank handle connected with a hand operated screw type jacking system. Flow spills into a large downstream tank and is re-circulated to the upstream header tank through a 6 inch pipe, with flow rates of up to 20 l/s. The control of the flow rate is done by a hand operated valve and the effective flow rate is shown in a digital display connected to an electromagnetic flow meter.

Sediment that is transported downstream is re-circulated separately from the main flow using a vortex pump which pumps a water-sediment mixture through a 1.5 inch pipe at high velocity. The re-circulated sediment is reintroduced to the flow at the upstream end of the flume and is distributed across the width of the channel. A V-notch weir is used to measure discharge and bedload transport samples can be collected by intercepting the flow as it spills from the end of the channel. However, the sediment line has not been used during the experiments.

(a) *Downstream tank.*

(b) *Upstream header tank.*

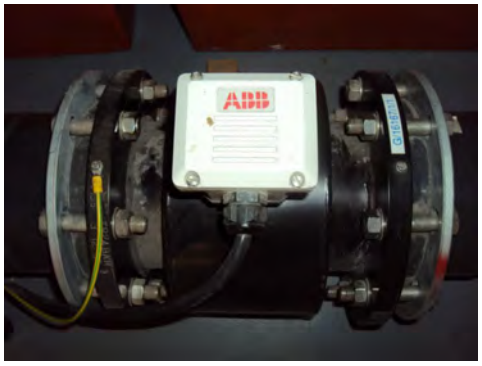

(c) *Electromagnetic flow meter.*

(d) *Pump.*

Figure 20: Blue Flume's details.

Along the flume there are ten equally distributed cross sections where a ruler glued to the glass wall of the channel and a piezometric intake take place. Rulers are used to measure the water depth and the deflected canopy height. The piezometric intakes are located in the middle of the width's flume and are connected to a board where the piezometric levels can easily be read. At the end of the channel there is a system of floodgates that can determine a different opening/closing ratio by

rotating. By opening or closing the gates it is possible to maintain the flow as uniform as possible during the experiments.

Figure 21: System of floodgates seated at the end of the flume.

6.1.2 *Ultrasonic Velocity Profile*

In order to inquire the velocity flow field, the instrument Ultrasonic Velocity Profile *UVP Monitor Model UVP-XW-PSi* was anaysed to become familiar with its principles of operation, technical specifications and measurement uncertainties. Investigations made with *UVP* however are not included in this thesis.

The instrument allows to take the velocity of the flow in a cross section. Since the transducer is rather small (8 mm diameter) it can be placed inside the flow while generating only a very small disturbance of measured flow field. The only required condition is that the tested fluid had to contain a sufficient amount of suspended small seeding particles, that can be added within the fluid in adequate quantity.

The UVP represents both a method and a device for measuring an instantaneous velocity profile in a liquid flow along the ultrasonic beam axis by detecting the Doppler shift frequency of echoed ultrasound as a function of time. The ultrasound-pulse-Doppler method allows the non-intrusive measurement of entire velocity profiles and is one of the latest advances in fluid engineering. It offers instantaneous results, thereby allowing calculation of flow as a function of both space and time.

Figure 22: UVP Monitor Model UVP-XW-PSi: main unit and 4-MHz transducer.

Functional principles of UVP

The technique uses the Doppler effect in which a sound wave, scattered by a moving particle, is subjected to a frequency shift, which is proportional to the velocity of the particle. An ultrasonic transducer transmits a short emission of ultrasound, which travels along the measurement axis and hits a small particle in the liquid. When we assume that the reflecting particle is small enough to represent the fluid flow adequately, its velocity equals the velocity of the fluid. When the collision occurs, part of the ultrasound energy scatters on the particles and echoes back. The echo reaches the transducer after a time delay:

$$t = \frac{2 \cdot x}{c} \tag{27}$$

where t [s] is the time delay between transmitted and received signal, x [m] is the distance of particle from transducer and c [m/s] is the speed of sound in the liquid.

The position of the particle can be determined from the length of time between the emission of the ultrasound wave to the reception of its echo t, if the speed of sound in the medium is known. If the echoes are received continuously within definite time windows (the velocity can be established in many separate space points along measurement axis), a complete velocity profile can be obtained, as shown in Fig. 23. The *channel width* is the width of the measurement volume and it determines the special resolution, the *channel distance* is the distance between two following measurement volumes.

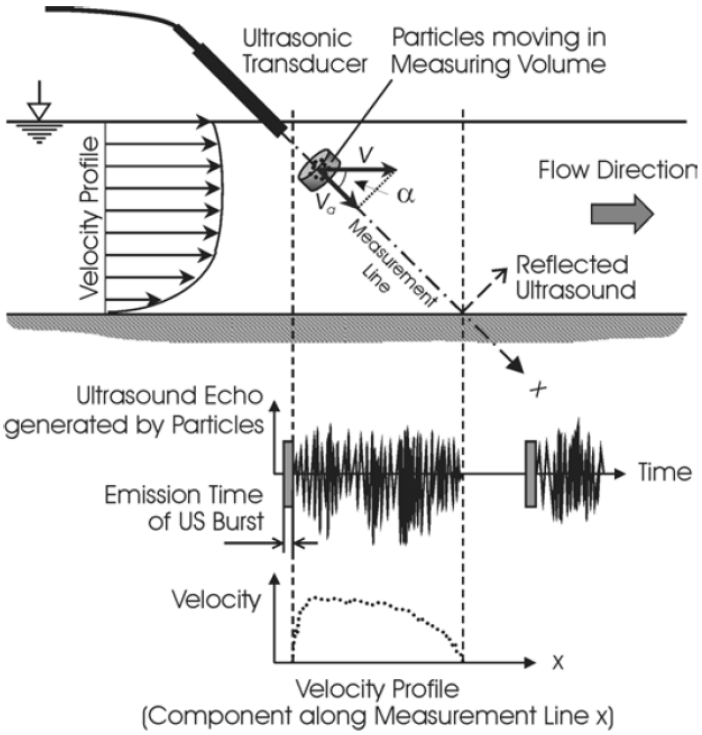

Figure 23: Scheme of UVP measurement system on a flow with free surface.

2D Velocity field

The velocity calculated using equations proposed by the UVP system (u, the velocity component along x-axis, calculated as the projection of u_f vector on x axis) is valid only if the components on the other directions (z and y axis) are equal to zero or could be neglected. In order to solve this issue and to consider as many velocity components as possible (2D or 3D), it is possible to use two probes with different inclinations as shown in Fig. 24. In the following, equations to determine the two components of the velocity is discussed. In Fig. 24, u_f is the velocity measured from UVP probe 1 (from upstream to downstream), d_f is the velocity measured from UVP probe 2 (from downstream to upstream), α is the Doppler angle, V the resultant velocity, u the component of velocity along x axis and w the component of velocity along z axis. If the aim is to measure time-averaged velocity profiles, since it is not necessary to have simultaneous velocity profile measurements, this method is correct. If the flow is regular and the Doppler angle is high, the error caused by the fact that the signals emitted from the probes hit each other only in one point, can be considered acceptable.

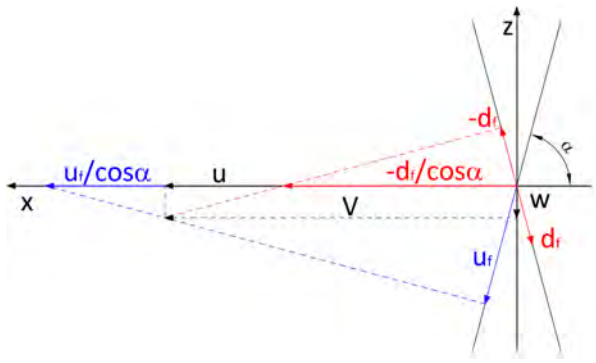

Figure 24: Scheme of UVP measurement and vector calculation with two probes.

The velocity components can be calculated as shown in Eq. 60:

$$u = \frac{1}{2cos\alpha}(u_f - u_d) \qquad w = -\frac{1}{2sen\alpha}(u_f + u_d) \tag{28}$$

6.2 EVERGREEN ARTIFICIAL GRASS

It has been proved [24, 23] that artificial grass behaves more or less like vegetation in natural open channels, particularly concerning its mechanical and hydraulic characteristics, among which waving motion and bending. This is a considerable advantage, given the many positive aspects that the artificial vegetation shows than the natural. Since natural vegetation is a highly variable material, many previous studies [17, 29, 13] had great difficulties in defining vegetation characteristics that influence the hydraulic resistance, such as the deflected canopy height due to the oscillatory movement of real plants. The high costs of real plants cannot be ignored. In addition it is not possible to run the experiments over a long period of time because the plants begin to decay. As a result of this, it has been decided to use artificial roughness elements. This was important also to allow cutting the elements

of grass of specific size. Vegetation considered is thus the artificial flexible garden grass EP100 made of uniformly distributed polyethylene plants.

Figure 25: Evergreen artificial vegetation EP100 that has been experienced.

The characteristics of the artificial grass were studied to know the properties of the experienced vegetation (see Section 7.1) and are summarized in Table 2.

M_p [plants/m^2]	M_s [stems/m^2]	H_v [cm]	w [cm]	t [cm]	A_w [-]	Φ [-]	E [N/m^2]	I_{ave} [m^4]	J [Nm^2]
15200	243600	3.53	0.119	0.020	20.40	0.969	$8.44{\cdot}10^{7}$	$1.06{\cdot}10^{-14}$	$8.92{\cdot}10^{-7}$

Table 2: Summary of the artificial flexible grass parameters.

6.3 FASTENER-BINDER SYSTEM

In order to fix the elements of vegetation in the correct position on the bed of the channel, a fastener-binder system was used. It is composed of two parts: a mushroom fastener used in combination with velours. The mushroom fastener part was cut of the same dimension of the bed of the channel and was positioned above it. The velours part was stitched to the elements of vegetation. By means of this system, a fast change of arrangement of the elements was possible, in order to create different configurations without damaging the glass bed of the flume.

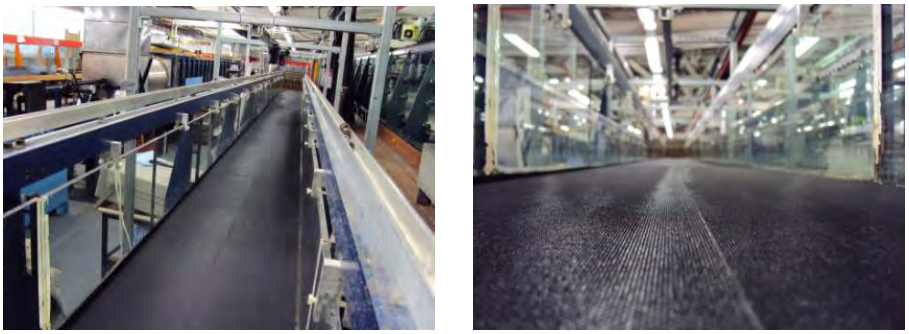

Figure 26: The mushroom fastener part positioned on the bottom of the channel.

7

PRELIMINARY TESTS AND RESULTS

7.1 VEGETATION CHARACTERISTICS

7.1.1 *Geometric characteristics of the vegetation*

The elements of artificial vegetation used for the experiments were analysed in their shape and geometry by measuring thirty randomly selected plants. These artificial plants were cut as close as possible to the polypropylene base. First of all it was measured for each plant the number of stems. At a later stage the height H_v, width w and thickness t of each stem were measured using a digital calliper.

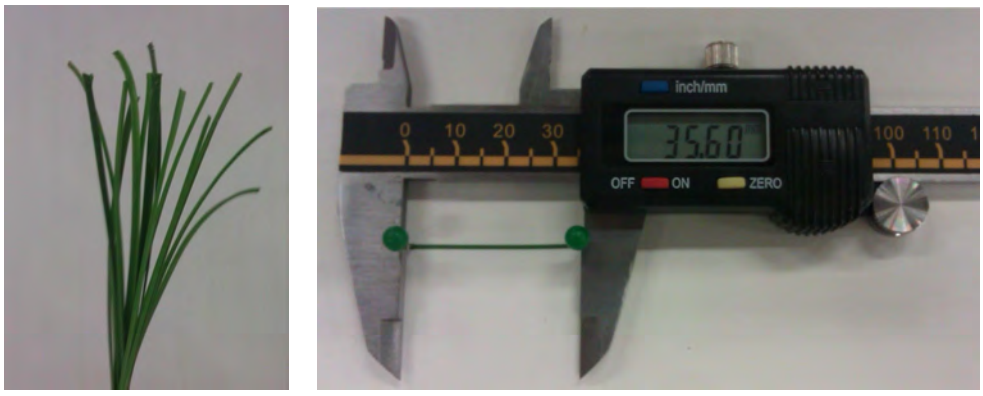

(a) *One plant of the grass layer with 16 stems.*

(b) *Digital calliper.*

Figure 27: Measuring method of the artificial grass geometry.

It was obtained the exact number of 16 stems per plant. Table 3 shows the average μ, the standard deviation σ and the coefficient of variation C_v of the geometric characteristics of the stems:

Dimension	Average μ [mm]	Standard deviation $\overline{\sigma}$ [mm]	Coefficient of variation C_v
un-deflected height H_v	35.297	0.757	0.021
width w	1.186	0.049	0.041
thickness t	0.200	0.013	0.067

Table 3: Vegetation characteristics.

It was also measured the canopy density in terms of plants M_p and stems M_s per square meter. By counting the number of plants in a square of side $(0.1\ m \cdot 0.1\ m)$, it

was obtained the average number of $M_p = 15200\ plants/m^2$. It was later calculated the number of stems per square meter, M_s, by multiplying the average number of plants by the average number of stems, as indicated in Eq. 29:

$$M_s = M_p \cdot \frac{stems}{plant} = 243600\ \frac{stems}{m^2} \tag{29}$$

The areal density A_w represents the wetted grass surface area per square meter and thus is described as the number of stems per square meter multiplied by the surface area of both sides of stems:

$$A_w = 2 \cdot M_s \cdot H_v \cdot w = 20.40 \tag{30}$$

7.1.2 *Mechanical characteristics of the vegetation*

The mechanical and geometrical properties of the artificial grass-like vegetation were studied in order to find the values of its flexural stiffness. A tension test of plastic specimens was carried out by using the *Hounsfield S-series bench up testing machine*. Five random samples of stems, from five different plants, for a total of 25 specimens, were analysed. Stems were cut as close as possible to the support with a cutter, and their dimensions were measured with a digital caliper. Each stem was positioned between the two clamps of the machine, paying attention to its alignment, because if the specimen is misaligned the machine exerts a bending force on the element. The length between grips (L_{sample}) was measured using the caliper. The test on the sample was then performed: the upper clamp is made up with a constant speed of 5 mm/minute and the machine records the values of the force F that correspond to the values of the extension ΔL. Fig. 28 shows the steps of the test: the sample to the starting position, the sample elongated and the sample broken at the end of the test.

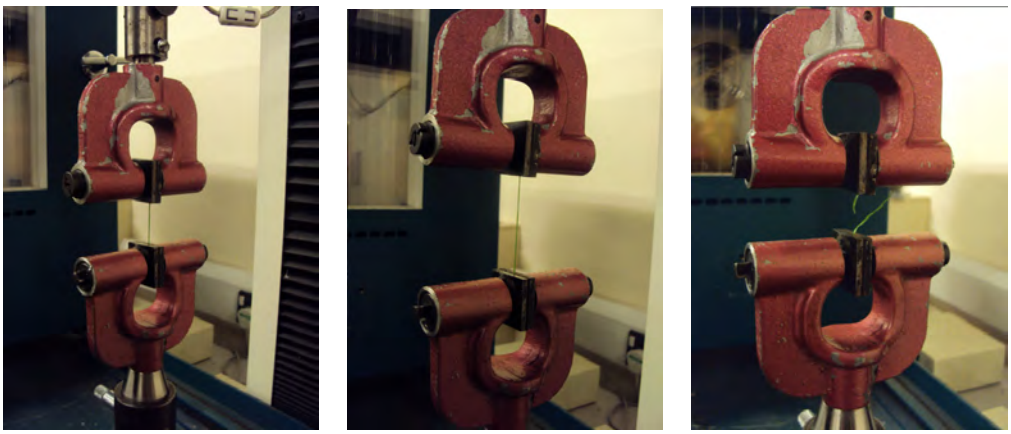

(a) *Sample at beginnig.* (b) *Sample elongated.* (c) *Sample broken.*

Figure 28: Steps of tension test.

Since the element can be invested by the flow in several directions, the second moment of area of an individual grass stem I_{ave} was calculated as an average of two

extreme values estimated depending on the orientation, i.e., when the grass stem was aligned with the flow, I_y, and perpendicular to the main flow direction, I_x.

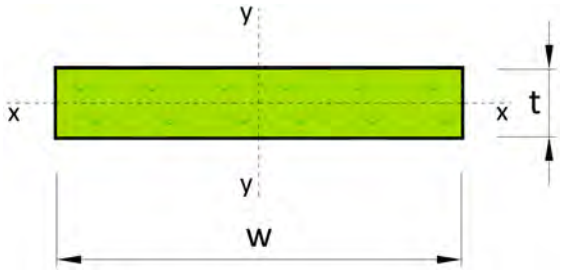

$$I_x = \frac{1}{12}t^3 w \qquad I_y = \frac{1}{12}w^3 t \qquad I_{ave} = \frac{I_x + I_y}{2} \tag{31}$$

The stem flexural rigidity is called J and it is the product between the Young's Modulus E and the second moment of area I_{ave} of the element, $J = E \cdot I_{ave}$.

The Young's Modulus is a measure of the stiffness of an elastic material and is calculated as following:

$$E = \frac{\sigma}{\epsilon} \tag{32}$$

where σ is the uniaxial stress and ϵ is the uniaxial strain. The uniaxial strain is defined as the ratio between the extension of the element over its initial length:

$$\epsilon = \frac{\Delta L}{L_{sample}} \tag{33}$$

The uniaxial stress is defined as the ratio between the applied force F and the cross section area of the stem A:

$$\sigma = \frac{F}{A} \tag{34}$$

Using Eq. 32, 33 and 34 the Young's Modulus can be expressed as following:

$$E = \frac{F \cdot L}{\Delta L \cdot A} \tag{35}$$

The term $F/\Delta L$ can be calculated as the slope of the tangent line to the graph force-extension in the first part where it follows the Hooks law. In Fig. 29 there is an example (for stem 1 on the first plant) of the graphs that were plotted by the machine for each run. The complete list of all the graphs obtained is in Appendix A and the table where there are listed the data of geometrical characteristics of the samples and the values of E, I_x and I_y obtained for each are also in Appendix A.

The results of mechanic properties of artificial grass-like vegetation are summarized in Table 4. The second moment of area is $I_{ave} = 1.06 \cdot 10^{-14}\ m^4$ and the stem flexural rigidity is $J = 8.92 \cdot 10^{-7}\ \mathrm{N}m^2$.

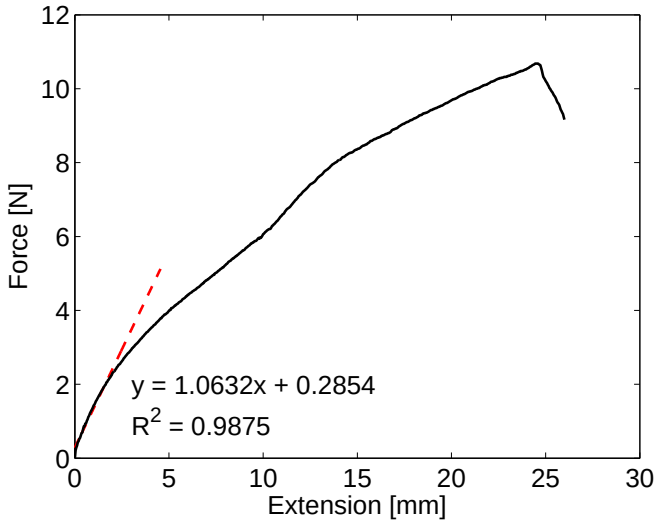

Figure 29: Curves Force - Extension for mechanic test on vegetation. Stem EP_P1_S1.

Dimension	Average	Standard deviation	Coefficient of variation
	μ	$\overline{\sigma}$	C_v
E $[N/m^2]$	$8.44 \cdot 10^7$	$1.63 \cdot 10^7$	0.193
I_x $[m^4]$	$3.99 \cdot 10^{-16}$	$1.48 \cdot 10^{-16}$	0.371
I_y $[m^4]$	$2.07 \cdot 10^{-14}$	$3.76 \cdot 10^{-15}$	0.182

Table 4: Mechanic properties of vegetation.

7.2 FLOW CHARACTERISTICS OVER SMOOTH BED AND FASTENER LAYER

Some preliminary tests were done to analyse the hydraulic behaviour of the channel under steady uniform flow conditions with (1) its own smooth bed and (2) with the fastener layer on it. Two bed slopes were investigated for both cases: 1:500 and 1:1000. About 18-19 values of flow conditions were analysed for each bed slope. Starting from the minimum value of depth, to the maximum, the water depth was step-by-step increased by a fixed value. The followed procedure for each water level can be summarized as follows:

1. Adjust flow rate and gates at the end of the flume to set the desire water depth;
2. Wait some minutes for the flow to stabilize;
3. Check water depth on 1-st, 5-th and 10-th cross sections, if not equal restart from point 1;
4. Record water depth on all cross-sections;
5. Record water surface level from all cross sections in the board of piezometers;

6. Check the quasi uniform steady flow conditions, if not restart from point 1;
7. Record flow rate discharge every 10 seconds for 2 minutes;
8. Increase the flow rare and start a new run from point 1.

The range of hydraulic parameters found is shown in Table 5.

	SMOOTH BED		FASTENER LAYER	
Bed slope:	1:500	1:1000	1:500	1:1000
Water depth H [mm]	$23 \div 70$	$25 \div 90$	$25 \div 90$	$25 \div 125$
Flow rate Q [l/s]	$2.9 \div 20.4$	$2.5 \div 20$	$1.7 \div 20.4$	$1.5 \div 21$
Cross sect. average velocity U [m/s]	$0.32 \div 0.72$	$0.25 \div 0.55$	$0.2 \div 0.6$	$0.15 \div 0.4$
Shear velocity u_* [m/s]	$0.02 \div 0.03$	$0.01 \div 0.02$	$0.02 \div 0.04$	$0.02 \div 0.03$
Reynolds number R_e $[\cdot 10^4]$	$0.7 \div 5.1$	$0.6 \div 5$	$0.4 \div 5.1$	$0.4 \div 5.3$
Gauckler-Strickler K_s	$95 \div 120$	$95 \div 110$	$50 \div 80$	$58 \div 77$
Chezy C	$50 \div 70$	$50 \div 70$	$25 \div 50$	$31 \div 50$
Weisbach f	$0.02 \div 0.03$	$0.02 \div 0.03$	$0.03 \div 0.07$	$0.03 \div 0.08$

Table 5: Range of values of the hydraulic conditions. Preliminary tests with smooth bed and fastener layer on the bed.

Fig. 73 shows the graphs of Darcy-Weisbach's f, Chezy's C, Manning's n and Gauckler-Strickler K_s as a function of the dimensionless Reynolds number for each bed slope and bed layer.

In Fig. 73(a) there is also underlined the well known Blasius formula (1913) for smooth pipes $f = 0.224/R_e^{0.25}$ for $700 < R_e < 25000$, which is often used as an approximation for wide smooth channels [6]. It is encouraging to see that friction factors behave as reported in the literature for the case of impermeable bed surface. The friction factor decreases as R_e increases since all points collapse at the same line. But the conventional 'hydraulically-rough regime', for which the friction factor depends only on the ratio of the roughness size to the flow thickness, does not apply to flows over permeable walls [27]. It has been showed that at high Reynolds number, the friction factor progressively increases with increasing Re over permeable bed. The increasing trend can be explained by a progressively deeper momentum penetration within the porous bed as Re increases.

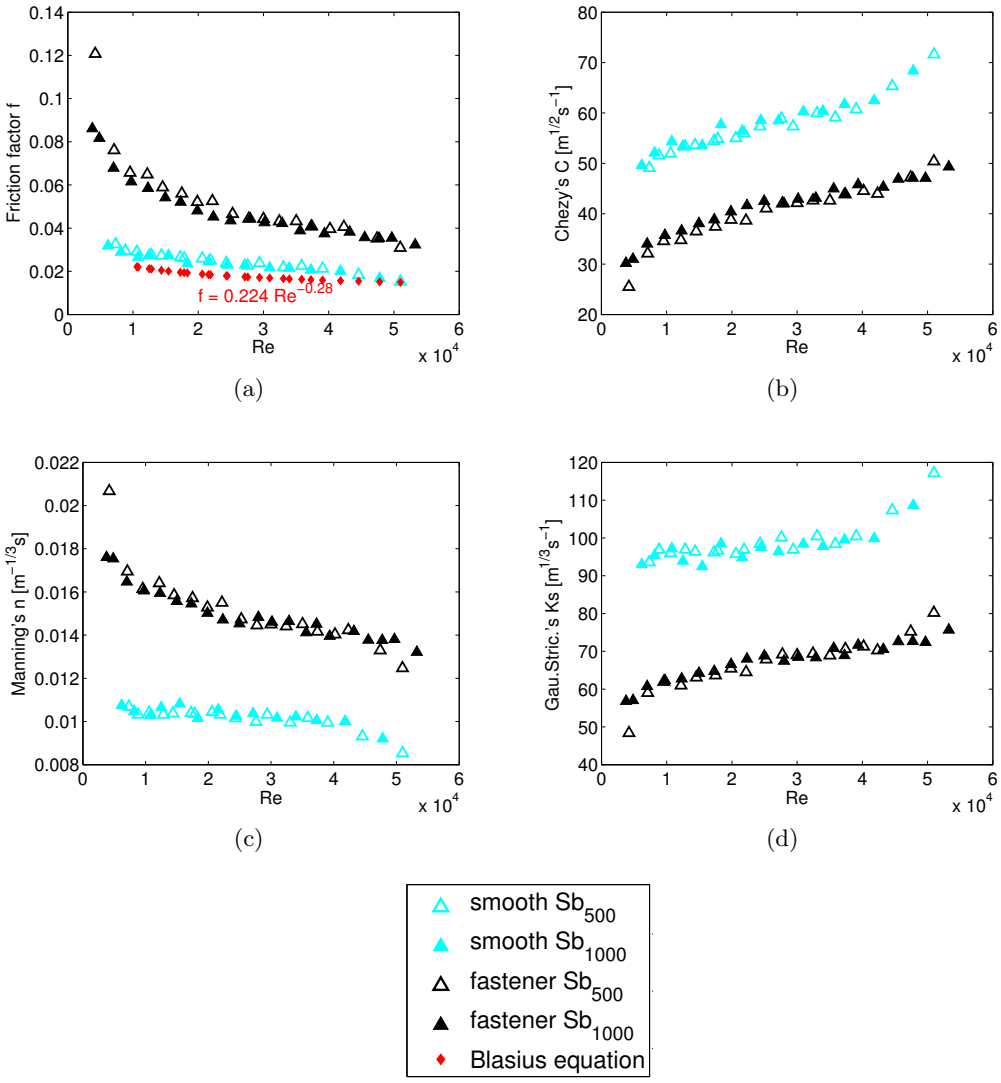

Figure 30: Relationships (a) $f = F(R_e)$; (b) $C = F(R_e)$; (c) $n = F(R_e)$; (d) $K_s = F(R_e)$; for preliminary test runs.

8

EXPERIMENTAL SET-UP AND PROTOCOL

The purpose of the experiments is to study the hydraulic resistance produced by sparse vegetation patches placed on the bed of the flume. The main parameters involved are patch spatial arrangements and blockage factor B. A series of laboratory experiments were carried out, in order to test the resistance and to answer the main questions made in Section 5.1. In this Section the design of the experiments are explained.

8.1 PATCH SHAPE AND BLOCKAGE FACTOR

Due to the geometry and the dimensions of the open-channel laboratory flume (e.g. channel width b), it was decided to use square elements of vegetation of area 0.01 m^2 and size 10 cm $\cdot$ 10 cm. A single square element of vegetation is shown in Fig. 31.

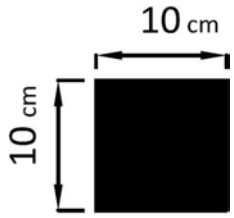

Figure 31: Square vegetation patch.

The elements were obtained by cutting squares from artificial grass, whose characteristics have been investigated and discussed in Section 7.1. The bottom of the flume was covered by the mushroom fastener, where the patches were attacked after being sewn to the velour. In order to determine the influence of vegetation density, the experimental set-up included the analysis of the flow with surface-area blockage factors B^{SA} ranging between $10 \div 30\%$. As a function of the blockage factor, the number of square elements needed can be derived, and it is shown in Table 6.

Blockage factor B^{SA} [%]	10	20	30
Bed area [m^2/m]	0.4	0.4	0.4
Vegetation area [m^2/m]	0.04	0.08	0.12
Square elements [#/m]	4	8	12

Table 6: Number of vegetation elements as a function of the blockage factor.

The simulated vegetation was set in two different configurations: *aligned* elements and *staggered* elements. For each configuration, various runs were made. In the aligned configuration, elements were placed at the same distance, both in x-axis direction and y-axis direction. Staggered configuration was obtained form the aligned one by moving laterally the patches in the direction of the x axis. This is shown in Fig. 32. In Fig. 33 the configurations of the plan are shown.

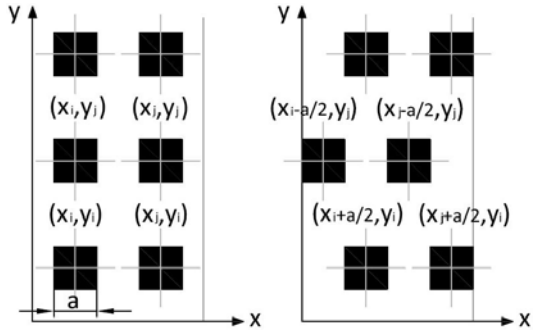

Figure 32: Change from aligned to staggered configuration.

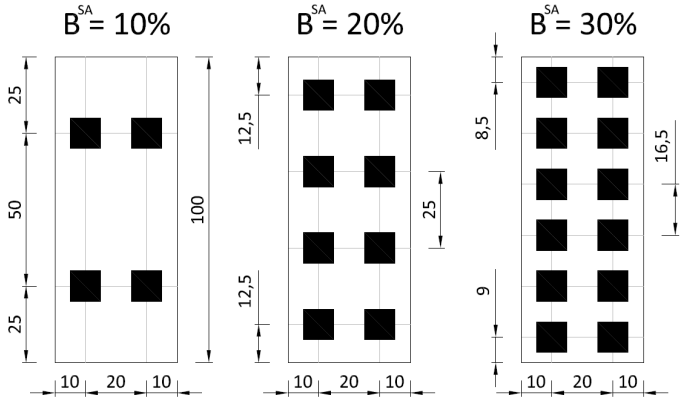

(a) *Arrangement with aligned elements.*

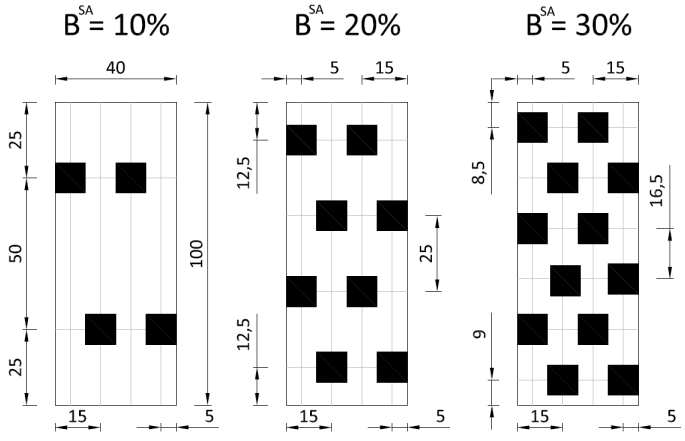

(b) *Arrangement with staggered elements.*

Figure 33: Experimental set-up configurations. The top view of the channel refers to a linear meter of the total length.

In Fig. 35 and 34 there are some pictures taken during the setting of the configurations in the laboratory.

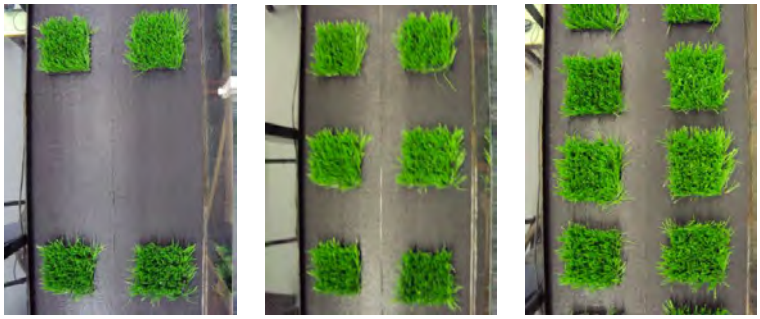

(a) B^{SA}=10%,aligned (b) B^{SA}=20%,aligned (c) B^{SA}=30%,aligned

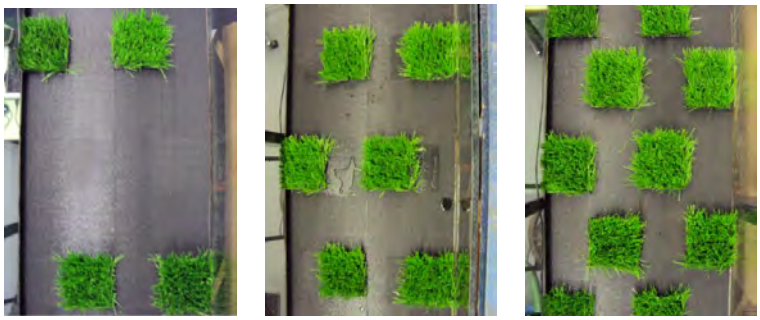

(d) B^{SA}=10%,staggered (e) B^{SA}=20%,staggered (f) B^{SA}=30%,staggered

Figure 34: Experimental set-up configurations, top view of the channel.

(a) B^{SA}=10%,aligned (b) B^{SA}=20%,aligned (c) B^{SA}=30%,aligned

(d) B^{SA}=10%,staggered (e) B^{SA}=20%,staggered (f) B^{SA}=30%,staggered

Figure 35: Experimental set-up configurations, frontal view of the channel.

8.3 EXPERIMENTAL DESIGN AND PROTOCOL

This section contains the measurement protocol that was followed for each run. Each run included measurements of a number of hydraulic parameters that allow to develop knowledge on the blockage factor-hydraulic resistance relationship, and to study the importance of spatial configurations on hydraulic resistance.

Before any experiments it is important to check the flume, the position of the grass and the fastener-binder system inside it and the instrumentations. It is also a good practice to avoid the presence of air bubbles inside the pipes that load to the piezometers for their correct reading.

After the desired configuration of vegetation has been placed on the bed of the channel, the first step is setting the bed slope and checking it from a dipstick where the current bed slope is indicated. By manually operating the valve connected to the pump, it is possible to establish a specific flow rate in the flume. After the system has settled, quasi-steady uniform flow condition must be guaranteed. The control is done on the upstream and downstream water depths, which have to be as equal as possible. Water levels can be adjusted by opening or closing the floodgates seated at the end of the flume. A series of discharges were investigated, starting with the minimum flow rate that cover the tips of the patches to the one that the pump capability allows. For each subsequent run, the discharge was increased so that the level ascended about 5 mm at a time. Moreover, each configuration has been studied with two bed slopes: 1:500 and 1:1000.

Quasi-steady uniform flow condition is verified in the following way: water depths H in the ten cross sections X-Si (i = 1÷10) where rules are placed are collected by reading the value from the rules themselves, and water surface levels h in sections MTi (i = 1÷10), from the piezometers in the board, are collected too. The current bed slope must not exceed more than 3% the desired bed slope.

By linear interpolation of water surface level values, we obtain the coefficients a and b of the straight line (equation: $y = a \cdot x + b$). Since piezometric intakes are not exactly in the same position of the rules, h were corrected using the linear relationship just found and the running distance of the rules. We obtain the adjusted values, called h'. The current bed slope S_b is equal to the a coefficient of the best fit straight line through the values of the water depth minus the corrected water surface levels for each cross section. The error is calculated by using Eq. 36:

$$E\% = \frac{S_{b,desired} - S_{b,current}}{S_{b,desired}} \cdot 100 \tag{36}$$

An example of graphic calculation of the current bed slope is shown in Fig. 36; it is taken from the preliminary experiments on fastener-binder layer resistance. In this case, with $Q = 1.51$ l/s, the desired slope was 1:1000 and the current slope was 1: 977.77. The error was thus 2.22%.

When all these steps have been completed, and quasi-steady uniform flow condition rules in the flume, the hydraulic parameters can be finally collected. For every run the following data are taken:

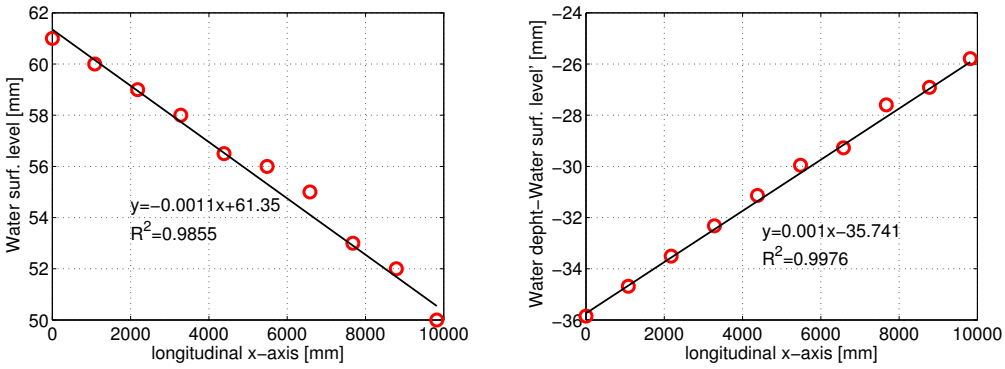

(a) (b)

Figure 36: Relationships (a) $h = F(x)$; (b) $H - h' = F(x)$; for calculating the current bed slope.

1. water depth at the ten cross sections with rules;
2. deflected canopy height at the ten cross sections with rules, due to oscillating movements it has been taken an average position of the tips;
3. water surface level at the piezometers in the board;
4. twelve values of flow rate from the flow meters, one every 10 seconds.

In Table 7 there is an example of the sheets where data were saved. Every run has a specific identifier name (e.g. "$EP100\_B10\_A\_Sb1000\_26Jun2014$" where $EP100$ = easy plant 100% density; $B10$ = blockage factor 10%; A = aligned configuration (otherwise S = staggered configuration); $Sb1000$ = bed slope 1:1000 and $26Jun2014$ = date).

Running distance				0	1084	2179	3282	4383	5482	6579	7675	8776	9820	
Date-Run ID	Q [l/s]	Channel slope [1:]	WD	X-S1	X-S2	X-S3	X-S4	X-S5	X-S6	X-S7	X-S8	X-S9	X-S10	Average [mm]
...	...	...		...	...	...	...	...	...	...	...	...	...	...

(a) *Water depths sheet.*

Running distance				0	1084	2181	3283	4387	5487	6582	7679	8789	9821		
Date-Run ID	Q [l/s]	Channel slope [1:]	WSL	MT1	MT2	MT3	MT4	MT5	MT6	MT7	MT8	MT9	MT10	a	b
...	...	...		...	...	...	...	...	...	...	...	...	...	...	...

(b) *Water surface levels sheet.*

Running distance				0	1084	2179	3282	4383	5482	6579	7675	8776	9820	
Date-Run ID	Q [l/s]	Channel slope [1:]	h_v	h_v 1	h_v 2	h_v 3	h_v 4	h_v 5	h_v 6	h_v 7	h_v 8	h_v 9	h_v 10	Average h_v
...	...	...		...	...	...	...	...	...	...	...	...	...	...

(c) *Canopy height sheet.*

Date-Run ID	Q [l/s]	1	2	3	4	5	6	7	8	9	10	11	12	Average Q
...		...	...	...	...	...	...	...	...	...	...	...	...	...

(d) *Flow rate sheet.*

Table 7: Examples of Excel worksheets to collect and analyse data.

9 CALCULATION OF HYDRAULIC PARAMETERS

The data collected following the protocol of measures (see the experimental protocol in Section 8.3) have been used for the calculation of the main hydraulic parameters. In this chapter is first described how main hydraulic parameters were calculated. Then, how they were used to calculate traditional formulas that describe the channel roughness. These formulas were first derived for pipes, but they are also used for describing resistance in channels. All data collected and all hydraulic parameters calculated during the experiments are summarized in tables in Appendix B.

9.1 MAIN HYDRAULIC PARAMETERS

9.1.1 *Mean water depth and mean deflected canopy height*

The average water depth $\overline{H}$ and the average deflected canopy height $\overline{h_v}$ were calculated using these relationships:

$$\overline{H} = \frac{\sum_{i=1}^{10} Hi}{10} \quad [mm] \tag{37}$$

$$\overline{h_v} = \frac{\sum_{i=1}^{10} h_v i}{10} \quad [mm] \tag{38}$$

where Hi is the measured water depth at the X-Si cross section and $h_v i$ is the deflected canopy height at the X-Si cross section.

9.1.2 *Energy slope*

In a laboratory flume it is difficult to maintain the steady uniform flow conditions, such as constant water depth along the length of the flume. For a steady uniform flow the energy slope S_e is equal to the bed slope S_b, but in the performed experiments the flow is at most quasi-uniform, and this assumption would result in errors. The energy slope was thus calculated using the momentum equation 39:

$$-S_e = \frac{\partial E}{\partial x} \tag{39}$$

where S_e = energy slope, E = energy, and x = position on the longitudinal x-axis. The energy E can be expressed by Eq. 40:

$$E = H + \frac{U^2}{2g} + z \tag{40}$$

where H = water depth, U = averaged cross-sectional velocity, g = acceleration due to gravity, and z = height above the reference plane.

By substituting Eq. 40 in Eq. 39, and considering that $\partial z/\partial x = -S_b$, where S_b is the bed slope, we get:

$$-S_e = \frac{\partial H}{\partial x} + \frac{\partial}{\partial x}\left(\frac{U^2}{2g}\right) + \frac{\partial z}{\partial x} = \frac{\partial H}{\partial x} + \frac{\partial U}{\partial x}\cdot\frac{\partial}{\partial U}\left(\frac{U^2}{2g}\right) - S_b \tag{41}$$

$$-S_e = \frac{U}{g}\frac{\partial U}{\partial x} + \frac{\partial H}{\partial x} - S_b \tag{42}$$

The averaged cross-sectional velocity U can be express as $U = Q/(bH)$ where Q = flow rate, and b = channel width. By substituting this term into the term $U/g \cdot \partial U/\partial x$, it is possible to obtain the final equation that has been used to calculate the energy slope (Eq. 43):

$$-S_e = \frac{Q^2}{gb^2H}\frac{\partial(\frac{1}{H})}{\partial x} + \frac{\partial H}{\partial x} - S_b = \frac{Q^2}{gb^2H}\frac{\partial(\frac{1}{H})}{\partial x} + \frac{\partial h}{\partial x} \tag{43}$$

The component $\partial h/\partial x$ was graphically calculated as the slope of the interpolation line of the water surface levels as a function of the running distance x. The term $\partial(1/H)/\partial x$ was graphically calculated as the slope of the interpolation line of the reciprocal of the water depths as a function of the running distance x.

In Fig. 37 there is an example taken from the preliminary experiments on velcro resistance. In this case, with $Q = 1.51$ l/s, the desired slope was 1:1000, the current bed slope was 1:977.77 (error 2.22%) and the energy slope was 1:967.77.

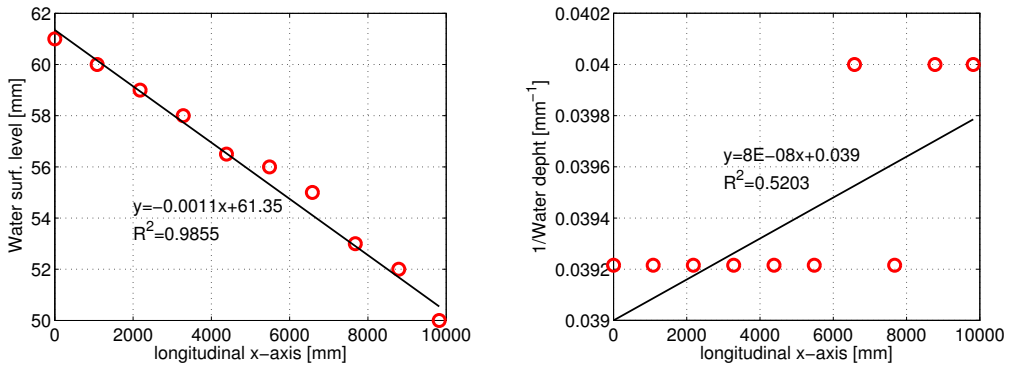

(a) (b)

Figure 37: Relationships (a) $h = F(x)$; (b) $1/H = F(x)$; for calculating the energy slope.

9.1.3 *Reynolds number*

The Reynolds number is a dimensionless parameter that can be defined as the ratio of the inertial forces to viscous or friction forces, and consequently quantifies

the relative importance of these two types of forces for given flow conditions. If interpreted as the ratio of twice the dynamic pressure and the shearing stress, it can be expressed as:

$$R_e = \frac{UL}{\nu} \tag{44}$$

Where U is the velocity based on the actual cross section area, L = characteristic length, and ν = kinematic viscosity $[m^2/s]$. The average water depth H was chosen as the representative length, and being U the average velocity, the Reynolds number was calculated as:

$$R_e = \frac{UH}{\nu} \tag{45}$$

It is used to characterize different flow regimes: laminar, transient or turbulent. Laminar flow occurs at low Reynolds numbers, where viscous forces are dominant, and is characterized by smooth, constant fluid motion. Turbulent flow occurs at high Reynolds numbers and is dominated by inertial forces, which tend to produce vortices and other flow instabilities. The flow is:

- *laminar* when $R_e < 2000$
- *transient* when $2000 > R_e < 10000$
- *turbulent* when $R_e > 10000$

9.1.4 *Froude number*

The Froude number is a dimensionless number and it is defined using the following equation:

$$F_r = \frac{U}{\sqrt{gH}} \tag{46}$$

So defined, it is equal to half of the ratio between the kinetic energy $v^2/2g$ and the energy of pressure and position, that is way it is also called *kinetic index*. It represents the ratio between the inertia forces and the weight force. It is a good parameter to characterize the energy state of motion: motions slow or subcritical ($H > H_c$) are qualified with $F_r < 1$ and motions rapid or supercritical ($H < H_c$) with $F_r > 1$. If $F_r = 1$ there are critical conditions.

9.1.5 *Shear velocity and shear stress*

The shear velocity, also known as friction velocity, is a form by which a shear stress may be re-written in units of velocity. Shear velocity is used to describe shear-related motion in moving fluids. In open channel flows with no vegetation or bed material, it is defined as following:

$$u_* = \sqrt{\frac{\tau}{\rho}} \tag{47}$$

where τ is the shear stress and ρ is the fluid density. It has the dimensions of a velocity.

The shear stress can be expressed as:

$$\tau = \gamma R S_e \tag{48}$$

where γ = specific weight of the water, R = hydraulic radius, and S_e = energy slope. Following Eq. 48, a first approach to express the shear velocity is using Eq. 49:

$$u_{*1,R} = \sqrt{gRS_e} \tag{49}$$

Of particular interest is the case of wide channel ($b \gg H$), which corresponds to the motion of a two-dimensional flow. If b is the width of the channel and H the flow depth, the hydraulic radius can be expressed as:

$$R = \frac{bH}{b+2H} = \frac{H}{(1+2\frac{H}{b})} \tag{50}$$

So, if $b \to \infty$ then $R \to H$ and the hydraulic radius R can be replaced with the water depth H in Eq. 49, getting:

$$u_{*1,H} = \sqrt{gHS_e} \tag{51}$$

Using the hydraulic radius R ($u_{*,R}$, Eq. 49) we obtain the minimum possible value of the shear velocity because we assume that the resistance of the walls of the flume and of the bottom of the channel are equal. Using the water depth ($u_{*,H}$, Eq. 51) we get the maximum possible value of the shear velocity because we assume that the effects of the walls of the channel are negligible.

Nikora et al. [36] proposed to take into account the vegetation porosity to calculate the shear velocity in open vegetated channels. Following this second approach, the shear velocity can be expressed using Eq. 52:

$$u_{*2} = \sqrt{gS_e(h_1 + \Phi h_v)} \tag{52}$$

where $h_1 = H - h_v$ and $\Phi = V_f/V_c$ = vegetation porosity, the ratio between the volume of fluid within the canopy volume, V_f, and the total canopy volume V_c which includes both the plant volume and the water volume within the canopy.

Both the two approaches to define the shear velocity, u_{*1} and u_{*2}, have been explored. Fig. 38 shows the comparison between the shear velocities calculated using the two different approaches. In Fig. 38 (a) values obtained with Eq. 49 are compared to those obtained with Nikora et al.'s equation [36], while in Fig. 38 (b)

values obtained with Eq. 51 are compared to those obtained with Nikora et al.'s equation [36].

It is evident from Fig. 38 (b) that the difference in the shear velocity values $u_{*1,H}$ and u_{*2} is negligible , as all the points are close to the $y = x$ line (perfect fit). The difference is not negligible, and the error increases as the shear velocity increases, if we compare $u_{*1,R}$ with u_{*2} (or equivalently $u_{*1,H}$ for what said before). $u_{*1,R}$ values are underestimated. This is reasonable since the walls of the channel (glass) and the bed (fastener-binder system and vegetation) have very different characteristics. The conclusion is that the effects of the walls of the channel on resistance are negligible if compared to the effects of the bed, which is confirmed by the good fit obtained between $u_{*1,H}$ and the values calculated with Nikora et al.'s equation [36]. Thus, values of shear velocity calculated with Eq. 51 were used to calculate the flow resistance parameters.

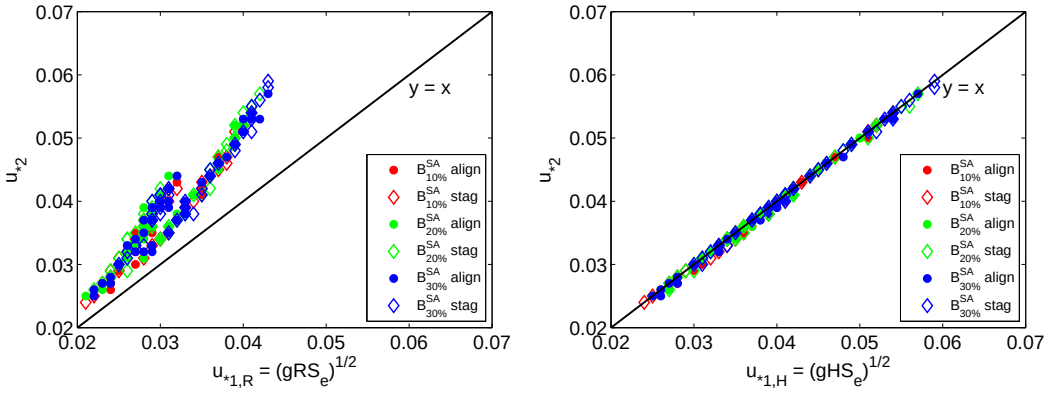

(a) (b)

Figure 38: Comparison between shear velocity u_{*1} and Nikora et al.'s u_{*2} [36].

9.2 FLOW RESISTANCE PARAMETERS

9.2.1 *Darcy-Weisbach friction factor*

The Darcy–Weisbach equation originally relates the head loss due to friction along a given length of pipe to the average velocity of the fluid flow. The equation is named after the combination of Julius Weisbach's formula (1845) and Henry Darcy's equation (1858):

$$j = \frac{fU^2}{2gD} \tag{53}$$

where $j =$ head loss, $D =$ pipe diameter, and $f =$ friction factor. The Darcy–Weisbach equation contains a dimensionless friction factor f, called the Darcy–Weisbach friction factor or Moody friction factor:

$$f = 8\left(\frac{u^*}{U}\right)^2 \tag{54}$$

The friction factor is not a constant and depends on the parameters of the pipe and the velocity of the fluid flow. It can be evaluated for given conditions by the use of various empirical or theoretical relations, or it can be obtained from published charts (Moody diagrams).

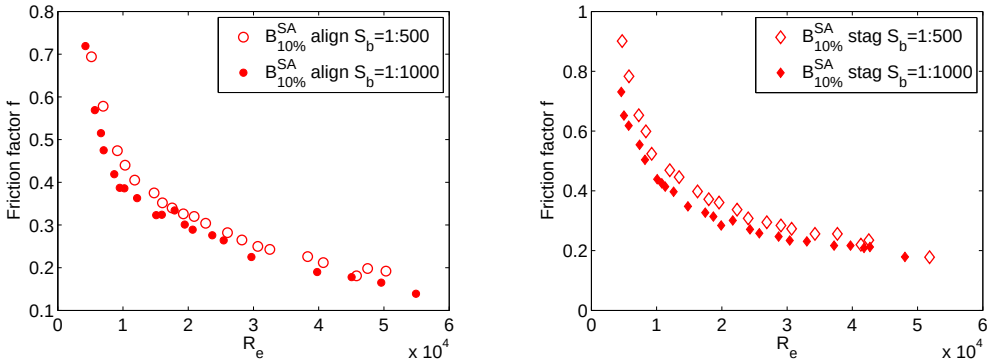

Figure 39: Relationships Darcy-Weisbach's friction factor $f = F(R_e)$ for $B^{SA} = 10\%$.

9.2.2 *Chezy coefficient*

Chezy formula is a conventional approach for describing the roughness of the bottom and side walls is steady open channel flow in turbulent conditions. The formula was established by the engineer Antoine Chézy (1769):

$$C = \frac{U}{\sqrt{RS_e}} \tag{55}$$

where U = average velocity, S_e = energy slope, C = Chézy coefficient, and R = hydraulic radius. A higher value of the Chézy coefficient means a smoother boundary.

9.2.3 *Manning coefficient*

A roughness description commonly used is the uniform-flow formula for open-channel flow derived by the engineer Manning (1889):

$$n = \frac{R^{2/3} S_e^{1/2}}{U} \tag{56}$$

The equations mentioned above are related in the following way:

$$\sqrt{\frac{f}{8}} = \frac{n\sqrt{g}}{R^{1/6}} = \frac{\sqrt{g}}{C} = \frac{\sqrt{gRS}}{U} \tag{57}$$

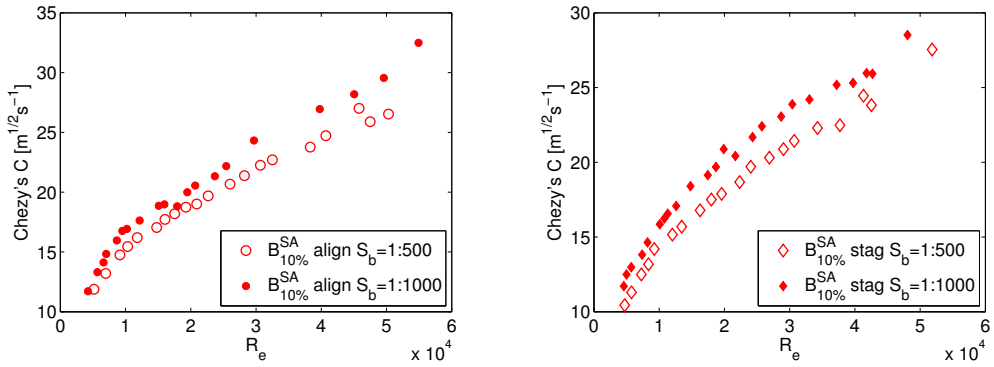

Figure 40: Relationships Chezy $C = F(R_e)$ for $B^{SA} = 10\%$.

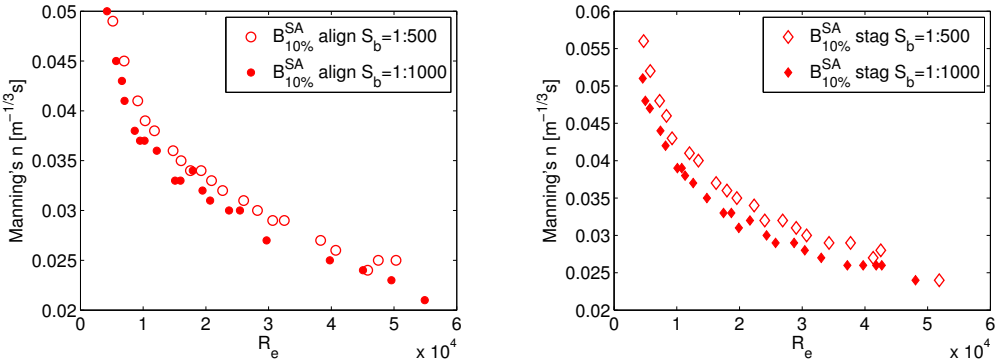

Figure 41: Relationships Manning $n = F(R_e)$ for $B^{SA} = 10\%$.

In the case of vegetated channels, these roughness parameters can be used for high submergence ratios, so that the vegetation can be approximated by a constant roughness coefficient.

Fig. 72, 73 and 74 show the resistance parameters as a function of the Reynolds number for the experienced runs with $B^{SA} = 10\%$. The complete list of graphs, in which the resistance coefficients are plotted against the Reynolds number, is in Appendix C. The two different bed slopes investigated (1:500 and 1:1000) gave similar results. Thus, in the following analysis of data no distinction has been made between them.

10 RESULTS

In this chapter the results obtained using the collected data from the laboratory tests are shown. The first part of the chapter includes a complete analysis of the hydraulic resistance due to the presence of vegetation patches. Attention is mainly focused on hydraulic resistance as a function of the number and the configuration of the patches. In the second part, the hydraulic resistance models described in Section 3.2 are studied and assessed.

The symbols used in the following plots are included in Fig. 42. Every surface area blockage factor is marked with a specific colour: $B^{SA} = 10\%$ = 'red', $B^{SA} = 20\%$ = 'green' and $B^{SA} = 30\%$ = 'blue'. All configurations with aligned patches are labelled with a full marker, while those with staggered patches are labelled with an empty marker.

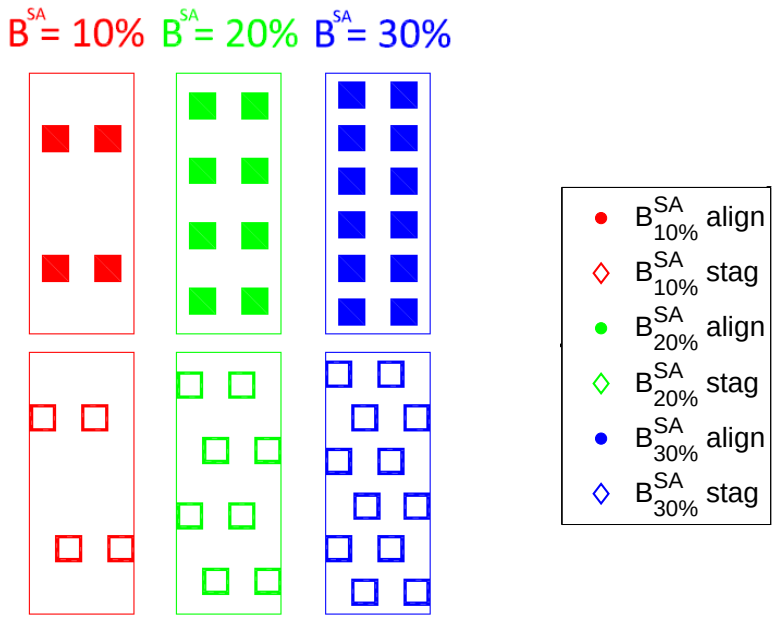

Figure 42: Patch configurations and symbols used for different scenarios.

In Table 8 a summary of the main hydraulic parameters collected during the experiments is given. As mentioned in Section 9.2 no distinction has been made between the two bed slopes (i.e. 1:500 and 1:1000) investigated for each configuration, since the bed slope did not influence the hydraulic resistance.

	$B^{SA} = 10\%$		$B^{SA} = 20\%$		$B^{SA} = 30\%$	
Configuration:	aligned	staggered	aligned	staggered	aligned	staggered
H [cm]	$5 \div 17$	$6 \div 17$	$5 \div 19$	$5.5 \div 19$	$5 \div 18$	$7 \div 18$
Q [l/s]	$1.7 \div 22$	$1.8 \div 20$	$1.6 \div 21$	$1.7 \div 21$	$2 \div 21$	$2 \div 21$
U [m/s]	$0.1 \div 0.3$	$0.08 \div 0.35$	$0.08 \div 0.3$	$0.08 \div 0.2$	$0.09 \div 0.3$	$0.08 \div 0.2$
u_* [m/s]	$0.03 \div 0.05$	$0.03 \div 0.04$	$0.04 \div 0.05$	$0.03 \div 0.06$	$0.03 \div 0.05$	$0.03 \div 0.06$
R_e $[\cdot 10^4]$	$0.4 \div 5.5$	$0.4 \div 5$	$0.4 \div 5$	$0.4 \div 5$	$0.5 \div 5.5$	$0.5 \div 5.5$
$C[m^{1/2}s^{-1}]$	$12 \div 30$	$12 \div 30$	$10 \div 30$	$8 \div 23$	$10 \div 30$	$8 \div 22$
f	$0.2 \div 0.7$	$0.2 \div 0.9$	$0.2 \div 0.9$	$0.3 \div 1.5$	$0.2 \div 0.9$	$0.3 \div 18$
$n[m^{-1/3}s]$	$0.02 \div 0.05$	$0.02 \div 0.05$	$0.02 \div 0.06$	$0.03 \div 0.07$	$0.02 \div 0.06$	$0.03 \div 0.08$
$K_s[m^{1/3}s^{-1}]$	$20 \div 50$	$20 \div 42$	$17 \div 40$	$14 \div 34$	$20 \div 40$	$14 \div 34$

Table 8: Range of values of the hydraulic parameters.

10.1 FLOW RESISTANCE PARAMETERS AS A FUNCTION OF REYNOLDS NUMBER

The main hydraulic resistance parameters Darcy-Weisbach's f, Chezy's C and Manning's n have been plotted as a function of the Reynolds number Re. These plots are shown respectively in Fig. 43, 45 and 44.

Fig. 43 shows the relationships $f = F(Re)$ found in the preliminary experiments with the smooth bed and with the fastener bed. A summary table of the averaged flow resistance parameters in the cases of smooth bed and fastener layer bed is given in Table 9.

	Manning n	Weisbach f	Chezy C	Gauckler-Strickler K_s
smooth	0.010	0.025	60	98
fastener	0.015	0.050	40	67

Table 9: Averaged values of the hydraulic parameters with smooth bed and fastener layer on the bed.

Comparing the friction factor due to the vegetation with that one due to the fastener layer, Fig. 43 shows that the first is much greater than the other. Fig. 43 shows also that friction factors due to the presence of the fastener bed and the smooth bed collapse in the same trend. Thus, the mushroom fastener that has been used to attach the patches of vegetation on the bottom can be regarded as a smooth surface.

Fig. 43, 44 and 45 show two different trends. Configurations aligned and staggered with $B^{SA} = 10\%$ experienced about the same resistance, while configurations with $B^{SA} = 20$ and 30% experienced two different hydraulic resistances, which are greater for the staggered configurations.

The flow resistance parameters for configurations $B^{SA} = 10\%$ *aligned*, $B^{SA} = 10\%$ *staggered*, $B^{SA} = 20\%$ *aligned* and $B^{SA} = 30\%$ *aligned* have the same

trend, and the collected points are close. Configurations $B^{SA} = 20\%$ *staggered* and $B^{SA} = 30\%$ *staggered* are also quite close, but the resistance is much greater.

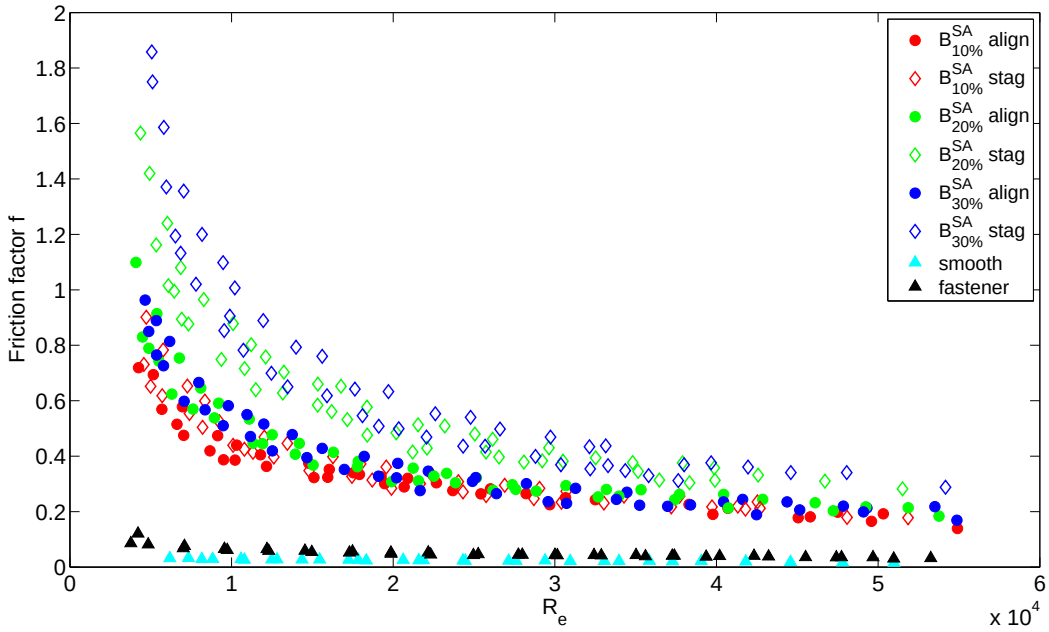

Figure 43: Relationship Darcy-Weisbach's friction factor $f = F(Re)$.

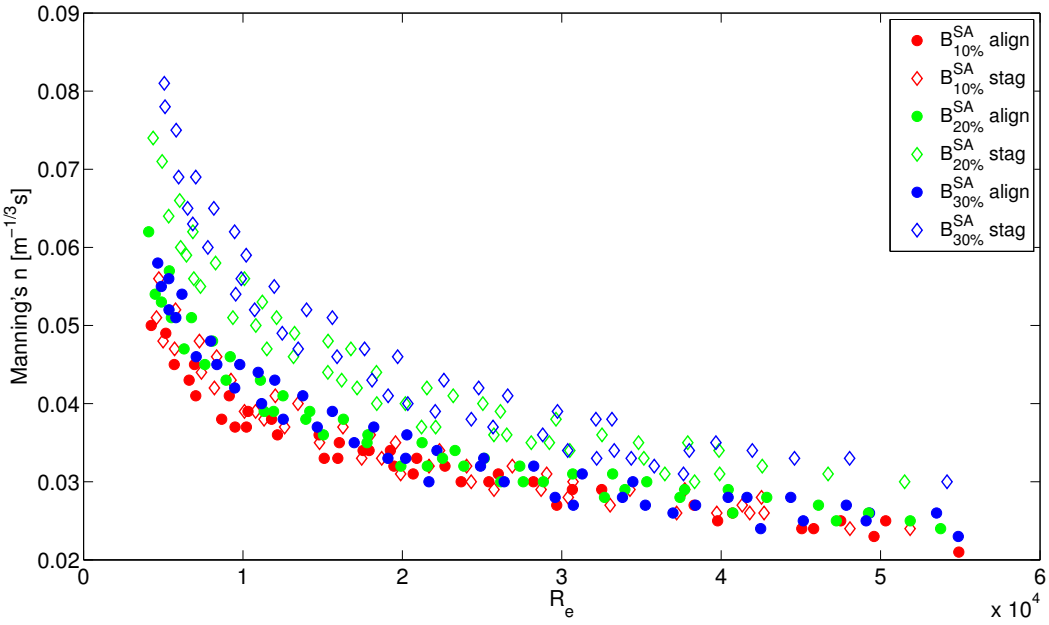

Figure 44: Relationship Manning's $n = F(Re)$.

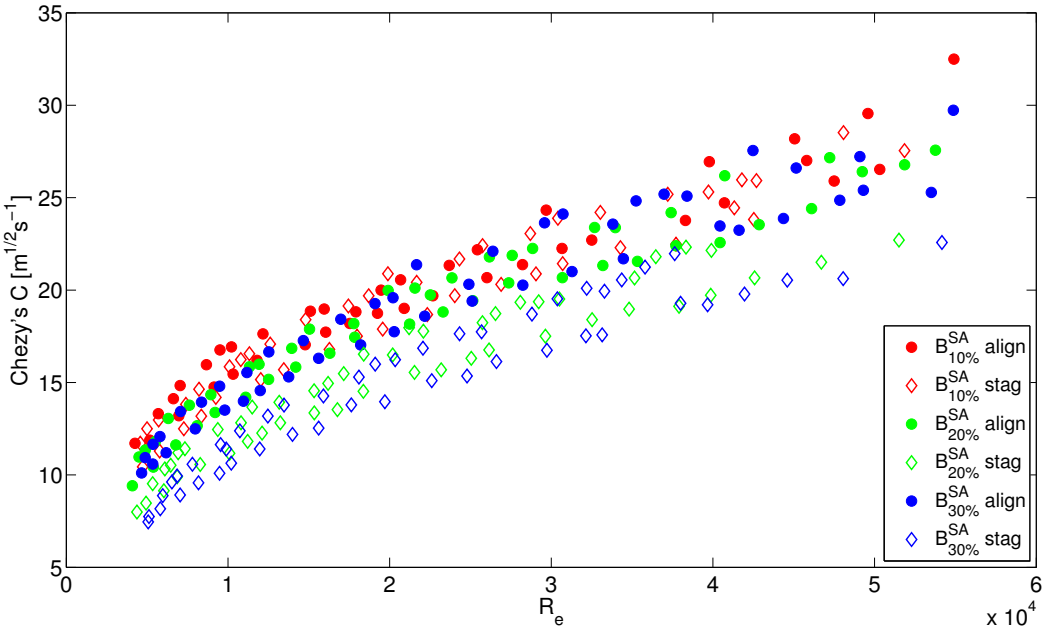

Figure 45: Relationship Chezy's $C = F(Re)$.

10.2 FLOW RESISTANCE PARAMETERS AS A FUNCTION OF RELATIVE ROUGHNESS

In Fig. 46, 47 and 48 Darcy-Weisbach's f, Manning's n and Chezy's C are shown as a function of the relative roughness.

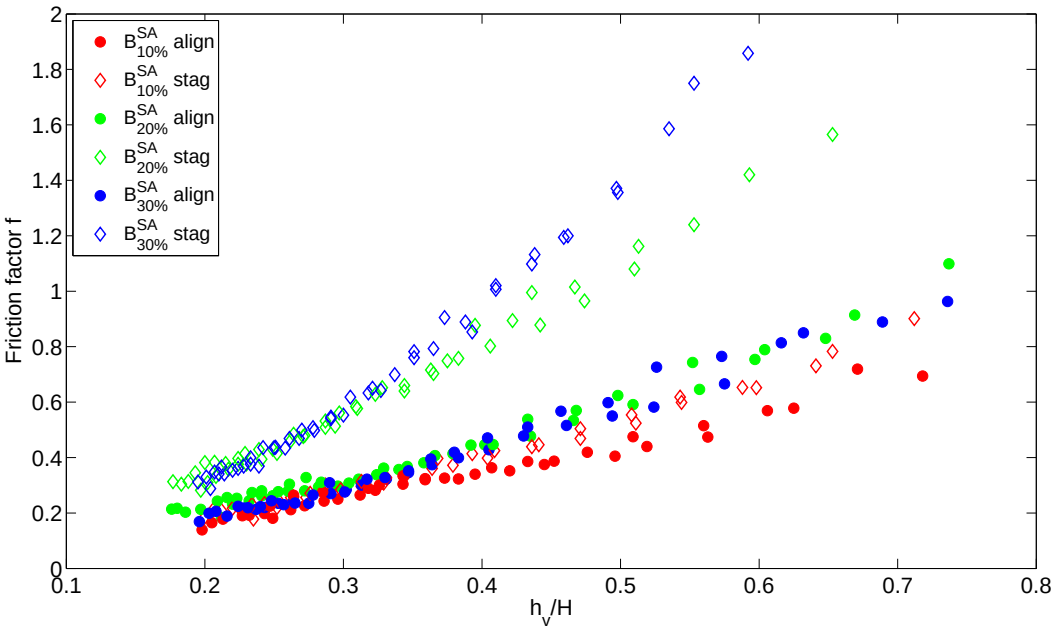

Figure 46: Relationship Darcy-Weisbach's friction factor $f = F(h_v/H)$.

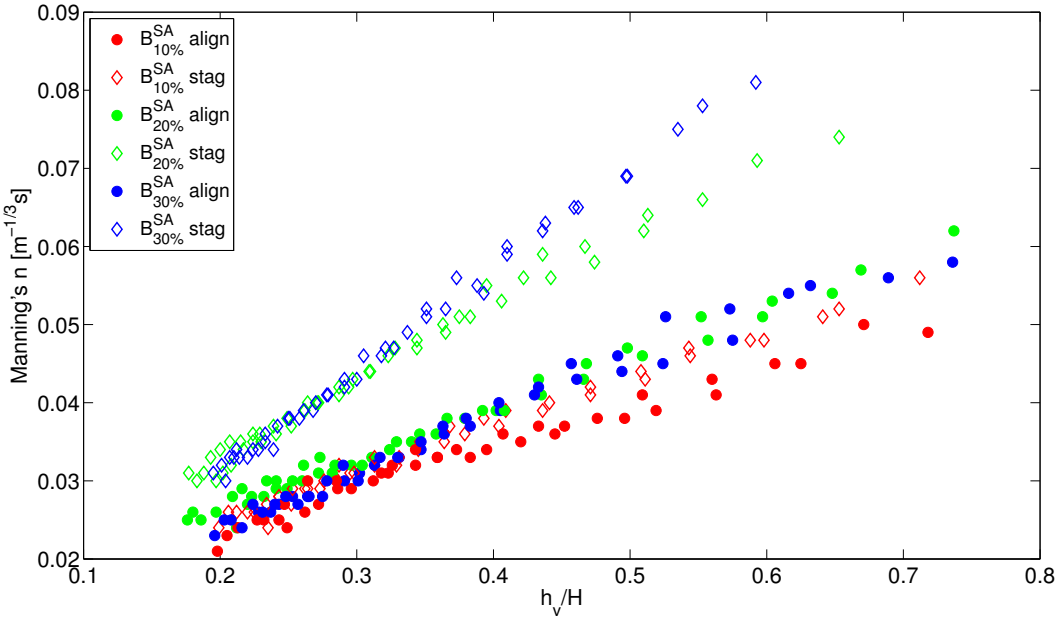

Figure 47: Relationship Manning's $n = F(h_v/H)$.

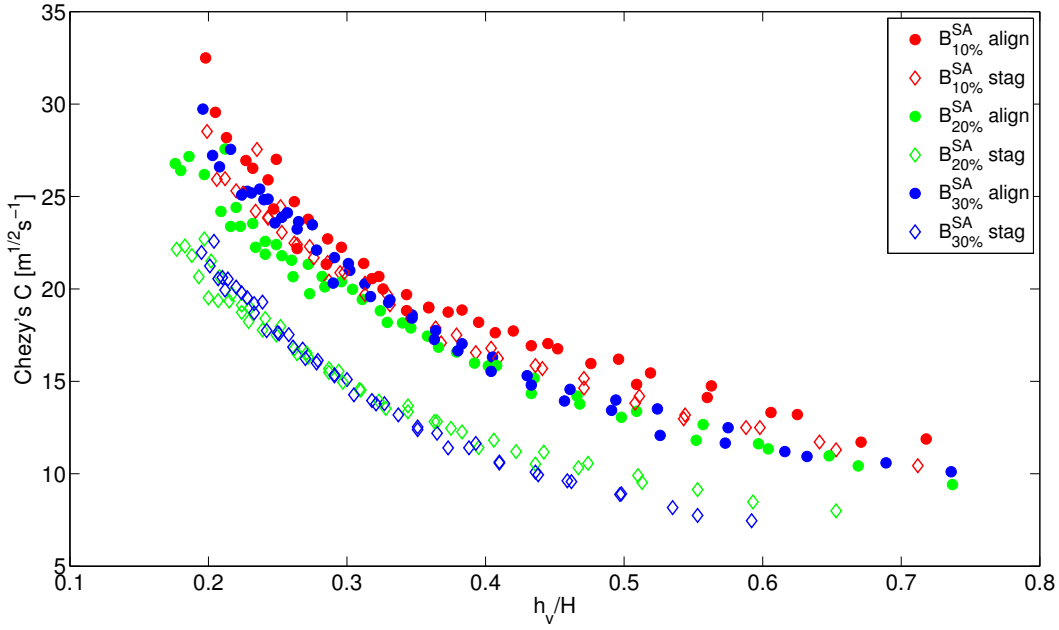

Figure 48: Relationship Chezy's $C = F(h_v/H)$.

Kouwen [24] found that for wide channel having artificial flexible roughness attached to the bed, the relative submergence H/h_v could be considered as a main hydraulic parameter. The relative roughness h_v/H has been chosen as key physical parameter of vegetation influencing the hydraulic resistance. Fig. 46, 47 and 48 show two main trend lines. They show that configurations aligned and staggered with $B^{SA} = 10\%$ experience about the same resistance, while configurations with

$B^{SA} = 20$ and 30% experience two different hydraulic resistances, which are greater for the staggered configurations.

10.3 FLOW RESISTANCE PARAMETERS AS A FUNCTION OF BLOCKAGE FACTORS

10.3.1 *Maximum cross-sectional blockage factor*

The maximum cross-sectional blockage factor considers a cross section that dissects the patch (i.e. where the vegetation area is the largest). It is the ratio between the cross-sectional area blocked by vegetation and the total cross-sectional area:

$$B^X = \frac{A_v}{A} \tag{58}$$

The ratio A_v/A was originally introduced for a bed uniformly covered by vegetation [24]. According to Nikora et al. [35], for streams with patchy vegetation, the ratio A_v/A can be interpreted as a site-averaged relative roughness, i.e. $A_v/A = (b_v h_v L)/(HbL) = (b_v h_v)/(Hb)$, where L is the length of flume, b the width, H the water depth, b_v the averaged width of the vegetation patches and h_v the averaged deflected canopy height (see Fig. 11). Since all the patches have the same shape, the averaged values in this study are equal to the values themselves: $b_v = 0.2\ m$ and $b = 0.4\ m$. The term b_v does not change as a function of the surface-area blockage factor, since the number of the patches increases along the longitudinal axis of the channel and not along the cross axis.

Darcy-Weisbach friction factor's f, Manning's n and Chezy's C have been represented as a function of the maximum cross-sectional blockage factor to determine the relationships $f = F(h_v b_v/Hb)$, $n = F(h_v b_v/Hb)$ and $C = F(h_v b_v/Hb)$.

Fig. 49 and 50 show the maximum cross-sectional blockage factor as a function of the friction factor.

A linear and an exponential fit were tested. The best fit line equations are shown in Fig. 50 and 49 respectively. Due to the different hydraulic resistance of staggered configurations with $B^{SA} = 20\%$ and 30%, two different equations were required. Exponential and linear functions provided both a good fit, with $R^2 = 0.95$ and 0.92 for the exponential equations, and $R^2 = 0.94$ and 0.91 for the linear equations.

Finally, Darcy-Weisbach's friction factor from the four fit equations, was used to calculate the ratio U/u_* and to compare it to the measured values. The value U/u_* can be obtained from the friction factor f using a simple relationship:

$$\frac{U}{u_*} = \sqrt{\frac{8}{f}} \tag{59}$$

The compared graphs are shown in Fig. 51. Both the exponential and the linear fit show good correlation between the calculated and the measured data (which is in agreement with the high value of R^2 in both cases). For configurations $B^{SA} = 10\%$ *aligned*, $B^{SA} = 10\%$ *staggered*, $B^{SA} = 20\%$ *aligned* and $B^{SA} = 30\%$ *aligned*

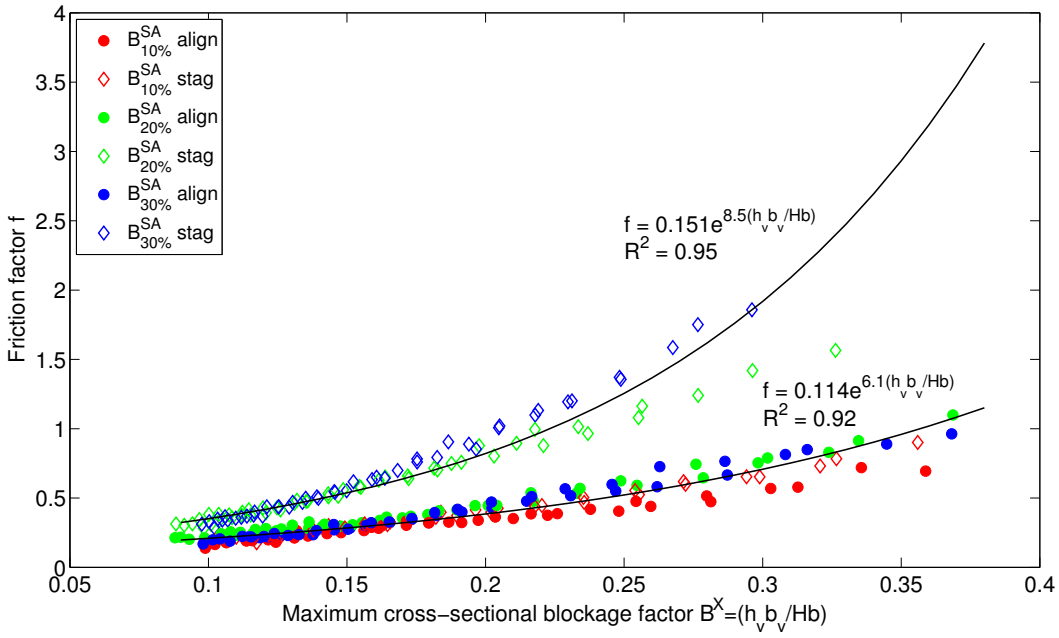

Figure 49: Relationship Darcy-Weisbach's friction factor $f = F(h_v b_v / Hb)$; exponential fit.

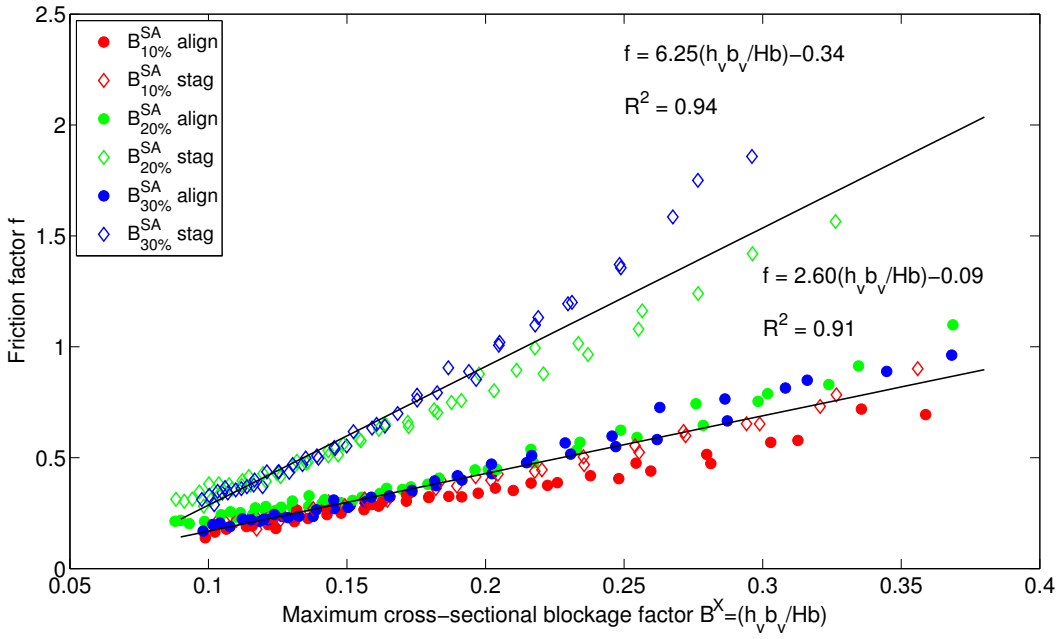

Figure 50: Relationship Darcy-Weisbach's friction factor $f = F(h_v b_v / Hb)$; linear fit.

the exponential interpolation is slightly better, while for configurations $B^{SA} = 20\%$ *staggered* and $B^{SA} = 30\%$ *staggered* the difference is smaller. For the highest flow rate, the points are not so close to the line $y = x$ (perfect fit) and this is probably due to the difficulties to create quasi-uniform steady flow conditions during the experiments. The water surface could be affected by turbulence effects, and thus data could have some errors. Moreover, the pump showed high oscillations in the

flow rate for the highest values. This can explain the scattered point on the right top of the graph.

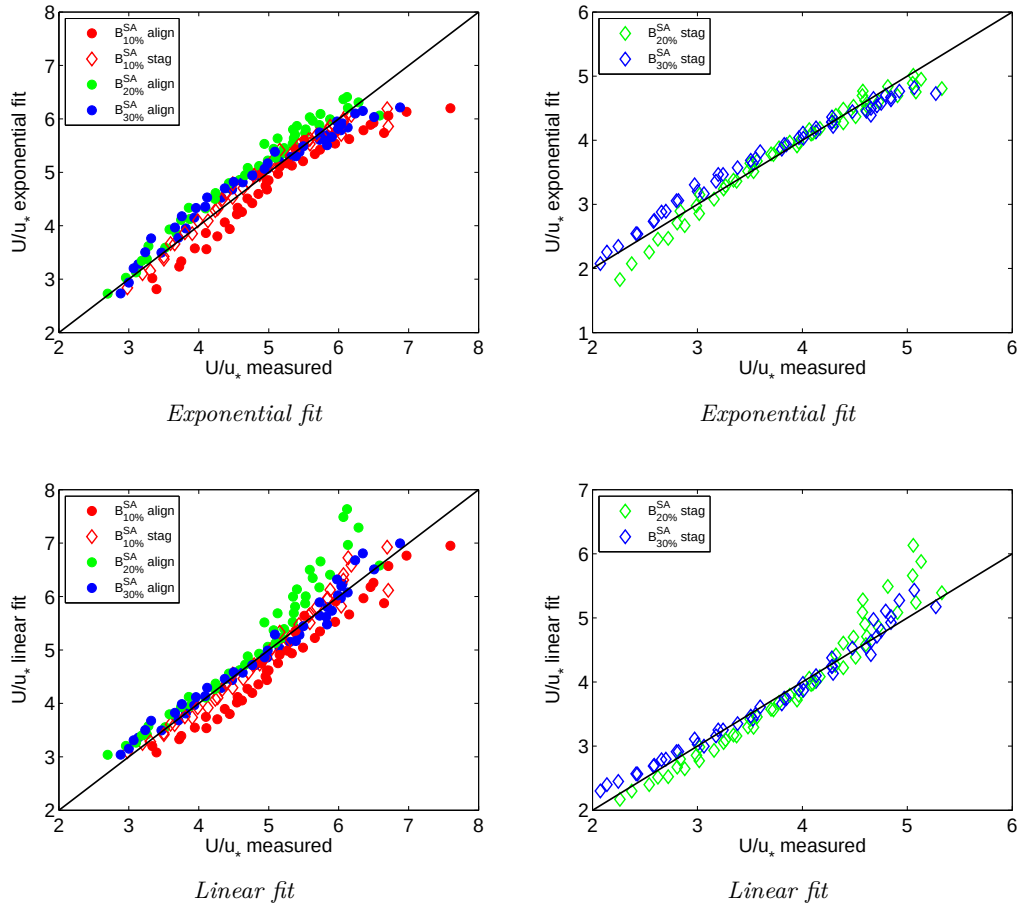

Figure 51: Comparison between measured U/u_* and calculated from $f = F(h_v b_v / Hb)$.

Fig. 52 and 53 show Manning's n as a function of the maximum cross-sectional blockage factor. As done for the friction factor, n values were interpolated using a linear and an exponential equation to find the best fit. The equations found and the R^2 values are shown in Fig. 52 and 53.

Green [5] found a theoretical relationship between the cross-sectional blockage factor and the hydraulic resistance expressed as Manning's n for channels with scattered blocks of plants. He expressed the averaged cross-sectional velocity using the following relationship:

$$U = B^X U_v + (1 - B^X) U_0 \tag{60}$$

where U_v is the mean flow velocity within the plants and U_0 is the mean flow velocity in the open channel. Substituting Eq. 60 into Manning's equation, we get:

$$n = \frac{R^{2/3} S_e^{1/2}}{B^X U_v + (1 - B^X) U_0} \tag{61}$$

Eq. 61 shows the non-linear nature of this relationship, with a dramatic increase in resistance toward a complete blockage. The aim is to verify if collected data follow this non-linear relationship.

Exponential and linear functions provided both a good fit (see Fig. 52 and 53), with $R^2 = 0.95$ and 0.92 for the two exponential equations and $R^2 = 0.97$ and 0.94 for the linear ones.

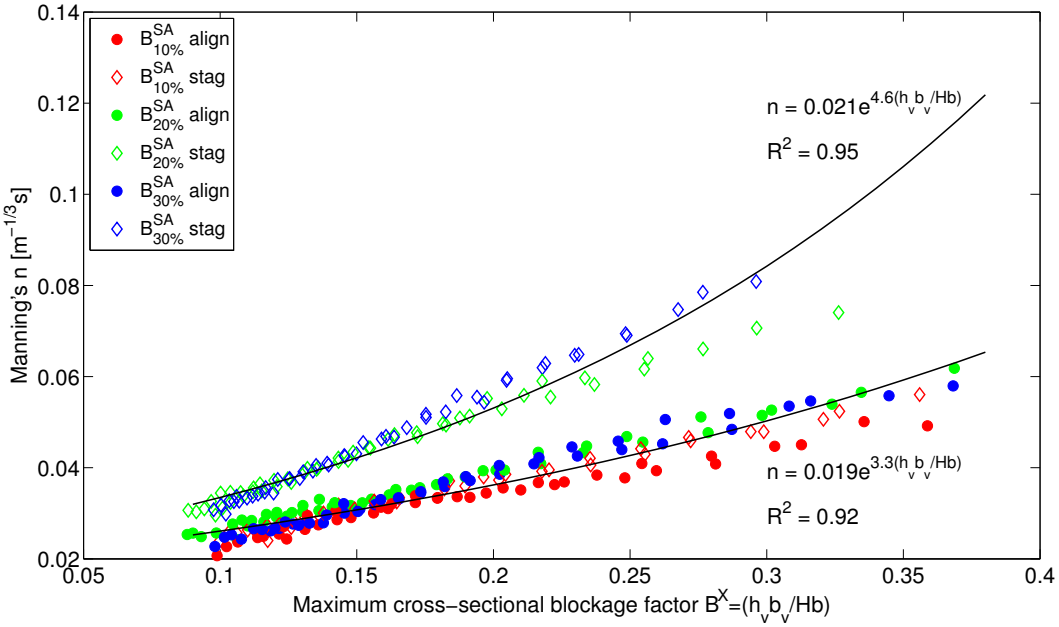

Figure 52: Relationship Manning's $n = F(h_v b_v / Hb)$; exponential fit.

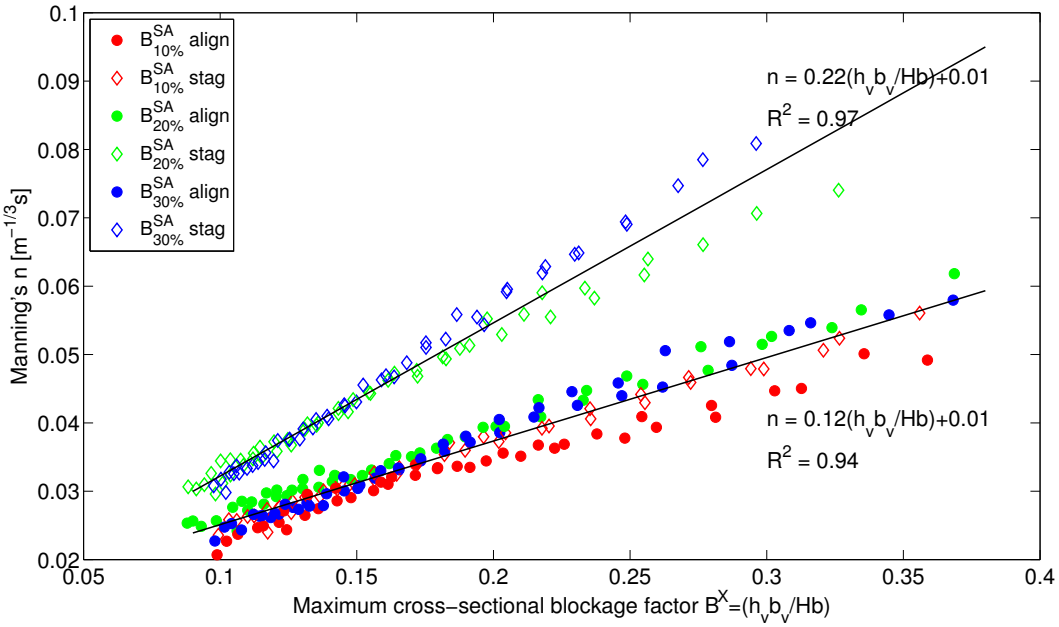

Figure 53: Relationship Manning's $n = F(h_v b_v / Hb)$; linear fit.

Fig. 54 and 55 shows Chezy's C as a function of the cross-sectional blockage factor. Data were interpolated using an exponential and a linear function. The coefficients of determination were $R^2 = 0.94 - 0.96$ for the exponential fit and $R^2 = 0.91 - 0.88$ for the linear fit.

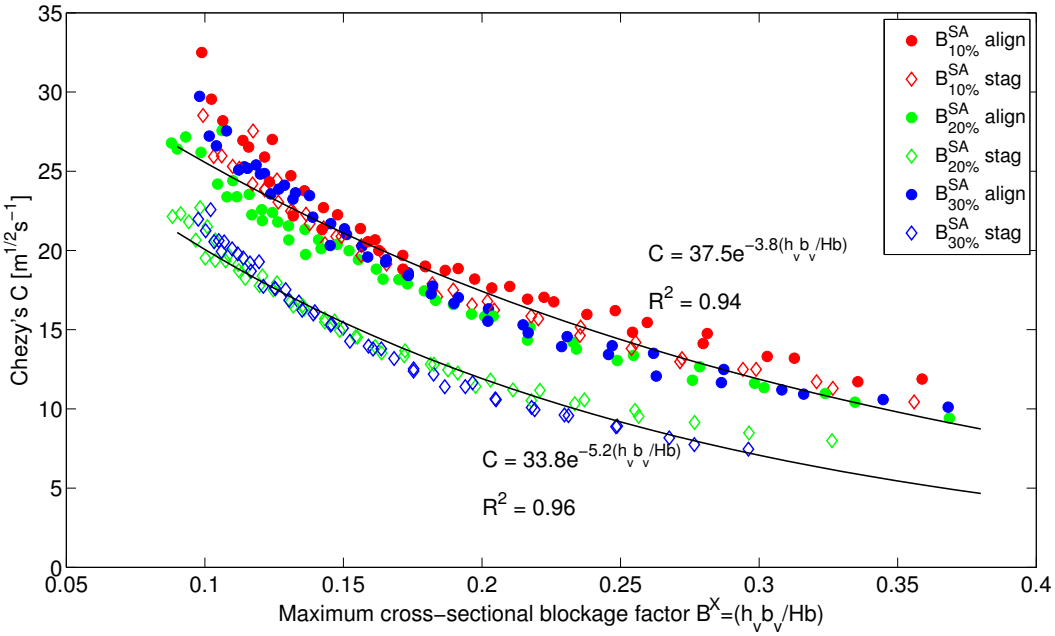

Figure 54: Relationship Chezy's $C = F(h_v b_v / Hb)$; exponential fit

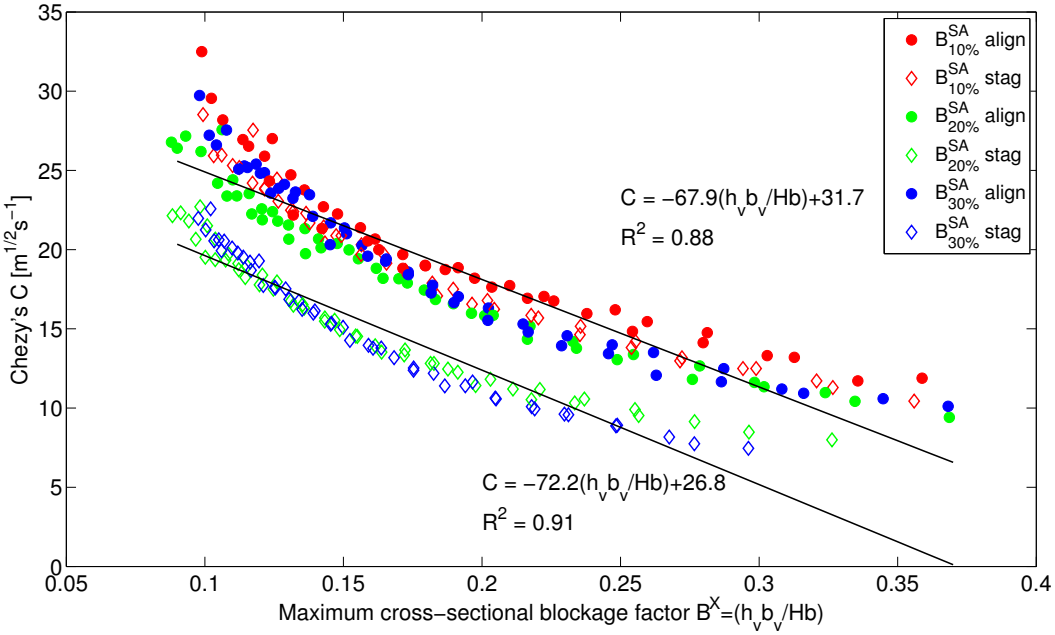

Figure 55: Relationship Chezy's $C = F(h_v b_v / Hb)$; linear fit

10.3.2 *Averaged cross-sectional blockage factor*

The cross sectional blockage factor was spatial averaged along the longitudinal axis of the channel to take into account the portions of the flume where the patches were not present. We get the *averaged cross-sectional blockage factor*.

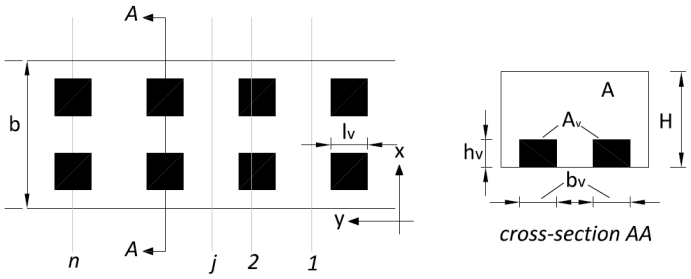

Figure 56: Averaged cross-sectional blockage factor B^{ave}.

Taking some random cross sections in the flume so that both sections with and without patches are considered, the averaged cross-sectional blockage factor (see Fig. 56) can be regarded as the average of the individual cross-sectional blockage factors:

$$B^{ave} = \frac{B^X_{,1} + B^X_{,2} + \cdots + B^X_{,n}}{n} \tag{62}$$

where:

$$B^X_{,j} = \frac{A_{v,j}}{A_j} = \frac{h_{v,,j} b_{v,j}}{H_j b_j} \qquad j = [1 \div n] \tag{63}$$

It stands to reason that in all cross sections of the channel where there is not vegetation, $B^X = 0$. By extending the sum to infinity along the total length L of the channel, and taking into account the consideration made, Eq. 62 can be rewritten as:

$$B^{ave} = \frac{h_v b_v n_x l_v n_y}{HbL} = B^{SA} \frac{h_v}{H} \tag{64}$$

in which n_x is the number of patches in the x direction and n_y is the number of patches in the y direction. All symbols are shown in Fig. 56.

The flow resistance parameters were plotted against the averaged cross-sectional blockage factor. Fig. 57, 58 and 59 show respectively the relationships $f = F(B^{ave})$, $n = F(B^{ave})$ and $C = F(B^{ave})$.

In these graphs the points are no longer overlapping, but the trend lines of the three different surface-area blockage factors are shifted. This is clear if we compare Fig. 46, 47 and 48 with Fig. 57, 58 and 59.

Since the term h_v/H is multiplied by B^{SA}, all points that correspond to the maximum surface-area blockage factor (i.e. 30%) are shifted to the right in Fig. 57, 58 and 59. Since the blockage factor is averaged on the length of the flume, configurations with $B^{SA} = 10\%$ take into account a greater number of sections in which B^X

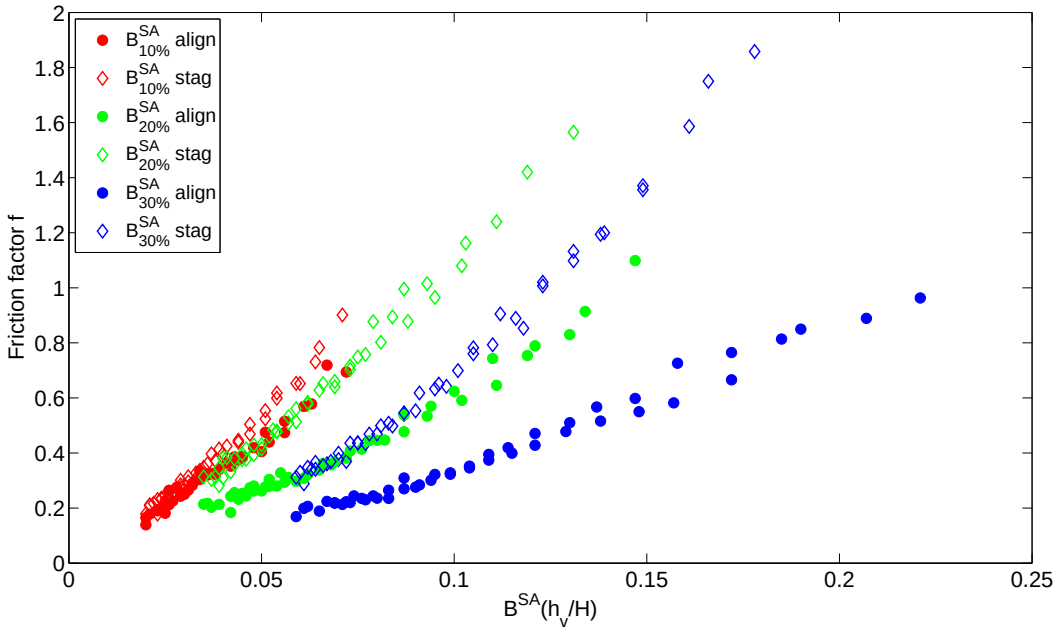

Figure 57: Relationship Darcy-Weisbach's friction factor $f = F(B^{SA}(h_v/H))$.

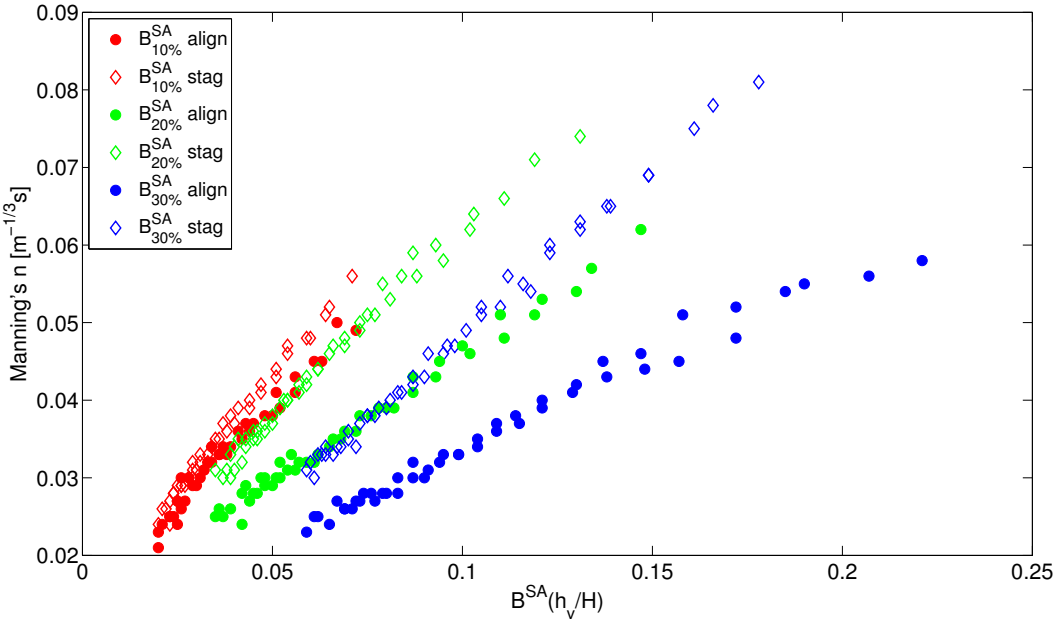

Figure 58: Relationship Manning's $n = F(B^{SA}(h_v/H))$.

is equal to zero. Thus the cross-sectional blockage factor is significantly decreased. The decrease is lower for a higher surface-area blockage factor, in which the cross sections where only fluid occurs are less due to the increased number of patches present along the longitudinal axis. The limit is when the maximum cross-sectional blockage factor is equal to the averaged cross-sectional blockage factor. It occurs when all the cross sections of the channel have the same blockage factor (i.e. two

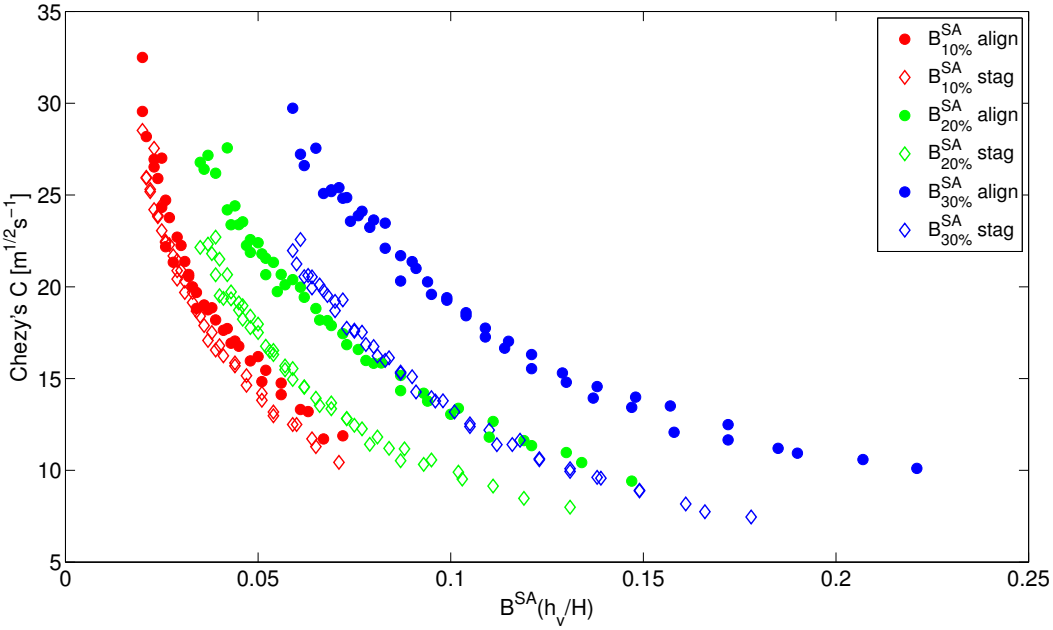

Figure 59: Relationship Chezy's $C = F(B^{SA}(h_v/H))$.

strips for the aligned configurations and attached staggered blocks for the staggered configurations).

It is interesting to distinguish data concerning the three surface-area blockage factor. Graphs are shown in Fig. 60, 61 and 62. We note that, as said before, configurations staggered and aligned with $B^{SA} = 10\%$ experienced about the same hydraulic resistance, while configurations aligned and staggered with $B^{SA} = 20\%$ and $B^{SA} = 30\%$ experienced different hydraulic resistances.

Considering the surface-area blockage factor $B^{SA} = 30\%$, the increase of resistance of the staggered configuration compared to that of the aligned configuration is slightly greater than for $B^{SA} = 20\%$.

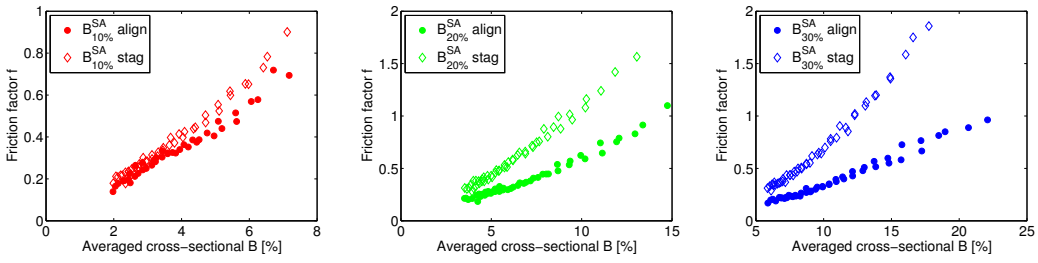

$B^{SA} = 10\%$ $B^{SA} = 20\%$ $B^{SA} = 30\%$

Figure 60: Friction factor f as a function of the averaged cross-sectional B.

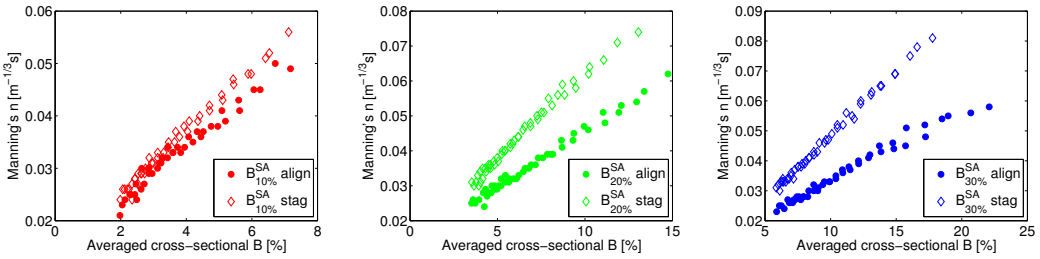

$B^{SA} = 10\%$ $B^{SA} = 20\%$ $B^{SA} = 30\%$

Figure 61: Manning's n as a function of the averaged cross-sectional B.

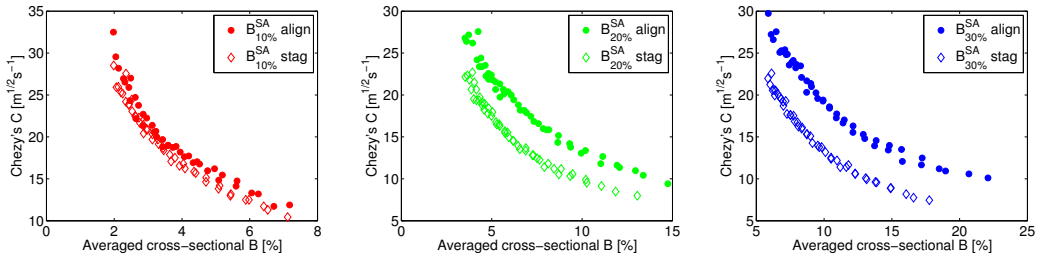

$B^{SA} = 10\%$ $B^{SA} = 20\%$ $B^{SA} = 30\%$

Figure 62: Chezy's C as a function of the averaged cross-sectional B.

10.4 ASSESSMENT OF CURRENT HYDRAULIC RESISTANCE MODELS

10.4.1 *Kouwen et al.'s logarithmic model (1969)*

The logarithmic relationship suggested by Kouwen et al. [24] is the following:

$$\frac{U}{u_*} = C_1 + C_2 ln\left(\frac{H}{h_v}\right) \tag{65}$$

where C_1 and C_2 are constants. The constant C_1 depends on the flow through the vegetation and hence is influenced by the vegetation density. The constant C_2 depends on the vegetation stiffness. For the artificial flexible vegetation experienced, Kouwen introduced two values of these coefficients, which were estimated from the least square fit to point of his collected data:

$C_1 = 0.16$ $C_2 = 2.41$

The measured values of U/u_* have been plotted against the measured $log(H/h_v)$ to see if the linear relationship suggested by Kouwen could be applied also in the case studied of patchy vegetation. They are shown in Fig. 63.

Fig. 63 demonstrates that our data closely match Kouwen et al.'s equation $U/u_* = C_1 ln(H/h_v) + C_2$. Two different equations had to be determined, one for configurations $B^{SA} = 10\%$ *aligned*, $B^{SA} = 10\%$ *staggered*, $B^{SA} = 20\%$ *aligned* and

$B^{SA} = 30\%$ *aligned*, and another for configurations $B^{SA} = 20\%$ *staggered* and $B^{SA} = 30\%$. The coefficient of determinations were respectively $R^2 = 0.92$ and $R^2 = 0.97$.

The assessed values of the coefficients of the two equations are:

$C_1 = 0.71 \qquad C_2 = 2.59$

for configurations $B^{SA} = 10\%$ *aligned*, $B^{SA} = 10\%$ *staggered*, $B^{SA} = 20\%$ *aligned* and $B^{SA} = 30\%$ *aligned*;

$C_1 = 2.00 \qquad C_2 = 2.72$

for configurations $B^{SA} = 20\%$ *staggered* and $B^{SA} = 30\%$.

The coefficients C_2 are very similar to that calibrated by Kouwen, and this is reasonable since artificial grass-like vegetation was used by Kouwen et al. [24]. Kouwen's grass was simulated by flexible elements cut out of sheets of styrene, 0.03 cm thick, 0.50 cm wide and 10 cm high.

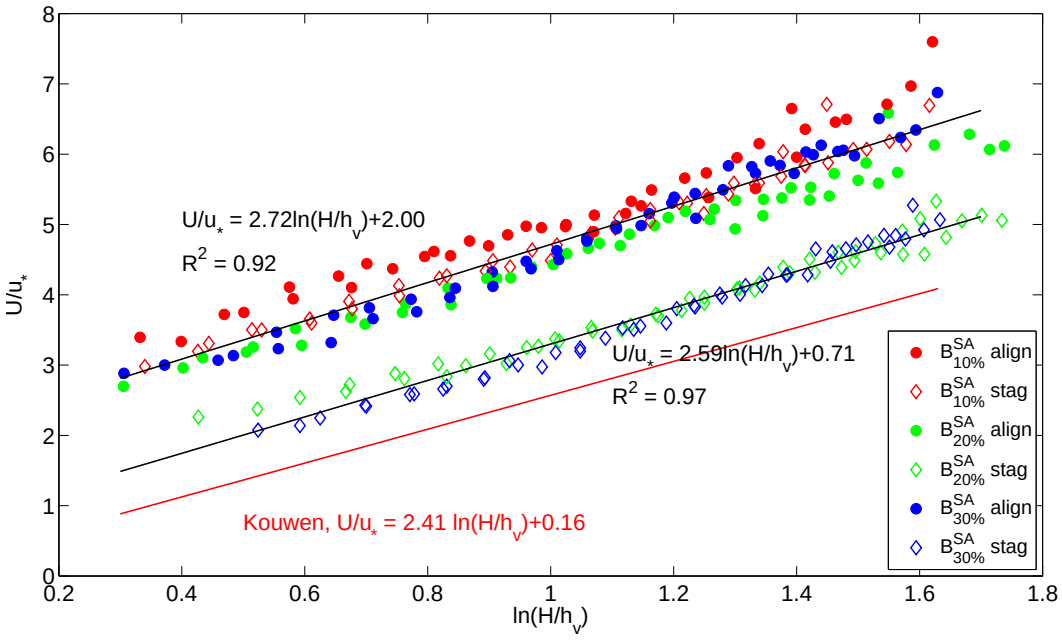

Figure 63: Application of Kouwen's hydraulic resistance model (1969); relationship $U/u_* = F(H/h_v)$.

In Fig. 64 U/u_* is plotted as a function of the site-averaged relative submergence $(Hb)/(h_v b_v)$. Since the vegetation has regular shape and the geometry is the same for all patches, the coefficients of determinations are the same of those calculated for the ratio H/h_v. The constants C_2 are +0.11 and -1.09, which are similar to those found by Nikora et al.'s [35].

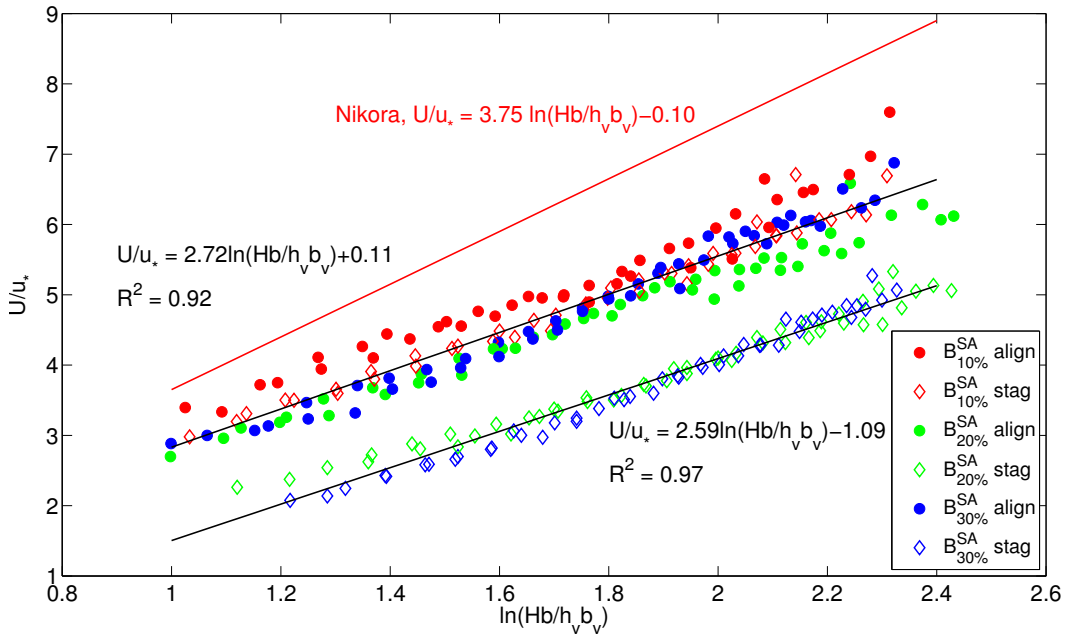

Figure 64: Application of Kouwen's hydraulic resistance model (1969); relationship $U/u_* = F(Hb/h_v b_v)$.

10.4.2 *Carollo et al.'s power function model (2005)*

Carollo, Ferro and Termini [14] introduced the following resistance law:

$$\frac{U}{u_*} = A_0(M) \cdot \left(\frac{H}{h_v}\right)^{a_1} \cdot \left(\frac{u_* h_v}{\nu}\right)^{a_2} \cdot \left(\frac{H_v}{h_v}\right)^{a_3} \tag{66}$$

where a_1, a_2, a_3 are numerical coefficients that have to be determined using the available measurements and A_0 is a function of the vegetation density M , which assumes a constant value for a given concentration. Carollo et al.'s model was applied using the coefficients proposed by the authors: $a_1 = 1.168$, $a_2 = -1.023$ and $a_3 = -0.861$. Moreover, it has been considered Eq. 66 with $a_2 = 0$ not to take into account the Reynolds number of the flow inside the vegetation layer. To determine the constant A_0, the measured values of U/u_* were plotted on the y-axis and the term on the right side of Eq. 66 (without $A_0(M)$) was plotted on the x-axis. Using a linear regression method it was possible to determine the density parameter. The calculated $A_0(M)$ was 1796.1 considering $a_2 \neq 0$ and 1.23 and 0.85 for the two best fit lines that interpolated data considering $a_2 = 0$.

The comparison between the measured and the calculated U/u_* in Fig. 65 shows a poor agreement with the line of perfect agreement for all the three cases in fact there are a lot of scattered points, particularly concerning the case with $a_2 \neq 0$. In order to correct this distortion the parameters A_0, a_1, a_2 and a_3 were recalibrated using a linear regression method. The coefficients found and the comparison between measured and calculated values of U/u_* are shown in Fig. 66. The assessed values of the coefficient a_2 are approximately equal to zero, which shows that this parameter could be neglected.

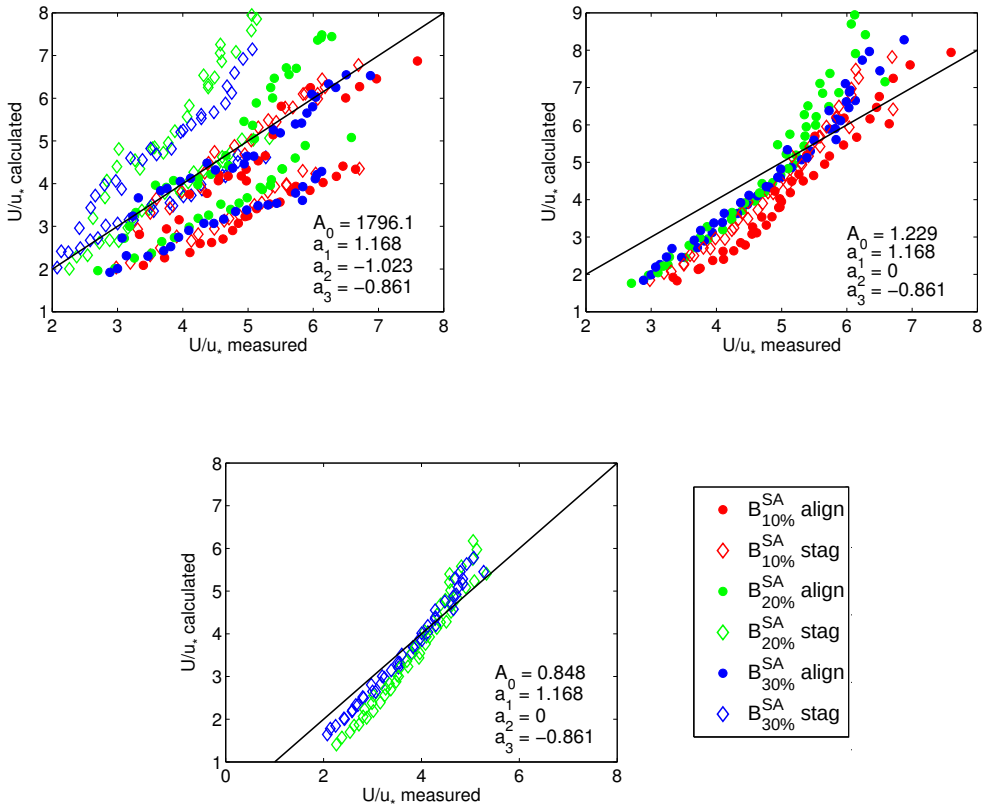

Figure 65: Comparison between measured U/u_* and obtained U/u_* from Carollo et al.'s model (2005).

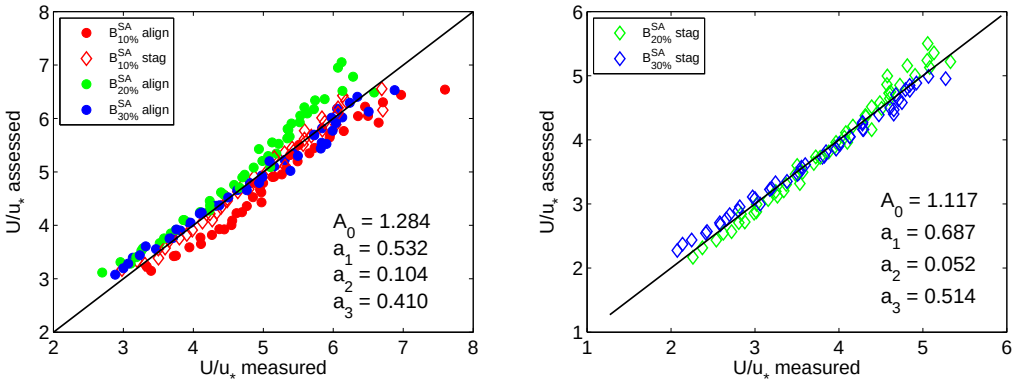

Figure 66: Comparison between measured and assessed values of U/u_*.

Since we noticed that the parameter a_2 should not be taken into account, and that $a_1 \simeq -a_3$, we set $a_2 = 0$ and $a_1 = -a_3 = a$. Eq. 66 can be rewritten as:

$$\frac{U}{u_*} = A_0(M) \cdot \left(\frac{H}{h_v}\right)^a \cdot \left(\frac{H_v}{h_v}\right)^{-a} = A_0(M) \cdot \left(\frac{H}{H_v}\right)^a \tag{67}$$

Following Nikora et al.'s approach [35] for patchy vegetation channels, instead of the ratio (H/H_v) we considered the ratio $(Hb/H_v b_v)$ to take into account for both the relative 'submergence' and the relative patch size. Fig. 67 shows U/u_* as a function of the ratio $(Hb/H_v b_v)$.

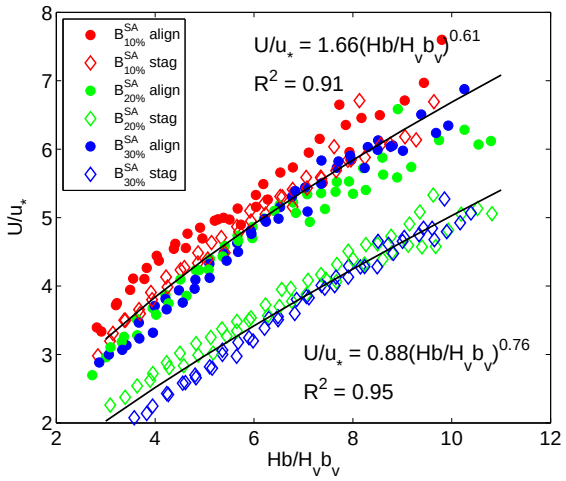

Figure 67: Relationship $U/u_* = F(h_v b_v/Hb)$.

In Fig. 68 there is the comparison between U/u_* calculated and U/u_* measured.

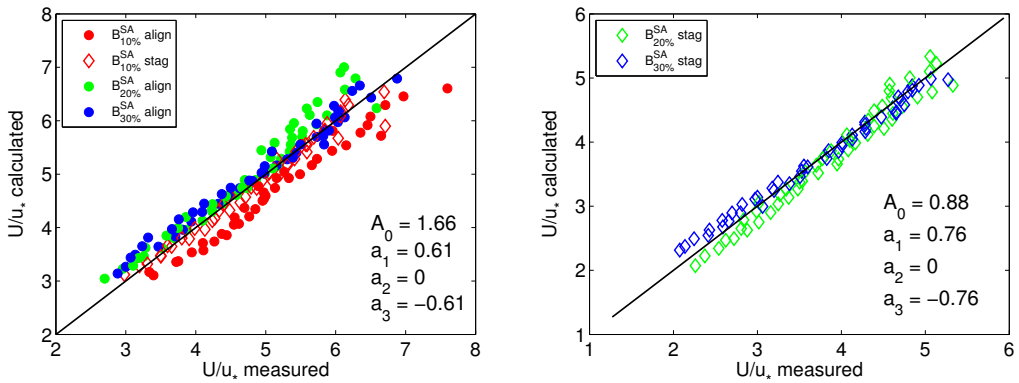

Figure 68: Comparison between measured and calculated values of $U/u_* = F(h_v b_v/Hb)$.

11 DISCUSSION

11.1 HYDRAULIC RESISTANCE DUE TO VEGETATION CONFIGURATIONS

It has been shown in Chapter 10 that the configurations investigated experienced different hydraulic resistance, connecting with the surface area blockage factor and the configuration pattern (aligned or staggered).

Configurations with $B^{SA} = 10\%$ experienced about the same hydraulic resistance for both the aligned and the staggered configurations. Configurations aligned and staggered with $B^{SA} = 20\%$ experienced different hydraulic resistance, which was greater for the staggered configuration. Configurations aligned and staggered with $B^{SA} = 30\%$ also experienced different hydraulic resistance, which was greater for the staggered configuration. Moreover, configurations $B^{SA} = 20\%$ *aligned* and $B^{SA} = 30\%$ *aligned* experienced the same hydraulic resistance which was also similar to that one of configuration $B^{SA} = 10\%$ *aligned*. The hydraulic resistance caused by configuration $B^{SA} = 30\%$ *staggered* was slightly greater than that one of configuration $B^{SA} = 20\%$ *staggered*.

We tried to give an explanation of these results by analysing the wakes that the patches caused, as Li and Shen (1973) did for their cylinders set-ups.

In an attempt to give a preliminary explanation based on Nepf study [16] on turbulence at the patch scale, and considering a high blockage due to the high density of the vegetation patches (24.36 $stems/cm^2$), we can consider a ratio $L_1/D = 2.5$. The term D is set equal to the characteristic geometrical measure of the patch, which is the side (i.e. 0.1 m). We obtain that the von Karman vortex street is formed at a distance L_1 of about 0.25 m behind the patch of vegetation. We compared the L_1 value thus obtained with the investigated configurations. The different scenarios are shown in Fig. 69.

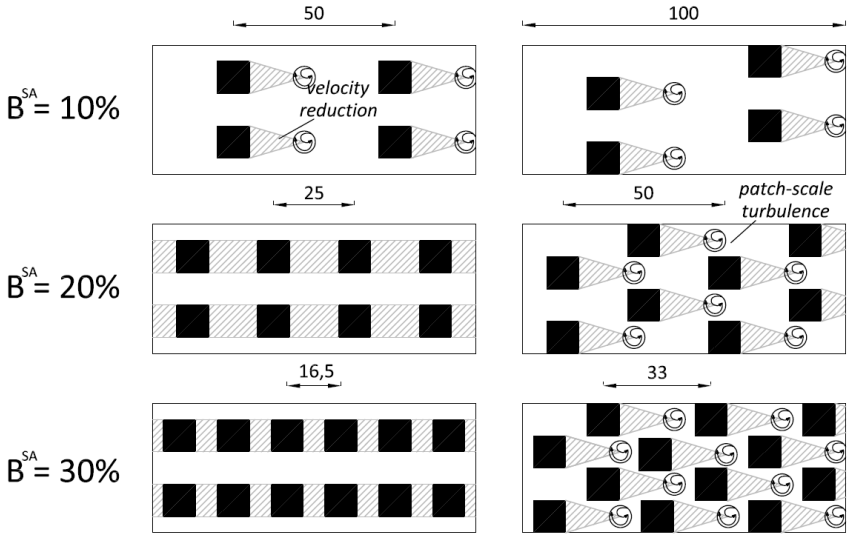

Figure 69: Turbulence fenomena for different configurations.

When $B^{SA} = 10\%$ it is likely that the von Karman vortex street can be generated but the different pattern does not influence the hydraulic resistance since the patches are very far and the flow can return undisturbed after a distance behind them. The staggered and the aligned configurations do not differ in this case since the low number of patches does not cause major obstacles on the flow.

When $B^{SA} = 20\%$ the patches are very close in the aligned configuration, and since their distance is 0.25 m, the von Karman vortex street does not have space enough to be generated. Conversely, in the staggered configuration, the distance of the patches is increased (i.e. 0.50 m) and the von Karman vortex can generate, causing energy losses and turbulence.

The same situation described above occurs when $B^{SA} = 30\%$.

It is interesting to note that, based on this hypothetical model, configurations $B^{SA} = 20\%$ *aligned* and $B^{SA} = 30\%$ *staggered* experience the same hydraulic resistance, since they behaves as two strips. Configuration $B^{SA} = 30\%$ *staggered* causes a greater hydraulic resistance than configuration $B^{SA} = 20\%$ *staggered* due to the higher boundary of the elements that force the flow to weave between the stands, increasing turbulence losses.

This explanation is in agreement with Bal's results [21] on different configurations. The vegetation patterns 2 and 3 of Fig. 16 had the same hydraulic resistance since they behave like configurations $B^{SA} = 20\%$ *aligned* and $B^{SA} = 30\%$ *staggered*.

It can also be possible that Nikora et al. [35] in their field study did not find out any dependence on patch mosaic patterns since the aquatic plants at the investigated stream reaches covered $40 - 100\%$ of the bed. Since the B^{SA} is very high, the vegetation patches could be very close and a change in their spatial configuration will not result in the onset of turbulent phenomena.

In the determination of the resistance laws, the configurations have been divided into two groups, since their hydraulic resistance did not differ much: (1) $B^{SA} = 10\%$ *aligned*, $B^{SA} = 10\%$ *staggered*, $B^{SA} = 20\%$ *aligned*, $B^{SA} = 30\%$ *aligned*; (2) $B^{SA} = 20\%$ *staggered*, $B^{SA} = 30\%$ *staggered*.

11.2 Flow resistance parameters as a function of vegetation parameters

The key physical parameters of vegetation that have been taken into account were the relative roughness h_v/H, the maximum cross-sectional blockage factor $(h_v b_v/Hb)$ and the averaged cross-sectional blockage factor $B^{SA}(h_v/H)$. Darcy-Weisbach friction factor f, Manning's n and Chezy's C have been plotted as a function of these parameters.

Due to the different hydraulic resistance that configurations $B^{SA} = 20\%$ *staggered* and $B^{SA} = 30\%$ *staggered* experienced, it was not possible to identify a unique resistance law, but for every vegetation parameter two equations were determined, as said in the previous section.

Correlations between the hydraulic resistance parameters and the vegetation parameters were high ($R^2 > 0.9$). Since b_v, b and B^{SA} were constants, the three parameters had the same predictive power in this study, and the considerations

that can be made for one of them are the same for all. We chose to show the relationships between the hydraulic resistance parameters and the maximum cross-sectional blockage factor. Relationships $f = F(h_v b_b / Hb)$, $n = F(h_v b_b / Hb)$ and $C = F(h_v b_b / Hb)$ were interpolated with both a linear and an exponential equation. Both the equations showed a high coefficient of determination for all three hydraulic parameters, with f ($R^2_{linear} = 0.94 - 0.91; R^2_{exp} = 0.95 - 0.92$) and C ($R^2_{linear} = 0.9 - 0.87; R^2_{exp} = 0.96 - 0.94$) interpolated slightly better from the exponential equation and n ($R^2_{linear} = 0.97 - 0.94; R^2_{exp} = 0.95 - 0.92$) from the linear one.

The limits of the hydraulic parameters when $(h_v b_v / Hb) \to 0$ (i.e. no vegetation) were calculated for both the exponential and the linear fit. The results showed that the values obtained from the exponential equations ($f = 0.1; n = 0.02, C = 38 \div 34$) were more similar to those calculated for the fastener layer (Table 9) than the ones obtained from the linear fit ($f = -0.34 \div -0.09; n = 0.01; C = 32 \div 27$). Equations $f = f_b exp[b_1(h_v b_v / Hb)]$, $n = n_b exp[b_2(h_v b_v / Hb)]$ and $C = C_b exp[b_3(h_v b_v / Hb)]$, where b_1, b_2, b_3 are coefficients, could best approximate the data. This is in agreement with Nikora et al.'s field study [35] and with Green's non-linear theoretical relationship [5], suggesting an increase in resistance towards a complete blockage. The linear fit had equally a very high predictive power and this can be due to the low value of the cross-sectional blockage factor that was investigated. Its maximum value was about 38%, and it can be possible that in this range of cross-sectional blockage factor the linear and the exponential equation do not differ much from each other.

11.3 Assessment of current hydraulic resistance models

Both Kouwen et al.'s [24] and Carollo et al.'s [14] models showed a good agreement with collected data, which is consistent with Nikora et al. [35] conclusion that they can both extended for conditions of patchy vegetation if site-averaged vegetation measures are used. Although it is possible that the velocity profile is not logarithmic due to the vegetation patchiness, data were approximated very well by Kouwen et al's models ($R^2 = 0.92 - 0.97$). The coefficients C_1 and C_2 need to be calibrated according to the vegetation characteristics.

Carollo et al.'s model also provided a good fit ($R^2 = 0.91 - 0.95$), but the coefficients of the functional law have to be calibrated for the specific situation since it is likely that the vertical velocity profile differs from that considered in Carollo et al.'s analysis. It is interesting to observe that a_2 was found to be 0. This suggests a non-dependence on this parameter.

Part III

CONCLUSIONS

12

CONCLUSIONS

A laboratory study in an open-channel flume was carried out in order to investigate the hydraulic resistance in presence of flexible submerged patchy vegetation. Elements of vegetation were cut out from artificial grass-like vegetation, whose geometrical and mechanical characteristics have been studied and explained in Chapter 7. The experimental set-up and the configurations investigated have been shown in Chapter 8. Hydraulic resistance was expressed in form of Manning's n, Darcy-Weisbach frinction factor f and Chezy's C. The key physical parameters of vegetation considered (i.e. the relative roughness h_v/H, the maximum cross-sectional blockage factor $(h_v b_v/Hb)$ and the averaged cross-sectional blockage factor $B^{SA}(h_v/H)$) had the same predictive power in this study, with $R^2 > 0.9$ for all of them. The investigated patterns of vegetation experienced different hydraulic resistance. The hydraulic resistance was not much different for configurations with $B^{SA} = 10\%$ for the staggered and the aligned pattern. Configurations with $B^{SA} = 20\%$ and $B^{SA} = 30\%$, instead, showed a different hydraulic resistance which was greater for the staggered configuration. A preliminary explanation of these results that involved the patch-scale turbulence has been given. The pattern of the vegetation patches influenced or did not influence the hydraulic resistance as a function of the surface-area blockage factor.

Both Kouwen et al.'s [24] model and Carollo et al's [14] model were found to be extended for conditions of patchy vegetation.

Developing knowledge on hydrodynamics in patchy vegetation channel is important since, as suggested by Bal [21], vegetation removal patterns could be good alternatives to create a management system that minimally increases hydraulic resistance but still guarantees the ecological functions.

13

FUTURE WORK

A rigorous explanation of the different hydraulic resistance that the configurations experienced has to be given. The velocity field has to be investigated above and between the vegetation patches. A plan to detect the velocity field that uses the UVP instrument has been made. The set-up of the measurements is shown in Fig. 70. The instrument will be placed on a trolley which can slide freely on the lateral beams of the flume. Data will be collected along both x axis and y axis, to obtain a double-averaged profile of the velocity field.

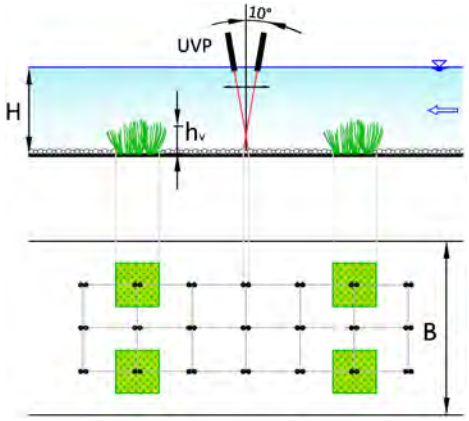

Figure 70: Planned scheme of velocity experiments for future work.

Further experiments are scheduled in order to investigate the hydraulic resistance for aligned and staggered patterns with a higher value of cross-sectional blockage factor: $B^{SA} = 40\%$ and 60%. The configurations are shown in Fig. 71. The aim is to verify if the hypothesis made of a non-dependence of the hydraulic resistance for the higher values of B^{SA} could be correct.

Next steps will be to inquire different patch shapes in order to express the hydraulic resistance not only as a function of the vegetation pattern, but also of the patch shape and size.

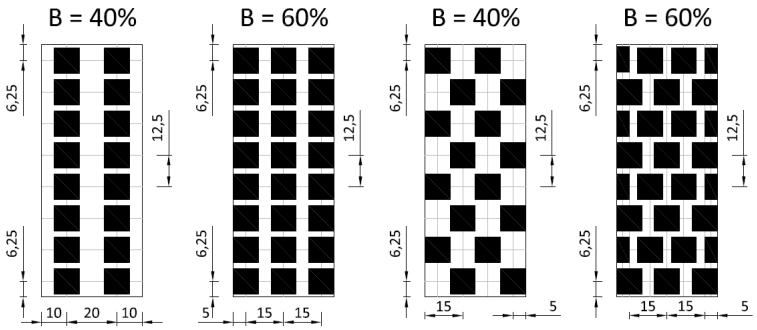

Figure 71: Planned configurations for future work.

Part IV

APPENDIX

A

APPENDIX A: CURVES FORCE - EXTENSION FOR MECHANIC TEST ON VEGETATION

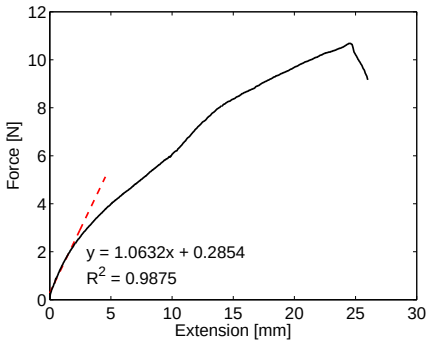

Stem EP_P1_S1.

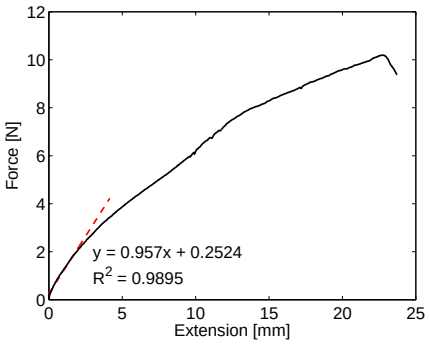

Stem EP_P1_S2.

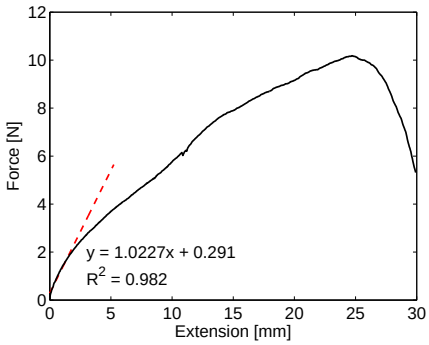

Stem EP_P1_S3.

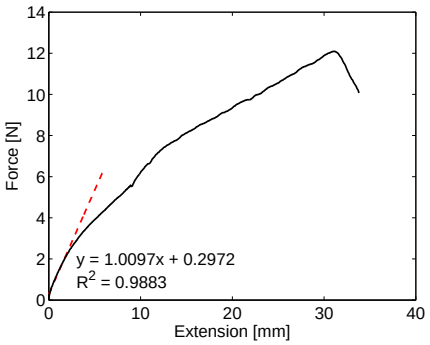

Stem EP_P1_S4.

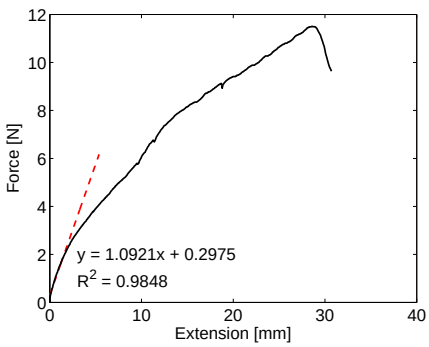

Stem EP_P1_S5.

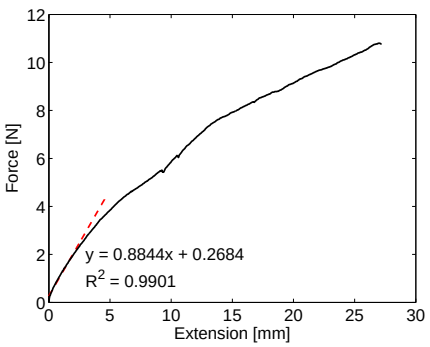

Stem EP_P2_S1.

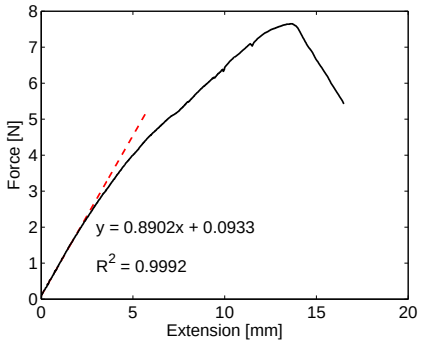

Stem EP_P2_S2.

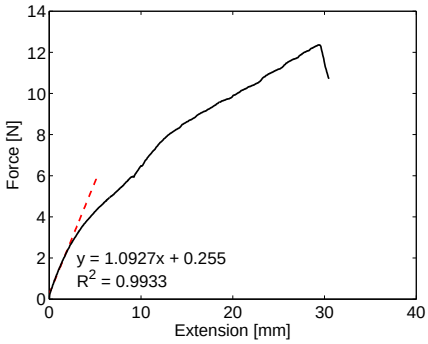

Stem EP_P2_S3.

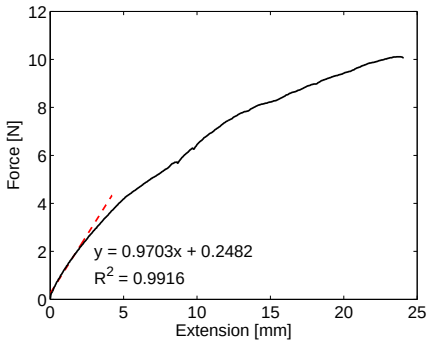

Stem EP_P2_S4.

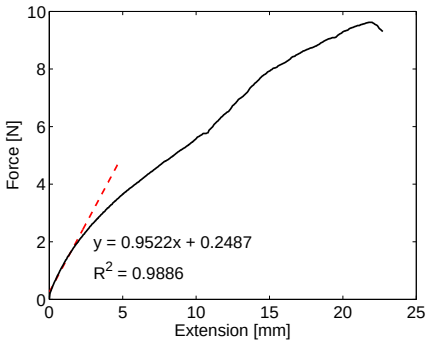

Stem EP_P2_S5.

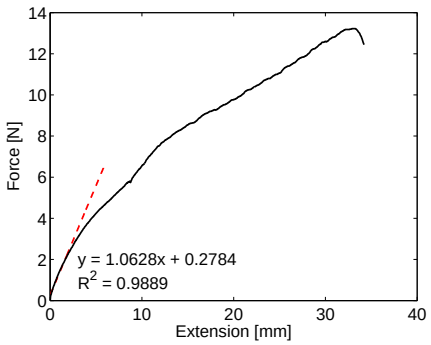

Stem EP_P3_S1.

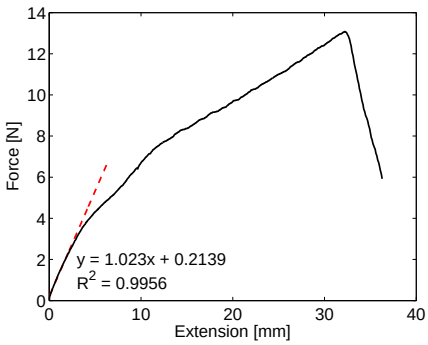

Stem EP_P3_S2.

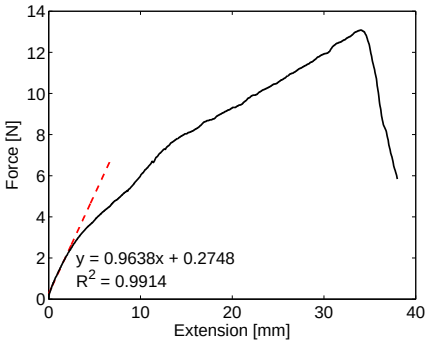

Stem EP_P3_S3.

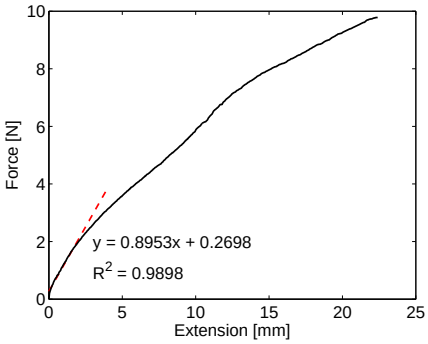

Stem EP_P3_S4.

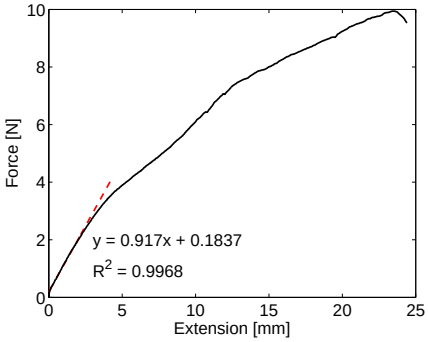

Stem EP_P3_S5.

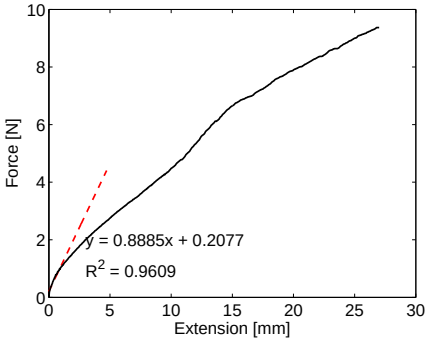

Stem EP_P4_S1.

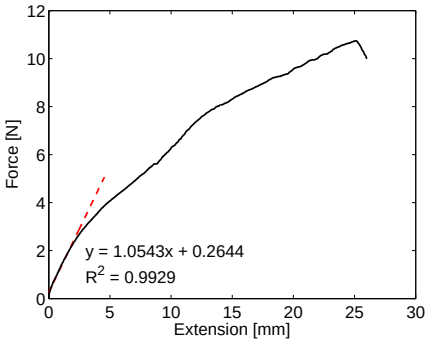

Stem EP_P4_S2.

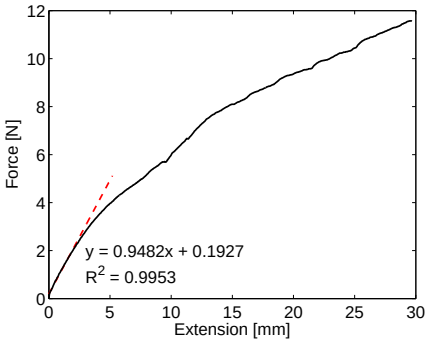

Stem EP_P4_S3.

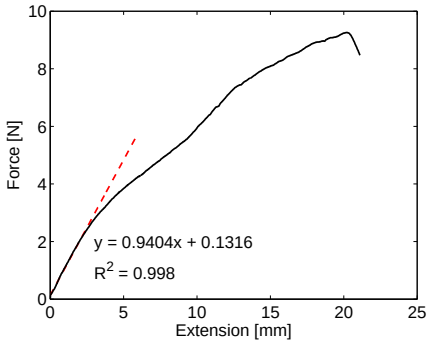

Stem EP_P4_S4.

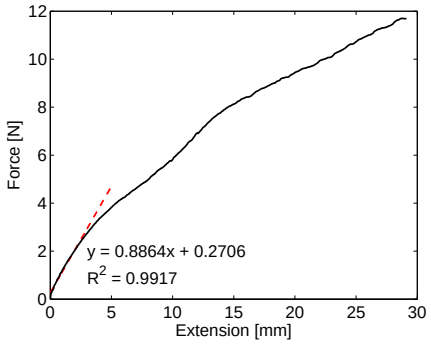

Stem EP_P4_S5.

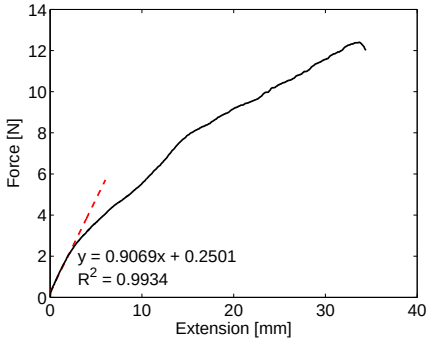

Stem EP_P5_S1.

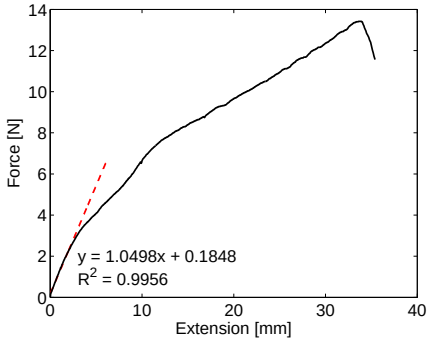

Stem EP_P5_S2.

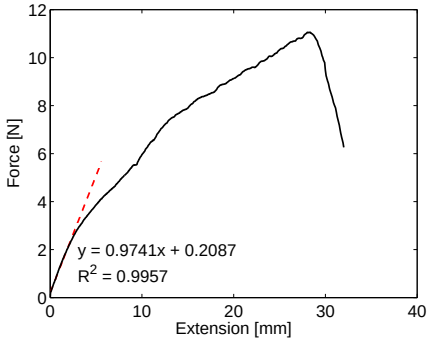

Stem EP_P5_S3.

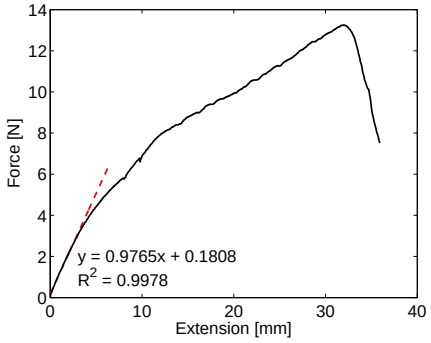

Stem EP_P5_S4.

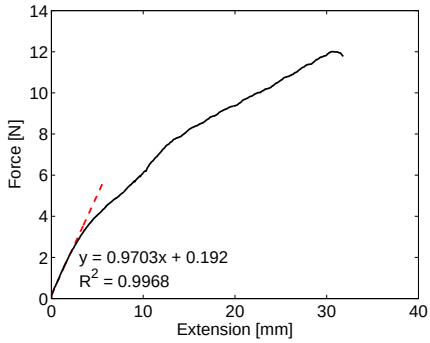

Stem EP_P5_S5.

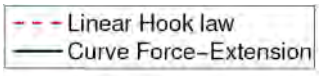

Legend.

stem_ID	w	t	L	A	I_x	I_y	L_{samp}	F/ΔL	E
	[mm]	[mm]	[mm]	[m^2]	[m^4]	[m^4]	[mm]	[N/m]	[N/m^2]
EP_P1_S1	1.2	0.16	35.96	1.92E-07	4.10E-16	2.30E-14	19.07	1063.16	1.06E+08
EP_P1_S2	1.1	0.14	33.3	1.54E-07	2.52E-16	1.55E-14	17.03	956.97	1.06E+08
EP_P1_S3	1.17	0.14	33.97	1.64E-07	2.68E-16	1.87E-14	18.17	1022.65	1.13E+08
EP_P1_S4	1.18	0.15	33.42	1.77E-07	3.32E-16	2.05E-14	18.48	1009.74	1.05E+08
EP_P1_S5	1.2	0.15	36.15	1.80E-07	3.38E-16	2.16E-14	19.84	1092.11	1.20E+08
EP_P2_S1	1.12	0.15	35.49	1.68E-07	3.15E-16	1.76E-14	25.19	884.36	1.33E+08
EP_P2_S2	1.19	0.17	34.06	2.02E-07	4.87E-16	2.39E-14	20.39	890.19	8.97E+07
EP_P2_S3	1.2	0.14	33.88	1.68E-07	2.74E-16	2.02E-14	18.97	1092.73	1.23E+08
EP_P2_S4	1.2	0.17	33.18	2.04E-07	4.91E-16	2.45E-14	20.88	970.32	9.93E+07
EP_P2_S5	1.04	0.18	36.55	1.87E-07	5.05E-16	1.69E-14	21.63	952.21	1.10E+08
EP_P3_S1	1.15	0.21	35.11	2.42E-07	8.88E-16	2.66E-14	18.62	1062.81	8.19E+07
EP_P3_S2	1.14	0.15	36	1.71E-07	3.21E-16	1.85E-14	19.23	1023.01	1.15E+08
EP_P3_S3	1.2	0.16	36.57	1.92E-07	4.10E-16	2.30E-14	18.86	963.78	9.47E+07
EP_P3_S4	1.22	0.17	33.68	2.07E-07	4.99E-16	2.57E-14	16.79	895.27	7.25E+07
EP_P3_S5	1.22	0.18	33.92	2.20E-07	5.93E-16	2.72E-14	19.69	917.01	8.22E+07
EP_P4_S1	1.23	0.15	36.6	1.85E-07	3.46E-16	2.33E-14	25.94	888.55	1.25E+08
EP_P4_S2	1.2	0.18	33.8	2.16E-07	5.83E-16	2.59E-14	18.56	1054.32	9.06E+07
EP_P4_S3	1.13	0.14	35.51	1.58E-07	2.58E-16	1.68E-14	21.38	948.21	1.28E+08
EP_P4_S4	1.22	0.15	33.53	1.83E-07	3.43E-16	2.27E-14	19.07	940.42	9.80E+07
EP_P4_S5	1.14	0.15	33.6	1.71E-07	3.21E-16	1.85E-14	20.96	886.44	1.09E+08
EP_P5_S1	1.13	0.15	36.71	1.70E-07	3.18E-16	1.80E-14	21.9	906.88	1.17E+08
EP_P5_S2	1.06	0.15	33.64	1.59E-07	2.98E-16	1.49E-14	17.65	1049.81	1.17E+08
EP_P5_S3	1.14	0.18	35.28	2.05E-07	5.54E-16	2.22E-14	20.07	974.07	9.53E+07
EP_P5_S4	1.1	0.14	32.83	1.54E-07	2.52E-16	1.55E-14	18.66	976.47	1.18E+08
EP_P5_S5	1.11	0.15	34.36	1.67E-07	3.12E-16	1.71E-14	20.91	970.27	1.22E+08

A

APPENDIX B: SUMMARY TABLES OF THE MAIN HYDRAULIC PARAMETERS

Run ID	S_b	S_e	Q l/s	H mm	h_v mm	H/h_v	U m/s	u_* m/s	F_r	R_e	n $sm^{-1/3}$	K_s $m^{1/3}s^{-1}$	C $m^{1/2}s^{-1}$	f
B10_A_Sb500_Q2.06	0.002	0.0019	2.0648	49.75	35.70	1.3936	0.1038	0.0306	0.1485	5161.88	0.0492	20.3329	11.8828	0.6941
B10_A_Sb500_Q2.78	0.002	0.0020	2.7849	56.60	35.40	1.5989	0.1230	0.0331	0.1651	6962.14	0.0450	22.2039	13.1986	0.5780
B10_A_Sb500_Q3.66	0.002	0.0020	3.6559	62.75	35.30	1.7776	0.1457	0.0354	0.1856	9139.74	0.0408	24.4921	14.7529	0.4737
B10_A_Sb500_Q4.13	0.002	0.0019	4.1260	67.60	35.10	1.9259	0.1526	0.0358	0.1874	10315.11	0.0393	25.4143	15.4523	0.4398
B10_A_Sb500_Q4.72	0.002	0.0020	4.7193	71.15	35.30	2.0156	0.1658	0.0373	0.1985	11798.17	0.0378	26.4744	16.1991	0.4055
B10_A_Sb500_Q5.91	0.002	0.0022	5.9108	77.80	34.60	2.2486	0.1899	0.0411	0.2174	14777.04	0.0363	27.5509	17.0418	0.3753
B10_A_Sb500_Q6.42	0.002	0.0021	6.4181	82.15	34.50	2.3812	0.1953	0.0410	0.2176	16045.34	0.0351	28.4723	17.7262	0.3524
B10_A_Sb500_Q7.01	0.002	0.0020	7.0146	86.65	34.20	2.5336	0.2024	0.0417	0.2195	17536.54	0.0344	29.0429	18.1948	0.3398
B10_A_Sb500_Q7.70	0.002	0.0020	7.6994	91.85	34.30	2.6778	0.2096	0.0423	0.2208	19248.60	0.0336	29.7221	18.7458	0.3259
B10_A_Sb500_Q8.36	0.002	0.0021	8.3615	95.00	34.10	2.7859	0.2200	0.0440	0.2279	20903.64	0.0333	30.0281	19.0115	0.3203
B10_A_Sb500_Q9.07	0.002	0.0020	9.0682	100.05	34.30	2.9169	0.2266	0.0441	0.2287	22670.52	0.0323	30.9227	19.6919	0.3036
B10_A_Sb500_Q10.41	0.002	0.0020	10.4084	106.55	34.40	3.0974	0.2442	0.0458	0.2389	26020.98	0.0310	32.2365	20.6710	0.2815
B10_A_Sb500_Q11.29	0.002	0.0021	11.2886	109.20	34.10	3.2023	0.2584	0.0471	0.2497	28221.46	0.0301	33.2529	21.3796	0.2654
B10_A_Sb500_Q12.26	0.002	0.0020	12.2646	115.30	34.10	3.3812	0.2659	0.0470	0.2500	30661.55	0.0291	34.4124	22.2538	0.2498
B10_A_Sb500_Q13.00	0.002	0.0019	13.0015	119.75	34.20	3.5015	0.2714	0.0473	0.2504	32503.66	0.0286	34.9689	22.7038	0.2434
B10_A_Sb500_Q15.32	0.002	0.0021	15.3213	125.45	34.10	3.6789	0.3053	0.0513	0.2752	38303.25	0.0274	36.4320	23.7676	0.2261
B10_A_Sb500_Q16.28	0.002	0.0021	16.2837	129.35	33.90	3.8156	0.3147	0.0512	0.2794	40709.36	0.0265	37.7721	24.7188	0.2115
B10_A_Sb500_Q18.32	0.002	0.0019	18.3212	136.35	33.90	4.0221	0.3359	0.0505	0.2905	45802.96	0.0244	41.0517	27.0073	0.1810
B10_A_Sb500_Q19.00	0.002	0.0021	19.0007	138.65	33.70	4.1142	0.3426	0.0539	0.2938	47501.82	0.0254	39.2986	25.8966	0.1981
B10_A_Sb500_Q20.13	0.002	0.0021	20.1268	144.25	33.40	4.3189	0.3488	0.0540	0.2932	50317.03	0.0249	40.1032	26.5292	0.1919

Table 10: Summary table of the hydraulic parameters, configuration $B10\_A\_Sb500$

Run ID	S_b	S_e	Q l/s	H mm	h_v mm	H/h_v	U m/s	u_* m/s	F_r	R_e	n $sm^{-1/3}$	K_s $m^{1/3}s^{-1}$	C $m^{1/2}s^{-1}$	f
B10_A_Sb1000_Q1.70	0.001	0.0012	1.6983	51.40	34.50	1.4899	0.0826	0.0248	0.1163	4245.76	0.0501	19.9544	11.7123	0.7191
B10_A_Sb1000_Q2.28	0.001	0.0013	2.2771	56.95	34.50	1.6507	0.1000	0.0267	0.1337	5692.66	0.0447	22.3749	13.3109	0.5691
B10_A_Sb1000_Q2.65	0.001	0.0012	2.6496	61.65	34.50	1.7870	0.1074	0.0273	0.1382	6623.95	0.0425	23.5027	14.1251	0.5146
B10_A_Sb1000_Q2.82	0.001	0.0010	2.8152	66.75	33.95	1.9661	0.1054	0.0257	0.1303	7037.94	0.0409	24.4413	14.8373	0.4755
B10_A_Sb1000_Q3.47	0.001	0.0011	3.4661	71.90	34.20	2.1023	0.1205	0.0276	0.1435	8665.15	0.0384	26.0544	15.9627	0.4187
B10_A_Sb1000_Q3.80	0.001	0.0010	3.8030	77.25	34.90	2.2135	0.1231	0.0271	0.1414	9507.48	0.0369	27.1168	16.7590	0.3874
B10_A_Sb1000_Q4.09	0.001	0.0009	4.0868	81.55	35.30	2.3102	0.1253	0.0275	0.1401	10217.09	0.0367	27.2145	16.9285	0.3855
B10_A_Sb1000_Q4.87	0.001	0.0010	4.8662	87.45	35.60	2.4565	0.1391	0.0296	0.1502	12165.43	0.0356	28.1148	17.6322	0.3628
B10_A_Sb1000_Q6.04	0.001	0.0012	6.0385	93.00	35.60	2.6124	0.1623	0.0326	0.1699	15096.13	0.0335	29.8603	18.8597	0.3232
B10_A_Sb1000_Q6.38	0.001	0.0011	6.3804	97.15	34.90	2.7837	0.1642	0.0330	0.1682	15951.09	0.0334	29.8999	18.9781	0.3237
B10_A_Sb1000_Q7.17	0.001	0.0013	7.1661	101.20	34.70	2.9164	0.1770	0.0362	0.1777	17915.13	0.0339	29.5169	18.8204	0.3337
B10_A_Sb1000_Q7.79	0.001	0.0012	7.7881	106.60	34.70	3.0720	0.1826	0.0354	0.1786	19470.30	0.0321	31.1803	19.9948	0.3009
B10_A_Sb1000_Q8.27	0.001	0.0012	8.2707	110.80	35.20	3.1477	0.1866	0.0354	0.1790	20676.66	0.0313	31.9212	20.5555	0.2886
B10_A_Sb1000_Q9.48	0.001	0.0011	9.4756	120.20	34.20	3.5146	0.1971	0.0366	0.1815	23689.06	0.0304	32.8490	21.3358	0.2760
B10_A_Sb1000_Q10.17	0.001	0.0010	10.1709	130.40	34.40	3.7907	0.1950	0.0354	0.1724	25427.20	0.0295	33.8668	22.1812	0.2635
B10_A_Sb1000_Q11.87	0.001	0.0009	11.8743	139.95	34.50	4.0565	0.2121	0.0356	0.1810	29685.87	0.0271	36.8798	24.3250	0.2254
B10_A_Sb1000_Q15.91	0.001	0.0011	15.9099	150.80	34.30	4.3965	0.2638	0.0406	0.2169	39774.78	0.0247	40.5619	26.9472	0.1896
B10_A_Sb1000_Q18.02	0.001	0.0011	18.0214	159.70	34.00	4.6971	0.2821	0.0420	0.2254	45053.61	0.0237	42.1990	28.1861	0.1777
B10_A_Sb1000_Q19.83	0.001	0.0011	19.8345	166.55	34.10	4.8842	0.2977	0.0427	0.2329	49586.34	0.0227	44.0723	29.5510	0.1647
B10_A_Sb1000_Q21.96	0.001	0.0010	21.9623	172.95	34.20	5.0570	0.3175	0.0418	0.2437	54905.78	0.0207	48.2995	32.4957	0.1386

Table 11: Summary table of the hydraulic parameters, configuration $B10\_A\_Sb1000$

Run ID	S_b	S_e	Q l/s	H mm	h_v mm	H/h_v	U m/s	u_* m/s	F_r	R_e	n $sm^{-1/3}$	K_s $m^{1/3}s^{-1}$	C $m^{1/2}s^{-1}$	f
B10_S_Sb500_Q1.89	0.002	0.0020	1.8886	50.15	35.70	1.4048	0.0941	0.0316	0.1342	4721.42	0.0561	17.8393	10.4367	0.9012
B10_S_Sb500_Q2.31	0.002	0.0021	2.3078	54.50	35.60	1.5309	0.1059	0.0331	0.1448	5769.44	0.0524	19.0917	11.2928	0.7831
B10_S_Sb500_Q2.91	0.002	0.0020	2.9068	60.00	35.30	1.6997	0.1211	0.0346	0.1579	7266.97	0.0479	20.8658	12.4969	0.6533
B10_S_Sb500_Q3.34	0.002	0.0019	3.3396	64.85	35.30	1.8371	0.1287	0.0352	0.1614	8349.06	0.0459	21.7836	13.1761	0.5986
B10_S_Sb500_Q3.70	0.002	0.0017	3.6990	69.10	35.30	1.9575	0.1338	0.0343	0.1625	9247.48	0.0430	23.2805	14.1936	0.5242
B10_S_Sb500_Q4.81	0.002	0.0021	4.8122	74.50	35.10	2.1225	0.1615	0.0391	0.1889	12030.56	0.0406	24.6350	15.1586	0.4688
B10_S_Sb500_Q5.38	0.002	0.0020	5.3819	79.65	35.10	2.2692	0.1689	0.0399	0.1911	13454.74	0.0395	25.2938	15.6897	0.4458
B10_S_Sb500_Q6.51	0.002	0.0021	6.5087	85.90	34.70	2.4755	0.1894	0.0422	0.2064	16271.68	0.0373	26.8279	16.7902	0.3980
B10_S_Sb500_Q7.20	0.002	0.0021	7.1959	90.70	34.40	2.6366	0.1983	0.0428	0.2103	17989.68	0.0360	27.7958	17.5056	0.3722
B10_S_Sb500_Q7.83	0.002	0.0021	7.8298	94.20	34.30	2.7464	0.2078	0.0441	0.2162	19574.45	0.0354	28.2790	17.8870	0.3608
B10_S_Sb500_Q8.93	0.002	0.0022	8.9336	99.80	34.40	2.9012	0.2238	0.0460	0.2262	22334.04	0.0341	29.3323	18.6739	0.3374
B10_S_Sb500_Q9.61	0.002	0.0020	9.6131	104.50	34.40	3.0378	0.2300	0.0451	0.2271	24032.81	0.0325	30.7876	19.7002	0.3079
B10_S_Sb500_Q10.76	0.002	0.0021	10.7577	109.60	34.30	3.1953	0.2454	0.0471	0.2367	26894.30	0.0317	31.5700	20.3056	0.2946
B10_S_Sb500_Q11.62	0.002	0.0020	11.6201	116.05	34.20	3.3933	0.2503	0.0472	0.2346	29050.16	0.0310	32.2651	20.8795	0.2845
B10_S_Sb500_Q12.28	0.002	0.0019	12.2808	119.70	34.20	3.5000	0.2565	0.0474	0.2367	30702.06	0.0303	33.0096	21.4307	0.2731
B10_S_Sb500_Q13.71	0.002	0.0020	13.7121	124.55	34.00	3.6632	0.2752	0.0493	0.2490	34280.14	0.0292	34.2004	22.2953	0.2562
B10_S_Sb500_Q15.09	0.002	0.0021	15.0864	129.75	34.00	3.8162	0.2907	0.0520	0.2577	37716.04	0.0291	34.3471	22.4845	0.2559
B10_S_Sb500_Q16.53	0.002	0.0020	16.5278	134.50	33.90	3.9676	0.3072	0.0509	0.2674	41319.50	0.0269	37.2138	24.4492	0.2196
B10_S_Sb500_Q17.01	0.002	0.0020	17.0119	139.40	33.90	4.1121	0.3051	0.0523	0.2609	42529.85	0.0277	36.1332	23.8234	0.2347
B10_S_Sb500_Q20.74	0.002	0.0021	20.7392	143.55	33.70	4.2596	0.3612	0.0538	0.3044	51848.09	0.0240	41.6540	27.5421	0.1777

Table 12: Summary table of the hydraulic parameters, configuration $B10\_S\_Sb500$

Run ID	S_b	S_e	Q l/s	H mm	h_v mm	H/h_v	U m/s	u_* m/s	F_r	R_e	n $sm^{-1/3}$	K_s $m^{1/3}s^{-1}$	C $m^{1/2}s^{-1}$	f
B10_S_Sb1000_Q1.83	0.001	0.0011	1.8294	55.50	35.60	1.5590	0.0824	0.0249	0.1117	4573.40	0.0506	19.7551	11.7130	0.7308
B10_S_Sb1000_Q2.00	0.001	0.0010	1.9973	59.55	35.60	1.6728	0.0838	0.0239	0.1097	4993.14	0.0479	20.8823	12.4947	0.6524
B10_S_Sb1000_Q2.28	0.001	0.0009	2.2835	65.20	35.40	1.8418	0.0876	0.0243	0.1095	5708.70	0.0467	21.4342	12.9735	0.6183
B10_S_Sb1000_Q2.96	0.001	0.0011	2.9579	69.50	35.30	1.9688	0.1064	0.0280	0.1289	7394.73	0.0442	22.6470	13.8172	0.5539
B10_S_Sb1000_Q3.28	0.001	0.0010	3.2847	75.00	35.30	2.1246	0.1095	0.0275	0.1276	8211.76	0.0421	23.7657	14.6356	0.5038
B10_S_Sb1000_Q4.04	0.001	0.0011	4.0381	81.05	35.30	2.2960	0.1246	0.0292	0.1397	10095.24	0.0392	25.5043	15.8531	0.4388
B10_S_Sb1000_Q4.32	0.001	0.0010	4.3177	85.85	35.10	2.4459	0.1257	0.0290	0.1370	10794.17	0.0385	25.9483	16.2385	0.4254
B10_S_Sb1000_Q4.53	0.001	0.0009	4.5292	89.35	35.10	2.5456	0.1267	0.0288	0.1354	11322.96	0.0380	26.3359	16.5576	0.4141
B10_S_Sb1000_Q5.05	0.001	0.0009	5.0454	95.45	35.10	2.7194	0.1321	0.0295	0.1366	12613.41	0.0371	26.9620	17.0794	0.3974
B10_S_Sb1000_Q5.92	0.001	0.0010	5.9210	100.55	34.80	2.8894	0.1472	0.0307	0.1482	14802.58	0.0346	28.8801	18.4013	0.3483
B10_S_Sb1000_Q6.98	0.001	0.0011	6.9791	104.80	34.70	3.0202	0.1665	0.0336	0.1642	17447.80	0.0334	29.8997	19.1380	0.3266
B10_S_Sb1000_Q7.48	0.001	0.0011	7.4821	110.00	34.40	3.1977	0.1700	0.0337	0.1637	18705.37	0.0327	30.6017	19.6905	0.3137
B10_S_Sb1000_Q7.96	0.001	0.0009	7.9574	115.25	34.40	3.3503	0.1726	0.0325	0.1623	19893.41	0.0310	32.2904	20.8806	0.2837
B10_S_Sb1000_Q8.67	0.001	0.0011	8.6682	119.65	34.30	3.4883	0.1811	0.0351	0.1672	21670.51	0.0318	31.4526	20.4190	0.3008
B10_S_Sb1000_Q9.73	0.001	0.0011	9.7278	124.80	34.40	3.6279	0.1949	0.0359	0.1761	24319.56	0.0301	33.2559	21.6840	0.2711
B10_S_Sb1000_Q10.30	0.001	0.0010	10.2991	129.95	34.30	3.7886	0.1981	0.0356	0.1755	25747.68	0.0292	34.2214	22.4056	0.2579
B10_S_Sb1000_Q11.48	0.001	0.0011	11.4808	135.20	34.20	3.9532	0.2123	0.0373	0.1843	28702.06	0.0285	35.0763	23.0567	0.2474
B10_S_Sb1000_Q12.17	0.001	0.0010	12.1650	140.50	34.20	4.1082	0.2165	0.0370	0.1844	30412.57	0.0276	36.1978	23.8843	0.2342
B10_S_Sb1000_Q13.21	0.001	0.0010	13.2143	145.50	34.10	4.2669	0.2271	0.0386	0.1900	33035.81	0.0274	36.5529	24.2008	0.2315
B10_S_Sb1000_Q14.88	0.001	0.0011	14.8815	151.20	34.00	4.4471	0.2461	0.0406	0.2020	37203.87	0.0264	37.8958	25.1823	0.2173
B10_S_Sb1000_Q15.89	0.001	0.0012	15.8886	154.50	34.00	4.5441	0.2571	0.0424	0.2088	39721.48	0.0263	38.0089	25.3091	0.2172
B10_S_Sb1000_Q16.72	0.001	0.0011	16.7175	159.80	33.90	4.7139	0.2615	0.0423	0.2089	41793.87	0.0257	38.8735	25.9664	0.2094
B10_S_Sb1000_Q17.08	0.001	0.0011	17.0770	163.80	33.80	4.8462	0.2606	0.0425	0.2056	42692.59	0.0258	38.7200	25.9228	0.2124
B10_S_Sb1000_Q19.23	0.001	0.0011	19.2297	170.15	33.80	5.0340	0.2825	0.0422	0.2187	48074.21	0.0236	42.4506	28.5188	0.1786

Table 13: Summary table of the hydraulic parameters, configuration $B10\_S\_Sb1000$

Run ID	S_b	S_e	Q l/s	H mm	h_v mm	H/h_v	U m/s	u_* m/s	F_r	R_e	n $sm^{-1/3}$	K_s $m^{1/3}s^{-1}$	C $m^{1/2}s^{-1}$	f
B20_A_Sb500_Q1.63	0.002	0.0021	1.6348	48.15	35.50	1.3563	0.0849	0.0315	0.1235	4087.02	0.0618	16.1760	9.4122	1.0992
B20_A_Sb500_Q2.15	0.002	0.0023	2.1517	53.05	35.50	1.4944	0.1014	0.0343	0.1406	5379.31	0.0565	17.6871	10.4250	0.9137
B20_A_Sb500_Q2.71	0.002	0.0021	2.7080	59.50	35.50	1.6761	0.1138	0.0349	0.1489	6770.05	0.0515	19.4240	11.6209	0.7540
B20_A_Sb500_Q3.24	0.002	0.0021	3.2392	63.90	35.60	1.7949	0.1267	0.0360	0.1601	8097.90	0.0477	20.9735	12.6625	0.6458
B20_A_Sb500_Q3.68	0.002	0.0019	3.6817	69.70	35.50	1.9634	0.1321	0.0359	0.1597	9204.33	0.0456	21.9166	13.3763	0.5915
B20_A_Sb500_Q4.44	0.002	0.0020	4.4375	74.30	34.60	2.1474	0.1493	0.0386	0.1749	11093.78	0.0433	23.0863	14.2010	0.5337
B20_A_Sb500_Q5.00	0.002	0.0019	5.0047	79.60	34.60	2.3006	0.1572	0.0384	0.1779	12511.77	0.0409	24.4570	15.1695	0.4768
B20_A_Sb500_Q5.68	0.002	0.0019	5.6770	85.10	34.20	2.4883	0.1668	0.0394	0.1825	14192.46	0.0395	25.3283	15.8343	0.4462
B20_A_Sb500_Q6.52	0.002	0.0019	6.5206	90.15	34.20	2.6360	0.1808	0.0411	0.1923	16301.55	0.0380	26.3499	16.5834	0.4140
B20_A_Sb500_Q7.14	0.002	0.0018	7.1355	95.45	34.20	2.7909	0.1869	0.0408	0.1931	17838.82	0.0363	27.5469	17.4499	0.3807
B20_A_Sb500_Q8.50	0.002	0.0021	8.4954	100.00	34.00	2.9412	0.2124	0.0449	0.2144	21238.45	0.0351	28.5178	18.1594	0.3570
B20_A_Sb500_Q9.32	0.002	0.0020	9.3213	105.35	34.10	3.0894	0.2212	0.0455	0.2176	23303.21	0.0340	29.3827	18.8179	0.3384
B20_A_Sb500_Q10.06	0.002	0.0020	10.0586	109.40	34.00	3.2176	0.2299	0.0461	0.2219	25146.41	0.0331	30.2074	19.4253	0.3217
B20_A_Sb500_Q10.95	0.002	0.0019	10.9477	115.05	34.00	3.3838	0.2379	0.0459	0.2239	27369.28	0.0317	31.5350	20.3884	0.2974
B20_A_Sb500_Q12.27	0.002	0.0020	12.2734	119.85	33.80	3.5459	0.2560	0.0490	0.2361	30683.44	0.0314	31.8406	20.6745	0.2936
B20_A_Sb500_Q13.27	0.002	0.0020	13.2749	124.90	34.00	3.6735	0.2657	0.0497	0.2400	33187.19	0.0306	32.7077	21.3283	0.2803
B20_A_Sb500_Q14.13	0.002	0.0020	14.1330	129.85	33.80	3.8417	0.2721	0.0508	0.2411	35332.57	0.0304	32.9244	21.5548	0.2786
B20_A_Sb500_Q15.08	0.002	0.0019	15.0845	135.45	33.70	4.0193	0.2784	0.0504	0.2415	37711.37	0.0294	34.0672	22.3975	0.2624
B20_A_Sb500_Q16.18	0.002	0.0020	16.1778	139.80	33.70	4.1484	0.2893	0.0523	0.2470	40444.45	0.0292	34.2242	22.5711	0.2617
B20_A_Sb500_Q17.14	0.002	0.0019	17.1445	144.85	33.60	4.3110	0.2959	0.0517	0.2482	42861.31	0.0281	35.5720	23.5412	0.2442
B20_A_Sb500_Q18.44	0.002	0.0018	18.4410	151.70	33.40	4.5419	0.3039	0.0517	0.2491	46102.53	0.0272	36.7169	24.4066	0.2317
B20_A_Sb500_Q21.51	0.002	0.0017	21.5061	157.25	33.40	4.7081	0.3419	0.0519	0.2753	53765.20	0.0242	41.3298	27.5658	0.1845

Table 14: Summary table of the hydraulic parameters, configuration $B20\_A\_Sb500$

Run ID	S_b	S_e	Q l/s	H mm	h_v mm	H/h_v	U m/s	u_* m/s	F_r	R_e	n $sm^{-1/3}$	K_s $m^{1/3}s^{-1}$	C $m^{1/2}s^{-1}$	f
B20_A_Sb1000_Q1.80	0.001	0.0013	1.7989	54.65	35.40	1.5438	0.0823	0.0265	0.1124	4497.16	0.0539	18.5427	10.9720	0.8300
B20_A_Sb1000_Q1.95	0.001	0.0012	1.9539	58.65	35.40	1.6568	0.0833	0.0262	0.1098	4884.73	0.0526	18.9958	11.3437	0.7887
B20_A_Sb1000_Q2.20	0.001	0.0011	2.2044	64.15	35.40	1.8121	0.0859	0.0262	0.1083	5510.91	0.0511	19.5513	11.8097	0.7432
B20_A_Sb1000_Q2.52	0.001	0.0009	2.5225	70.95	35.30	2.0099	0.0889	0.0248	0.1065	6306.18	0.0468	21.3467	13.0571	0.6236
B20_A_Sb1000_Q3.05	0.001	0.0010	3.0457	75.40	35.30	2.1360	0.1010	0.0269	0.1174	7614.13	0.0447	22.3516	13.7736	0.5696
B20_A_Sb1000_Q3.58	0.001	0.0010	3.5772	81.80	35.40	2.3107	0.1093	0.0283	0.1220	8943.04	0.0434	23.0489	14.3424	0.5376
B20_A_Sb1000_Q4.53	0.001	0.0011	4.5318	86.25	35.20	2.4503	0.1314	0.0310	0.1428	11329.38	0.0395	25.3186	15.8530	0.4469
B20_A_Sb1000_Q4.77	0.001	0.0011	4.7698	89.70	35.20	2.5483	0.1329	0.0314	0.1417	11924.45	0.0394	25.4097	15.9825	0.4450
B20_A_Sb1000_Q5.58	0.001	0.0012	5.5787	94.70	34.70	2.7291	0.1473	0.0332	0.1528	13946.65	0.0376	26.6233	16.8498	0.4073
B20_A_Sb1000_Q6.02	0.001	0.0011	6.0170	100.25	34.70	2.8890	0.1500	0.0322	0.1513	15042.38	0.0356	28.0888	17.8912	0.3681
B20_A_Sb1000_Q7.11	0.001	0.0012	7.1133	105.30	34.60	3.0434	0.1689	0.0359	0.1662	17783.20	0.0352	28.4005	18.1879	0.3622
B20_A_Sb1000_Q7.97	0.001	0.0011	7.9635	113.15	34.40	3.2892	0.1760	0.0345	0.1670	19908.78	0.0323	30.9615	19.9822	0.3077
B20_A_Sb1000_Q8.63	0.001	0.0010	8.6269	120.85	34.30	3.5233	0.1785	0.0352	0.1639	21567.37	0.0323	30.9466	20.1114	0.3113
B20_A_Sb1000_Q9.01	0.001	0.0011	9.0078	125.80	34.30	3.6676	0.1790	0.0362	0.1611	22519.39	0.0331	30.2510	19.7409	0.3281
B20_A_Sb1000_Q9.54	0.001	0.0010	9.5415	131.25	34.20	3.8377	0.1817	0.0355	0.1602	23853.78	0.0317	31.5284	20.6632	0.3044
B20_A_Sb1000_Q10.47	0.001	0.0010	10.4693	135.00	34.10	3.9589	0.1939	0.0361	0.1685	26173.21	0.0302	33.1652	21.7973	0.2767
B20_A_Sb1000_Q11.03	0.001	0.0010	11.0329	141.25	34.10	4.1422	0.1953	0.0365	0.1659	27582.25	0.0302	33.1405	21.8784	0.2797
B20_A_Sb1000_Q11.54	0.001	0.0009	11.5380	145.80	34.10	4.2757	0.1978	0.0366	0.1654	28845.06	0.0298	33.6061	22.2542	0.2740
B20_A_Sb1000_Q13.07	0.001	0.0010	13.0722	152.00	33.90	4.4838	0.2150	0.0382	0.1761	32680.53	0.0284	35.1770	23.3873	0.2525
B20_A_Sb1000_Q13.59	0.001	0.0010	13.5860	157.00	33.90	4.6313	0.2163	0.0387	0.1743	33964.97	0.0285	35.0589	23.3799	0.2563
B20_A_Sb1000_Q14.97	0.001	0.0010	14.9663	162.05	33.90	4.7802	0.2309	0.0402	0.1831	37415.71	0.0276	36.1677	24.1902	0.2428
B20_A_Sb1000_Q16.29	0.001	0.0009	16.2917	171.95	33.90	5.0723	0.2369	0.0386	0.1824	40729.24	0.0257	38.9454	26.1887	0.2128
B20_A_Sb1000_Q18.89	0.001	0.0010	18.8901	181.05	33.70	5.3724	0.2608	0.0415	0.1957	47225.16	0.0249	40.2133	27.1650	0.2026
B20_A_Sb1000_Q19.70	0.001	0.0010	19.6969	186.05	33.50	5.5537	0.2647	0.0436	0.1959	49242.19	0.0256	38.9920	26.4025	0.2173
B20_A_Sb1000_Q20.74	0.001	0.0011	20.7432	190.49	33.50	5.6863	0.2722	0.0445	0.1991	51857.95	0.0253	39.4717	26.7815	0.2136

Table 15: Summary table of the hydraulic parameters, configuration $B20\_A\_Sb1000$

Run ID	S_b	S_e	Q l/s	H mm	h_v mm	H/h_v	U m/s	u_* m/s	F_r	R_e	n $sm^{-1/3}$	K_s $m^{1/3}s^{-1}$	C $m^{1/2}s^{-1}$	f
B20_S_Sb500_Q1.75	0.002	0.0023	1.7477	54.55	35.60	1.5323	0.0801	0.0354	0.1095	4369.23	0.0740	13.5059	7.9897	1.5647
B20_S_Sb500_Q1.97	0.002	0.0020	1.9724	59.90	35.50	1.6873	0.0823	0.0347	0.1074	4931.07	0.0706	14.1553	8.4761	1.4195
B20_S_Sb500_Q2.41	0.002	0.0022	2.4138	64.15	35.50	1.8070	0.0941	0.0370	0.1186	6034.47	0.0661	15.1375	9.1436	1.2398
B20_S_Sb500_Q2.74	0.002	0.0019	2.7443	69.75	35.60	1.9593	0.0984	0.0361	0.1189	6860.65	0.0616	16.2227	9.9020	1.0795
B20_S_Sb500_Q3.31	0.002	0.0020	3.3129	74.70	35.40	2.1102	0.1109	0.0385	0.1295	8282.13	0.0582	17.1678	10.5673	0.9653
B20_S_Sb500_Q4.04	0.002	0.0023	4.0392	79.45	35.10	2.2635	0.1271	0.0421	0.1440	10097.92	0.0555	18.0168	11.1724	0.8785
B20_S_Sb500_Q4.49	0.002	0.0021	4.4877	85.20	34.60	2.4624	0.1317	0.0417	0.1440	11219.25	0.0529	18.8941	11.8135	0.8019
B20_S_Sb500_Q4.84	0.002	0.0019	4.8438	90.45	34.60	2.6142	0.1339	0.0412	0.1421	12109.42	0.0513	19.4790	12.2639	0.7578
B20_S_Sb500_Q5.30	0.002	0.0019	5.2959	94.45	34.50	2.7377	0.1402	0.0416	0.1456	13239.65	0.0494	20.2598	12.8186	0.7032
B20_S_Sb500_Q6.14	0.002	0.0020	6.1370	99.75	34.30	2.9082	0.1538	0.0442	0.1555	15342.56	0.0477	20.9749	13.3525	0.6597
B20_S_Sb500_Q6.71	0.002	0.0021	6.7090	104.10	34.10	3.0528	0.1611	0.0460	0.1594	16772.42	0.0473	21.1539	13.5301	0.6518
B20_S_Sb500_Q7.35	0.002	0.0019	7.3499	110.00	34.10	3.2258	0.1670	0.0449	0.1608	18374.84	0.0443	22.5712	14.5233	0.5767
B20_S_Sb500_Q8.61	0.002	0.0020	8.6148	115.80	34.00	3.4059	0.1860	0.0471	0.1745	21537.06	0.0416	24.0250	15.5436	0.5129
B20_S_Sb500_Q9.28	0.002	0.0021	9.2764	119.00	34.10	3.4897	0.1949	0.0491	0.1804	23190.92	0.0414	24.1791	15.6881	0.5086
B20_S_Sb500_Q10.02	0.002	0.0020	10.0206	125.15	34.00	3.6809	0.2002	0.0490	0.1807	25051.61	0.0400	25.0005	16.3059	0.4799
B20_S_Sb500_Q10.46	0.002	0.0018	10.4613	129.80	34.00	3.8176	0.2015	0.0483	0.1786	26153.29	0.0391	25.6030	16.7610	0.4607
B20_S_Sb500_Q11.86	0.002	0.0019	11.8551	135.50	33.80	4.0089	0.2187	0.0507	0.1897	29637.76	0.0376	26.6228	17.5038	0.4297
B20_S_Sb500_Q13.01	0.002	0.0020	13.0089	139.55	33.70	4.1409	0.2331	0.0517	0.1992	32522.33	0.0358	27.9009	18.3976	0.3937
B20_S_Sb500_Q13.93	0.002	0.0019	13.9263	145.85	33.60	4.3408	0.2387	0.0518	0.1996	34815.73	0.0349	28.6447	18.9693	0.3771
B20_S_Sb500_Q15.16	0.002	0.0020	15.1626	150.00	33.60	4.4643	0.2527	0.0548	0.2083	37906.58	0.0347	28.7957	19.1206	0.3757
B20_S_Sb500_Q15.94	0.002	0.0020	15.9449	154.85	33.60	4.6086	0.2574	0.0545	0.2089	39862.24	0.0338	29.6112	19.7215	0.3580
B20_S_Sb500_Q17.03	0.002	0.0018	17.0305	161.40	33.50	4.8179	0.2638	0.0538	0.2096	42576.28	0.0324	30.9026	20.6611	0.3322
B20_S_Sb500_Q18.68	0.002	0.0019	18.6839	165.10	33.30	4.9580	0.2829	0.0557	0.2223	46709.64	0.0312	32.1006	21.5067	0.3097
B20_S_Sb500_Q20.60	0.002	0.0019	20.6036	169.90	33.40	5.0868	0.3032	0.0569	0.2348	51508.98	0.0296	33.7968	22.7021	0.2816

Table 16: Summary table of the hydraulic parameters, configuration $B20\_S\_Sb500$

Run ID	S_b	S_e	Q l/s	H mm	h_v mm	H/h_v	U m/s	u_* m/s	F_r	R_e	n $sm^{-1/3}$	K_s $m^{1/3}s^{-1}$	C $m^{1/2}s^{-1}$	f
B20_S_Sb1000_Q2.14	0.001	0.0013	2.1380	68.80	35.30	1.9490	0.0777	0.0296	0.0946	5345.11	0.0640	15.6336	9.5263	1.1623
B20_S_Sb1000_Q2.44	0.001	0.0011	2.4378	75.60	35.30	2.1416	0.0806	0.0287	0.0936	6094.60	0.0597	16.7475	10.3235	1.0147
B20_S_Sb1000_Q2.58	0.001	0.0010	2.5817	80.80	35.20	2.2955	0.0799	0.0282	0.0897	6454.31	0.0590	16.9389	10.5251	0.9947
B20_S_Sb1000_Q2.77	0.001	0.0009	2.7687	85.95	36.30	2.3678	0.0805	0.0269	0.0877	6921.64	0.0559	17.8956	11.2006	0.8944
B20_S_Sb1000_Q2.94	0.001	0.0008	2.9358	91.30	36.10	2.5291	0.0804	0.0266	0.0849	7339.45	0.0552	18.1127	11.4159	0.8771
B20_S_Sb1000_Q3.75	0.001	0.0009	3.7490	96.15	36.10	2.6634	0.0975	0.0298	0.1004	9372.45	0.0509	19.6490	12.4571	0.7489
B20_S_Sb1000_Q4.32	0.001	0.0011	4.3224	99.75	36.20	2.7555	0.1083	0.0324	0.1095	10806.05	0.0497	20.1381	12.8198	0.7157
B20_S_Sb1000_Q4.60	0.001	0.0009	4.6004	104.80	36.10	2.9030	0.1097	0.0310	0.1082	11501.03	0.0468	21.3547	13.6686	0.6402
B20_S_Sb1000_Q5.27	0.001	0.0010	5.2696	110.85	35.80	3.0964	0.1188	0.0333	0.1140	13173.96	0.0462	21.6345	13.9321	0.6284
B20_S_Sb1000_Q6.13	0.001	0.0012	6.1302	114.95	35.50	3.2380	0.1333	0.0360	0.1256	15325.52	0.0444	22.5074	14.5504	0.5837
B20_S_Sb1000_Q6.48	0.001	0.0011	6.4774	119.40	35.50	3.3634	0.1356	0.0359	0.1253	16193.61	0.0434	23.0350	14.9510	0.5607
B20_S_Sb1000_Q6.87	0.001	0.0010	6.8650	124.60	35.70	3.4902	0.1377	0.0355	0.1246	17162.50	0.0421	23.7447	15.4798	0.5316
B20_S_Sb1000_Q7.36	0.001	0.0009	7.3573	131.55	35.60	3.6952	0.1398	0.0341	0.1231	18393.37	0.0396	25.2217	16.5337	0.4759
B20_S_Sb1000_Q8.08	0.001	0.0010	8.0755	135.30	35.70	3.7899	0.1492	0.0367	0.1295	20188.80	0.0399	25.0826	16.4888	0.4839
B20_S_Sb1000_Q8.48	0.001	0.0008	8.4802	141.25	35.60	3.9677	0.1501	0.0342	0.1275	21200.51	0.0368	27.2094	17.9629	0.4150
B20_S_Sb1000_Q8.84	0.001	0.0009	8.8360	145.35	34.80	4.1767	0.1520	0.0352	0.1273	22090.10	0.0372	26.8566	17.7793	0.4287
B20_S_Sb1000_Q10.30	0.001	0.0010	10.2965	151.85	34.80	4.3635	0.1695	0.0386	0.1389	25741.17	0.0365	27.4347	18.2382	0.4151
B20_S_Sb1000_Q10.62	0.001	0.0010	10.6186	155.05	34.80	4.4555	0.1712	0.0382	0.1388	26546.44	0.0356	28.1160	18.7279	0.3972
B20_S_Sb1000_Q11.23	0.001	0.0009	11.2334	160.95	34.60	4.6517	0.1745	0.0380	0.1389	28083.40	0.0346	28.9369	19.3418	0.3786
B20_S_Sb1000_Q11.69	0.001	0.0009	11.6883	165.85	34.40	4.8212	0.1762	0.0385	0.1381	29220.79	0.0346	28.8995	19.3701	0.3826
B20_S_Sb1000_Q12.20	0.001	0.0009	12.2027	170.75	34.20	4.9927	0.1787	0.0390	0.1380	30506.79	0.0344	29.0434	19.5179	0.3819
B20_S_Sb1000_Q14.06	0.001	0.0010	14.0593	175.25	33.90	5.1696	0.2006	0.0417	0.1530	35148.34	0.0326	30.6675	20.6573	0.3451
B20_S_Sb1000_Q14.59	0.001	0.0009	14.5870	179.90	33.90	5.3068	0.2027	0.0401	0.1526	36467.46	0.0310	32.2965	21.8049	0.3135
B20_S_Sb1000_Q15.33	0.001	0.0009	15.3321	185.70	33.90	5.4779	0.2064	0.0402	0.1529	38330.36	0.0303	32.9737	22.3237	0.3037
B20_S_Sb1000_Q15.96	0.001	0.0009	15.9624	190.85	33.70	5.6632	0.2091	0.0413	0.1528	39905.88	0.0306	32.6329	22.1449	0.3127

Table 17: Summary table of the hydraulic parameters, configuration $B20\_S\_Sb1000$

Run ID	S_b	S_e	Q l/s	H mm	h_v mm	H/h_v	U m/s	u_* m/s	F_r	R_e	n $sm^{-1/3}$	K_s $m^{1/3}s^{-1}$	C $m^{1/2}s^{-1}$	f
B30_A_Sb500_Q1.86	0.002	0.0020	1.8623	50.65	37.30	1.3579	0.0919	0.0319	0.1304	4655.85	0.0580	17.2542	10.1077	0.9627
B30_A_Sb500_Q2.14	0.002	0.0020	2.1392	54.10	37.30	1.4504	0.0989	0.0330	0.1357	5347.92	0.0558	17.9206	10.5898	0.8891
B30_A_Sb500_Q2.47	0.002	0.0018	2.4702	60.35	37.20	1.6223	0.1023	0.0326	0.1330	6175.51	0.0535	18.6883	11.2011	0.8143
B30_A_Sb500_Q3.19	0.002	0.0020	3.1903	64.75	37.20	1.7406	0.1232	0.0355	0.1546	7975.70	0.0484	20.6545	12.4907	0.6659
B30_A_Sb500_Q3.92	0.002	0.0020	3.9202	70.45	36.90	1.9092	0.1391	0.0375	0.1673	9800.43	0.0452	22.1050	13.5091	0.5815
B30_A_Sb500_Q4.38	0.002	0.0021	4.3836	74.30	36.70	2.0245	0.1475	0.0387	0.1728	10959.04	0.0440	22.7421	13.9893	0.5500
B30_A_Sb500_Q4.80	0.002	0.0019	4.7993	79.10	36.50	2.1671	0.1517	0.0385	0.1722	11998.33	0.0426	23.4991	14.5644	0.5163
B30_A_Sb500_Q5.50	0.002	0.0019	5.5020	84.95	36.50	2.3274	0.1619	0.0396	0.1774	13754.96	0.0408	24.4816	15.3018	0.4775
B30_A_Sb500_Q6.24	0.002	0.0018	6.2439	89.95	36.40	2.4712	0.1735	0.0401	0.1847	15609.72	0.0386	25.9189	16.3080	0.4278
B30_A_Sb500_Q7.28	0.002	0.0020	7.2823	95.05	36.40	2.6113	0.1915	0.0428	0.1984	18205.78	0.0372	26.8960	17.0295	0.3992
B30_A_Sb500_Q8.11	0.002	0.0020	8.1123	99.90	36.40	2.7445	0.2030	0.0439	0.2051	20280.86	0.0359	27.8781	17.7501	0.3735
B30_A_Sb500_Q8.87	0.002	0.0019	8.8692	104.70	36.30	2.8843	0.2118	0.0440	0.2090	22173.03	0.0344	29.0453	18.5892	0.3460
B30_A_Sb500_Q10.04	0.002	0.0020	10.0430	109.70	36.30	3.0220	0.2289	0.0460	0.2206	25107.40	0.0331	30.1685	19.4060	0.3227
B30_A_Sb500_Q11.30	0.002	0.0020	11.2968	115.20	36.10	3.1911	0.2452	0.0476	0.2306	28242.04	0.0319	31.3414	20.2660	0.3011
B30_A_Sb500_Q12.51	0.002	0.0021	12.5124	119.45	36.10	3.3089	0.2619	0.0494	0.2419	31281.08	0.0309	32.3556	21.0016	0.2842
B30_A_Sb500_Q13.78	0.002	0.0021	13.7842	124.15	36.10	3.4391	0.2776	0.0510	0.2515	34460.42	0.0300	33.2854	21.6916	0.2703
B30_A_Sb500_Q16.17	0.002	0.0022	16.1738	129.95	35.80	3.6299	0.3112	0.0533	0.2756	40434.56	0.0279	35.8437	23.4678	0.2351
B30_A_Sb500_Q16.65	0.002	0.0022	16.6482	135.45	35.70	3.7941	0.3073	0.0536	0.2666	41620.46	0.0283	35.3444	23.2372	0.2438
B30_A_Sb500_Q17.75	0.002	0.0021	17.7458	140.55	35.60	3.9480	0.3156	0.0540	0.2688	44364.52	0.0276	36.1764	23.8711	0.2345
B30_A_Sb500_Q19.14	0.002	0.0020	19.1383	146.50	35.60	4.1152	0.3266	0.0542	0.2724	47845.66	0.0267	37.5217	24.8586	0.2200
B30_A_Sb500_Q19.72	0.002	0.0019	19.7220	150.20	35.60	4.2191	0.3283	0.0536	0.2704	49304.93	0.0261	38.2444	25.3979	0.2130
B30_A_Sb500_Q21.40	0.002	0.0021	21.4031	155.40	35.50	4.3775	0.3443	0.0569	0.2789	53507.71	0.0264	37.9494	25.2832	0.2182

Table 18: Summary table of the hydraulic parameters, configuration $B30\_A\_Sb500$

Run ID	S_b	S_e	Q l/s	H mm	h_v mm	H/h_v	U m/s	u_* m/s	F_r	R_e	n $sm^{-1/3}$	K_s $m^{1/3}s^{-1}$	C $m^{1/2}s^{-1}$	f
B30_A_Sb1000_Q1.95	0.001	0.0013	1.9513	58.85	37.20	1.5820	0.0829	0.0270	0.1091	4878.29	0.0546	18.3026	10.9346	0.8495
B30_A_Sb1000_Q2.15	0.001	0.0010	2.1456	64.95	37.20	1.7460	0.0826	0.0255	0.1035	5364.06	0.0519	19.2732	11.6599	0.7647
B30_A_Sb1000_Q2.32	0.001	0.0009	2.3160	69.80	36.70	1.9019	0.0830	0.0250	0.1002	5790.11	0.0506	19.7763	12.0722	0.7264
B30_A_Sb1000_Q2.83	0.001	0.0009	2.8273	74.70	36.70	2.0354	0.0946	0.0259	0.1105	7068.21	0.0458	21.8208	13.4313	0.5975
B30_A_Sb1000_Q3.35	0.001	0.0010	3.3468	80.45	36.80	2.1861	0.1040	0.0277	0.1171	8366.97	0.0446	22.4409	13.9366	0.5666
B30_A_Sb1000_Q3.79	0.001	0.0010	3.7948	84.70	36.70	2.3079	0.1120	0.0283	0.1229	9487.04	0.0422	23.6890	14.8013	0.5099
B30_A_Sb1000_Q4.47	0.001	0.0010	4.4679	90.05	36.40	2.4739	0.1240	0.0301	0.1320	11169.75	0.0405	24.6953	15.5401	0.4713
B30_A_Sb1000_Q5.01	0.001	0.0009	5.0098	96.10	36.50	2.6329	0.1303	0.0298	0.1342	12524.40	0.0381	26.2762	16.6577	0.4187
B30_A_Sb1000_Q5.86	0.001	0.0011	5.8640	100.20	36.40	2.7527	0.1463	0.0325	0.1476	14660.07	0.0369	27.1091	17.2662	0.3951
B30_A_Sb1000_Q6.79	0.001	0.0011	6.7906	104.95	36.40	2.8832	0.1618	0.0340	0.1594	16976.48	0.0347	28.7812	18.4249	0.3525
B30_A_Sb1000_Q7.64	0.001	0.0011	7.6384	110.15	36.40	3.0261	0.1734	0.0351	0.1668	19096.03	0.0334	29.9438	19.2699	0.3277
B30_A_Sb1000_Q8.08	0.001	0.0011	8.0842	114.65	36.40	3.1497	0.1763	0.0354	0.1662	20210.46	0.0330	30.3014	19.5836	0.3219
B30_A_Sb1000_Q8.67	0.001	0.0009	8.6667	120.70	36.30	3.3251	0.1795	0.0333	0.1650	21666.63	0.0304	32.8872	21.3698	0.2756
B30_A_Sb1000_Q9.96	0.001	0.0013	9.9613	125.00	36.30	3.4435	0.1992	0.0392	0.1799	24903.16	0.0321	31.1529	20.3161	0.3090
B30_A_Sb1000_Q10.56	0.001	0.0011	10.5558	129.90	36.10	3.5983	0.2032	0.0370	0.1800	26389.58	0.0296	33.7576	22.1011	0.2650
B30_A_Sb1000_Q11.83	0.001	0.0010	11.8342	136.05	36.10	3.7687	0.2175	0.0374	0.1882	29585.57	0.0278	35.9345	23.6356	0.2360
B30_A_Sb1000_Q12.29	0.001	0.0010	12.2901	140.25	36.10	3.8850	0.2191	0.0371	0.1868	30725.27	0.0274	36.5558	24.1164	0.2296
B30_A_Sb1000_Q13.52	0.001	0.0012	13.5231	145.40	36.00	4.0389	0.2325	0.0406	0.1947	33807.67	0.0281	35.5998	23.5682	0.2440
B30_A_Sb1000_Q14.10	0.001	0.0010	14.0984	150.00	36.00	4.1667	0.2350	0.0392	0.1937	35245.96	0.0268	37.3820	24.8221	0.2229
B30_A_Sb1000_Q14.79	0.001	0.0010	14.7902	154.75	35.70	4.3347	0.2389	0.0396	0.1939	36975.58	0.0264	37.8186	25.1862	0.2194
B30_A_Sb1000_Q15.36	0.001	0.0010	15.3582	159.05	35.70	4.4552	0.2414	0.0404	0.1933	38395.45	0.0266	37.5682	25.0835	0.2239
B30_A_Sb1000_Q16.99	0.001	0.0010	16.9905	165.60	35.70	4.6387	0.2565	0.0394	0.2012	42476.20	0.0243	41.1093	27.5499	0.1890
B30_A_Sb1000_Q18.06	0.001	0.0011	18.0604	170.90	35.60	4.8006	0.2642	0.0424	0.2040	45151.12	0.0253	39.5813	26.6017	0.2057
B30_A_Sb1000_Q19.64	0.001	0.0011	19.6373	175.25	35.60	4.9228	0.2801	0.0442	0.2136	49093.23	0.0247	40.4086	27.2188	0.1988
B30_A_Sb1000_Q21.95	0.001	0.0011	21.9492	181.00	35.50	5.0986	0.3032	0.0441	0.2275	54873.12	0.0227	44.0124	29.7308	0.1691

Table 19: Summary table of the hydraulic parameters, configuration $B30\_A\_Sb1000$

Run ID	S_b	S_e	Q l/s	H mm	h_v mm	H/h_v	U m/s	u_* m/s	F_r	R_e	n $sm^{-1/3}$	K_s $m^{1/3}s^{-1}$	C $m^{1/2}s^{-1}$	f
B30_S_Sb500_Q2.03	0.002	0.0024	2.0270	63.15	37.40	1.6885	0.0802	0.0387	0.1020	5067.62	0.0809	12.3668	7.4551	1.8579
B30_S_Sb500_Q2.32	0.002	0.0020	2.3235	69.70	37.30	1.8686	0.0833	0.0371	0.1008	5808.82	0.0747	13.3861	8.1699	1.5855
B30_S_Sb500_Q2.82	0.002	0.0020	2.8152	74.75	37.20	2.0094	0.0942	0.0388	0.1100	7037.97	0.0690	14.4846	8.9164	1.3561
B30_S_Sb500_Q3.27	0.002	0.0020	3.2701	80.45	37.20	2.1626	0.1016	0.0394	0.1144	8175.21	0.0649	15.4168	9.5744	1.2005
B30_S_Sb500_Q3.79	0.002	0.0021	3.7919	84.90	37.00	2.2946	0.1117	0.0414	0.1223	9479.66	0.0619	16.1442	10.0900	1.0981
B30_S_Sb500_Q4.08	0.002	0.0018	4.0802	90.10	36.90	2.4417	0.1132	0.0402	0.1204	10200.55	0.0592	16.8962	10.6330	1.0068
B30_S_Sb500_Q4.78	0.002	0.0019	4.7846	94.60	36.70	2.5777	0.1264	0.0421	0.1313	11961.56	0.0555	18.0247	11.4064	0.8885
B30_S_Sb500_Q5.60	0.002	0.0020	5.5974	100.25	36.60	2.7391	0.1396	0.0439	0.1408	13993.38	0.0523	19.1384	12.1902	0.7928
B30_S_Sb500_Q6.24	0.002	0.0021	6.2434	104.10	36.50	2.8521	0.1499	0.0462	0.1484	15608.42	0.0510	19.5936	12.5321	0.7598
B30_S_Sb500_Q7.05	0.002	0.0018	7.0516	111.20	36.40	3.0549	0.1585	0.0449	0.1518	17629.07	0.0467	21.4045	13.7886	0.6423
B30_S_Sb500_Q7.88	0.002	0.0021	7.8829	114.45	36.40	3.1442	0.1722	0.0485	0.1625	19707.17	0.0463	21.6003	13.9576	0.6334
B30_S_Sb500_Q9.04	0.002	0.0020	9.0422	121.10	36.30	3.3361	0.1867	0.0491	0.1713	22605.57	0.0431	23.2259	15.0971	0.5528
B30_S_Sb500_Q9.92	0.002	0.0022	9.9161	124.60	36.30	3.4325	0.1990	0.0517	0.1800	24790.17	0.0425	23.5507	15.3534	0.5403
B30_S_Sb500_Q10.64	0.002	0.0020	10.6448	129.95	36.30	3.5799	0.2048	0.0511	0.1814	26612.02	0.0406	24.6363	16.1300	0.4976
B30_S_Sb500_Q11.89	0.002	0.0021	11.8925	135.15	36.20	3.7334	0.2200	0.0533	0.1911	29731.33	0.0393	25.4745	16.7446	0.4691
B30_S_Sb500_Q12.86	0.002	0.0021	12.8575	139.75	36.10	3.8712	0.2300	0.0536	0.1964	32143.72	0.0376	26.5752	17.5259	0.4340
B30_S_Sb500_Q13.26	0.002	0.0021	13.2597	143.90	36.10	3.9861	0.2304	0.0538	0.1939	33149.20	0.0376	26.5796	17.5789	0.4367
B30_S_Sb500_Q15.20	0.002	0.0020	15.1986	150.15	35.90	4.1825	0.2531	0.0544	0.2085	37996.40	0.0344	29.0399	19.2847	0.3695
B30_S_Sb500_Q15.87	0.002	0.0021	15.8688	153.90	35.80	4.2989	0.2578	0.0559	0.2098	39672.00	0.0347	28.8555	19.2070	0.3764
B30_S_Sb500_Q16.78	0.002	0.0020	16.7818	159.55	35.70	4.4692	0.2630	0.0558	0.2102	41954.54	0.0338	29.6207	19.7829	0.3605
B30_S_Sb500_Q17.84	0.002	0.0019	17.8407	166.40	35.60	4.6742	0.2680	0.0553	0.2098	44601.71	0.0326	30.6348	20.5394	0.3408
B30_S_Sb500_Q19.22	0.002	0.0021	19.2226	169.50	35.60	4.7612	0.2835	0.0585	0.2199	48056.41	0.0326	30.7053	20.6210	0.3410
B30_S_Sb500_Q21.67	0.002	0.0020	21.6672	173.90	35.50	4.8986	0.3115	0.0591	0.2385	54168.03	0.0298	33.5389	22.5759	0.2879

Table 20: Summary table of the hydraulic parameters, configuration $B30\_S\_Sb500$

Run ID	S_b	S_e	Q l/s	H mm	h_v mm	H/h_v	U m/s	u_* m/s	F_r	R_e	n $sm^{-1/3}$	K_s $m^{1/3}s^{-1}$	C $m^{1/2}s^{-1}$	f
B30_S_Sb1000_Q2.04	0.001	0.0019	2.0443	67.60	37.40	1.8075	0.0756	0.0354	0.0928	5110.66	0.0785	12.7391	7.7456	1.7503
B30_S_Sb1000_Q2.39	0.001	0.0015	2.3873	75.30	37.40	2.0134	0.0793	0.0328	0.0922	5968.20	0.0694	14.4070	8.8765	1.3710
B30_S_Sb1000_Q2.61	0.001	0.0012	2.6123	81.40	37.40	2.1765	0.0802	0.0310	0.0898	6530.83	0.0647	15.4646	9.6175	1.1938
B30_S_Sb1000_Q2.74	0.001	0.0011	2.7420	85.15	37.30	2.2828	0.0805	0.0303	0.0881	6854.99	0.0629	15.9034	9.9429	1.1318
B30_S_Sb1000_Q3.12	0.001	0.0011	3.1196	90.95	37.30	2.4383	0.0858	0.0306	0.0908	7799.01	0.0596	16.7922	10.5789	1.0201
B30_S_Sb1000_Q3.82	0.001	0.0012	3.8184	94.60	37.20	2.5430	0.1009	0.0329	0.1048	9546.11	0.0544	18.3966	11.6418	0.8530
B30_S_Sb1000_Q3.96	0.001	0.0011	3.9577	99.70	37.20	2.6801	0.0992	0.0334	0.1003	9894.37	0.0558	17.9066	11.3986	0.9051
B30_S_Sb1000_Q4.29	0.001	0.0010	4.2935	105.55	37.00	2.8527	0.1017	0.0318	0.0999	10733.81	0.0517	19.3313	12.3831	0.7819
B30_S_Sb1000_Q4.99	0.001	0.0011	4.9878	109.65	36.90	2.9715	0.1137	0.0336	0.1096	12469.57	0.0488	20.4932	13.1817	0.6993
B30_S_Sb1000_Q5.39	0.001	0.0010	5.3873	114.50	36.80	3.1114	0.1176	0.0335	0.1110	13468.14	0.0469	21.3225	13.7787	0.6500
B30_S_Sb1000_Q6.36	0.001	0.0011	6.3620	120.45	36.70	3.2820	0.1320	0.0367	0.1215	15904.94	0.0455	21.9632	14.2684	0.6176
B30_S_Sb1000_Q7.24	0.001	0.0012	7.2400	125.50	36.50	3.4384	0.1442	0.0377	0.1300	18099.98	0.0427	23.4406	15.2929	0.5461
B30_S_Sb1000_Q7,64	0.001	0.0010	7.6423	131.15	36.50	3.5932	0.1457	0.0367	0.1284	19105.85	0.0410	24.3992	15.9896	0.5083
B30_S_Sb1000_Q8.14	0.001	0.0011	8.1366	134.70	36.40	3.7005	0.1510	0.0377	0.1314	20341.51	0.0405	24.6997	16.2299	0.4986
B30_S_Sb1000_Q8.82	0.001	0.0011	8.8250	139.55	36.40	3.8338	0.1581	0.0383	0.1351	22062.47	0.0391	25.5642	16.8568	0.4689
B30_S_Sb1000_Q9.73	0.001	0.0011	9.7305	145.35	36.40	3.9931	0.1674	0.0391	0.1402	24326.18	0.0375	26.6367	17.6338	0.4358
B30_S_Sb1000_Q10.28	0.001	0.0011	10.2762	149.90	36.30	4.1295	0.1714	0.0400	0.1413	25690.46	0.0374	26.7164	17.7389	0.4363
B30_S_Sb1000_Q11.52	0.001	0.0011	11.5207	155.60	36.30	4.2865	0.1851	0.0413	0.1498	28801.63	0.0356	28.0607	18.6973	0.3991
B30_S_Sb1000_Q12.15	0.001	0.0011	12.1499	158.95	36.20	4.3909	0.1911	0.0411	0.1530	30374.85	0.0342	29.2487	19.5276	0.3694
B30_S_Sb1000_Q12.88	0.001	0.0010	12.8759	164.80	36.20	4.5525	0.1953	0.0411	0.1536	32189.67	0.0333	30.0021	20.0974	0.3544
B30_S_Sb1000_Q13.32	0.001	0.0010	13.3173	170.30	36.10	4.7175	0.1955	0.0418	0.1513	33293.13	0.0337	29.6729	19.9362	0.3656
B30_S_Sb1000_Q13.74	0.001	0.0010	13.7421	174.70	36.10	4.8393	0.1967	0.0410	0.1502	34355.21	0.0328	30.5197	20.5519	0.3481
B30_S_Sb1000_Q14.32	0.001	0.0009	14.3202	179.50	36.00	4.9861	0.1994	0.0405	0.1503	35800.61	0.0318	31.4719	21.2440	0.3300
B30_S_Sb1000_Q15.05	0.001	0.0009	15.0545	183.35	35.80	5.1215	0.2053	0.0405	0.1531	37636.14	0.0308	32.4880	21.9706	0.3116

Table 21: Summary table of the hydraulic parameters, configuration $B30\_S\_Sb1000$

A

APPENDIX C: FLOW RESISTANCE PARAMETERS AS A FUNCTION OF REYNOLDS

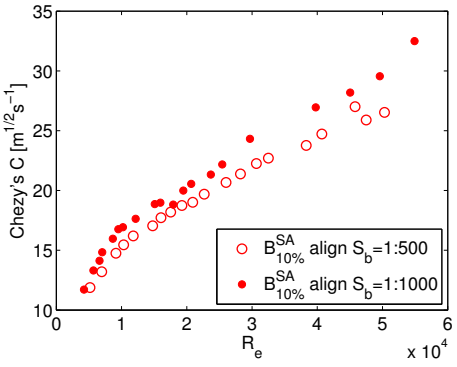

$B^{SA} = 10\%$, *aligned*

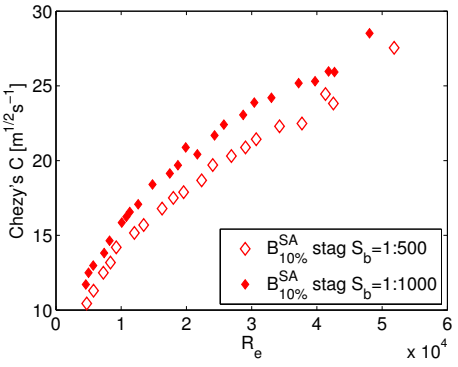

$B^{SA} = 10\%$, *staggered*

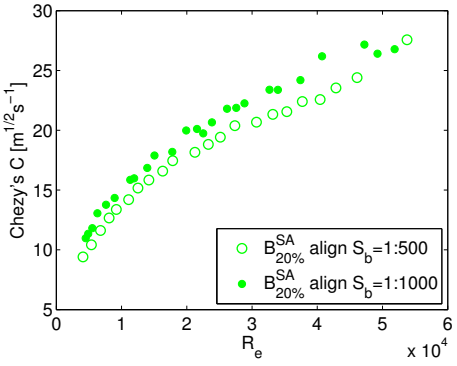

$B^{SA} = 20\%$, *aligned*

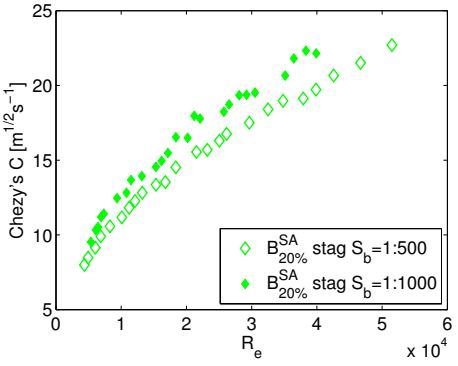

$B^{SA} = 20\%$, *staggered*

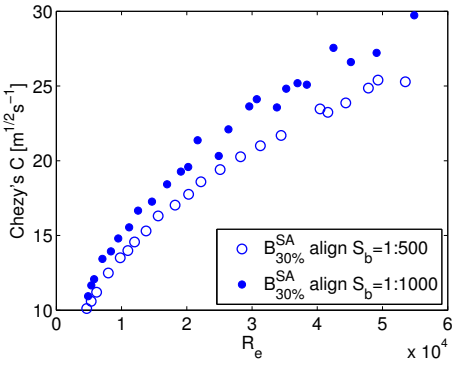

$B^{SA} = 30\%$, *aligned*

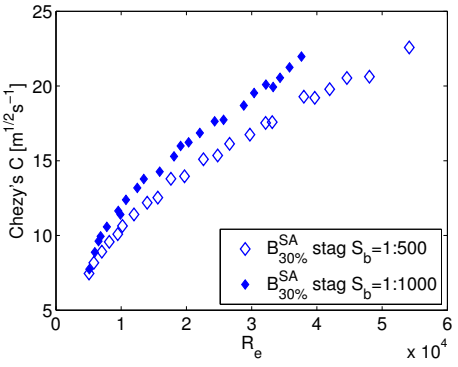

$B^{SA} = 30\%$, *staggered*

Figure 72: Relationships Chezy $C = F(R_e)$.

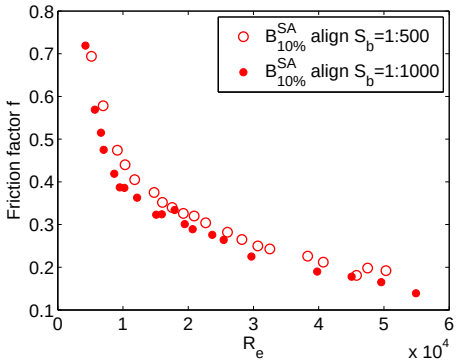

$B^{SA} = 10\%,\ aligned$

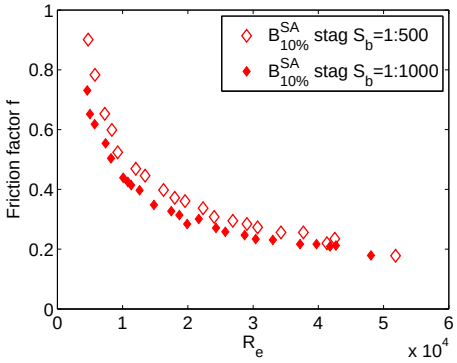

$B^{SA} = 10\%,\ staggered$

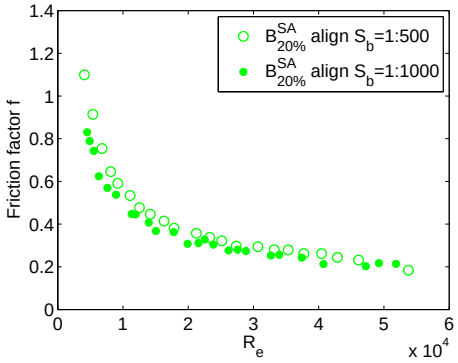

$B^{SA} = 20\%,\ aligned$

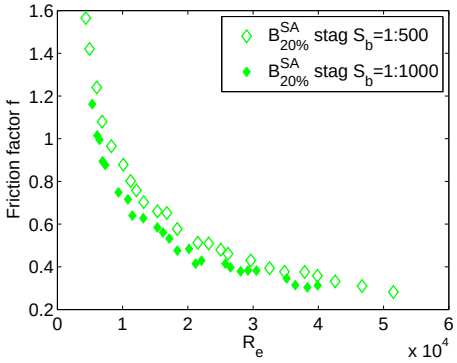

$B^{SA} = 20\%,\ staggered$

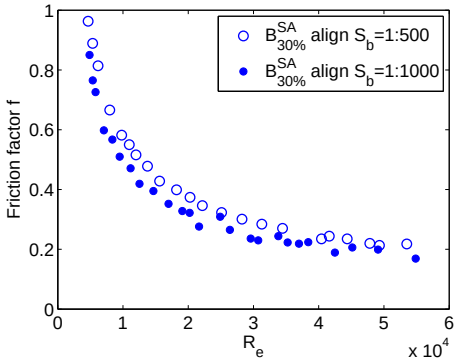

$B^{SA} = 30\%,\ aligned$

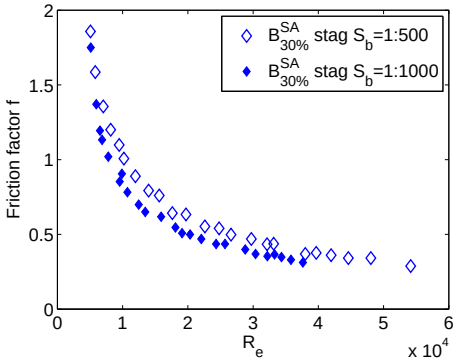

$B^{SA} = 30\%,\ staggered$

Figure 73: Relationships Darcy-Weisbach's friction factor $f = F(R_e)$.

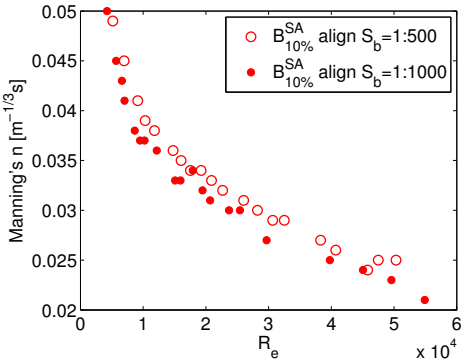

$B^{SA} = 10\%,\ aligned$

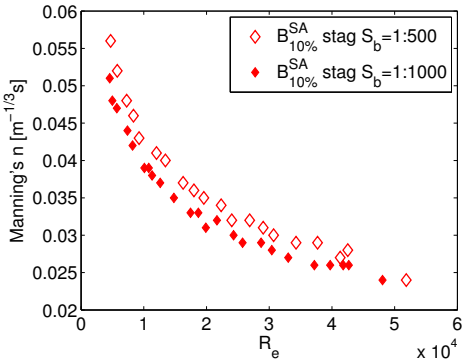

$B^{SA} = 10\%,\ staggered$

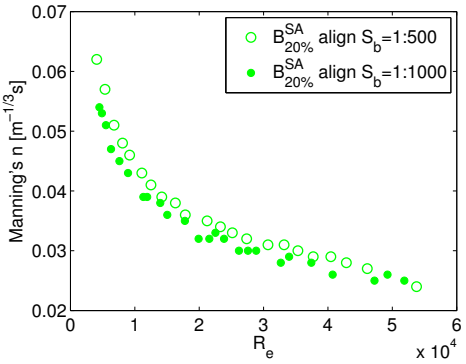

$B^{SA} = 20\%,\ aligned$

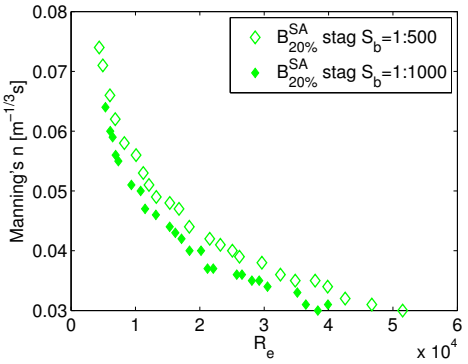

$B^{SA} = 20\%,\ staggered$

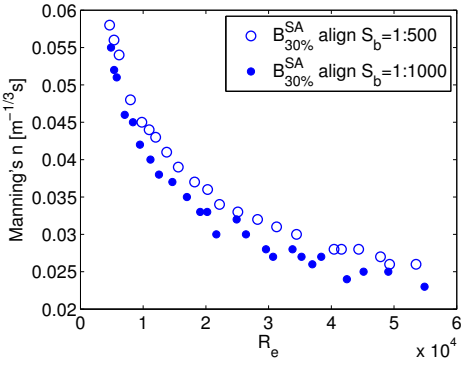

$B^{SA} = 30\%,\ aligned$

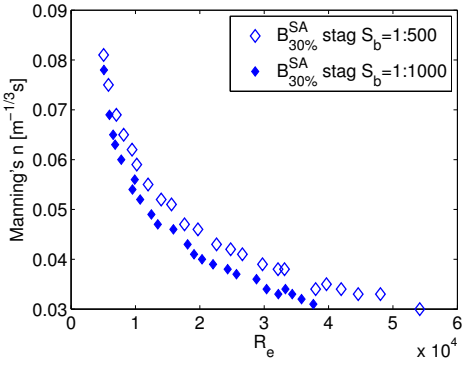

$B^{SA} = 30\%,\ staggered$

Figure 74: Relationships Manning $n = F(R_e)$.

A

APPENDIX D: FLOW RESISTANCE PARAMETERS AS A FUNCTION OF RELATIVE SUBMERGENCE

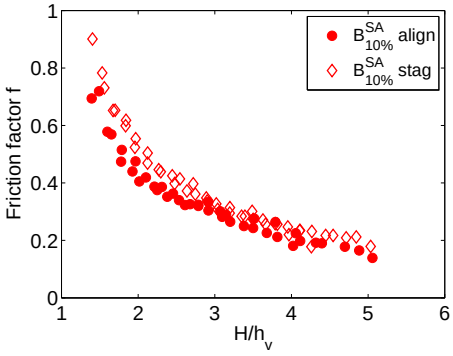

$B^{SA} = 10\%$

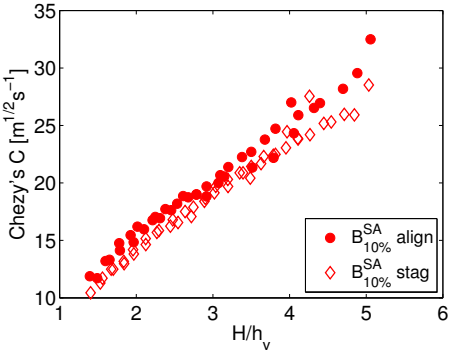

$B^{SA} = 10\%$

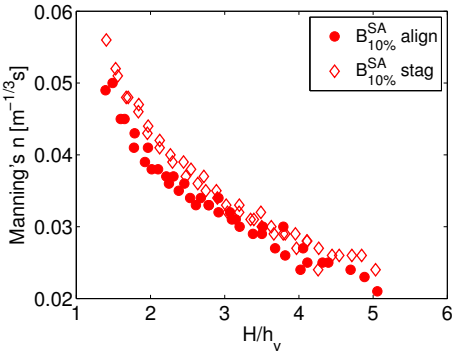

$B^{SA} = 10\%$

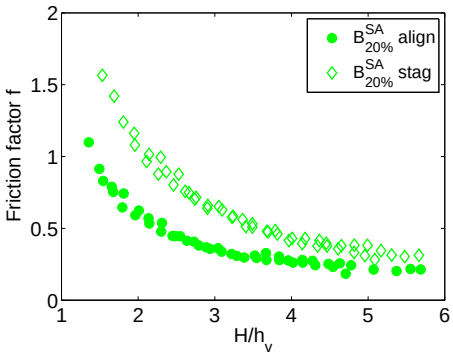

$B^{SA} = 20\%$

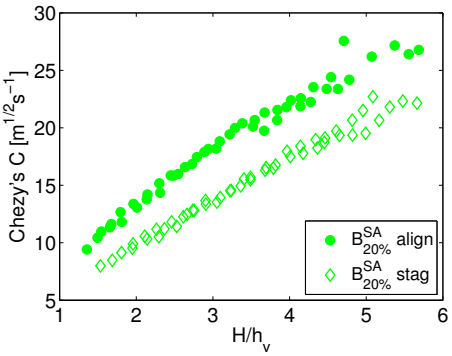

$B^{SA} = 20\%$

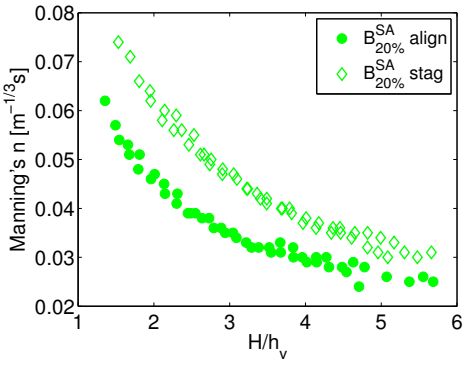

$B^{SA} = 20\%$

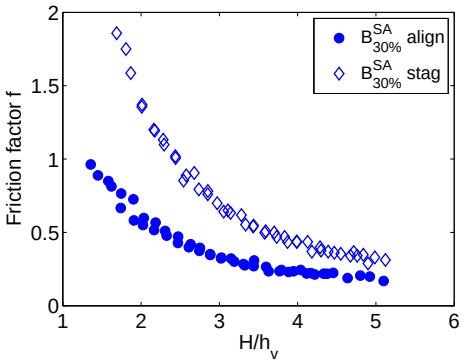

$B^{SA} = 30\%$

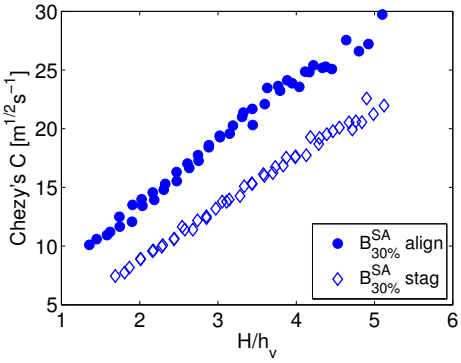

$B^{SA} = 30\%$

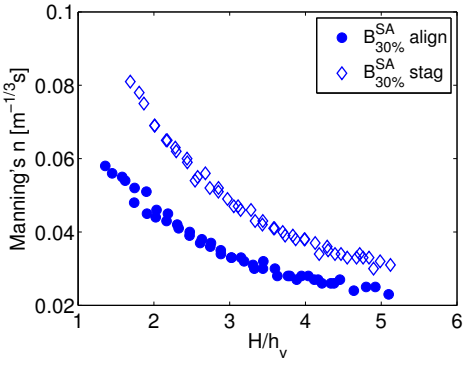

$B^{SA} = 30\%$

BIBLIOGRAPHY

[1] Gottauf A. *Einfluß aquatischer Vegetation auf das Widerstandsverhalten des Fließgewassers Brenz*. 1997: Vertieferarbeit am Institut fur Wasserbau und Kulturtechnik der Universitat Karlsruhe.

[2] University of Aberdeen website. *School of Engineering*. URL: http://www.abdn.ac.uk/engineering/research/environmental-industrial-fluid-mechanics-122.php.

[3] Stone BM and Shen HT. *Hydraulic resistance of flow in channels with cylindrical roughness*. 2002: Journal of Hydraulic Engineering, 128(5): 500-506.

[4] Green Julian C. *Comparison of blockage factors in modelling the resistance of channels containing submerged macrophytes*. 2005: River Res. Applic. 21: 671-686 (2005).

[5] Green Julian C. *Modelling flow resistance in vegetated streams: review and development of new theory*. 2005: Hydrol. Process. 19, 1245-1259.

[6] Yen Ben Chie. *Open Channel Flow Resistance*. January 2002: Journal of Hydraulic Engineering, Am Soc Civil Eng, 128(1):20-39.

[7] James CS. and Jordanova AA. *Reach-scale resistance of distributed roughness in channels*. 2010: River Flow 2012; Dittrich, Koll, Aberle & Geisenhainer (eds).

[8] Watson D. *Hydraulic effects of aquatic weeds in UK rivers*. 1987: Regulated Rivers: Research and Management 1: 211-227.

[9] Watson D. *The effect of aquatic macrophytes on channel roughness and flow parameters*. 1986: PhD thesis, University of Southampton (unpublished).

[10] Bogart DB. *The effects of aquatic weeds on flow in Everglades canals*. 1948: Proceedings of the Soil Science Society of Florida 9: 32-52.

[11] Green EP and Short FT. *World Atlas of Seagrasses*. 2003: Berkeley, Univ. Calif. Press.

[12] Koch EW. *Hydrodynamics, diffusion-boundary layers and photosynthesis of the seagrasses, Thalassia testudinum and Cymodocea nodosa*. 1994: Mar. Biol. 118:767-76.

[13] R. N. Fenzl and J. R. Davis. *Hydraulic Resistance Relationships for Surface Flows in Vegetated Channels*. 1964: Transactions, American Society of Agricultural Engineers, Vol. 7, No 1, pp 46-55.

[14] Carollo FG, Ferro V, and Termini D. *Flow Resistance Law in Channels with Flexible Submerged Vegetation*. 2005: J. Hydraul. Eng. 131(7), 554-564.

[15] Nepf H. *Flow and transport in regions with aquatic vegetation*. 2012: Ann. Rev. Fluid Mech. 44, 123–142.

[16] Nepf H. *Hydrodynamics of vegetated channels*. 2012: Journal of Hydraulic Research Vol. 50, No. 3 (2012).

[17] Eastgate W. I. *Vegetated Stabilization of Grassed Waterways and Dam Bywashes*. 1966: thesis presented to the University of Qeensland, at St. Lucia, Queensland, Australia, in partial fulfillment of the requirements for the degree of Masters of Engineering Science.

[18] Green JC. *Effect of macrophyte spatial variability on channel resistance*. 2006: Advances in Water Resources.

[19] Ackerman JD. *Submarine pollination in the marine angiosperm Zostera marina*. 1997: Am. Bot. 84:1110-19.

[20] Dijkstra J.T. and Uittenbogaard R.E. *Modelling hydrodynamics in flexible vegetation*. 2006: Physical Processes in Natural Waters workshop, Sept 4-7, Lancaster, England.

[21] Bal K., Struyf E., Vereecken H., Viaene P., De Doncker L., de Deckere E., Mostaert F., and Meire P. *How do macrophyte distribution patterns affect hydraulic resistances?* 2011: Ecological Engineering 37 (2011) 529–533.

[22] Fisher K. *The Hydraulic Roughness of Vegetated Channels*. 1992: Report SR 305. Hydraulics Research Ltd: Wallingford.

[23] N. Kouwen and R-M. Li. *Biomechanics of Vegetative Channel Linings*. June 1980: Journal of the Irrigation and Drainage Division, ASCE, Vol. 106, No. HY6, Proc. Paper 15464, pp. 1085-1103.

[24] N. Kouwen, T. E. Unny, and H. M. Hill. *Flow Retardance in Vegetated Channels*. June 1969: Journal of the Irrigation and Drainage Division, ASCE, Vol. 95, No. IR2, Proc. Paper 6633, pp. 329-342.

[25] Kleinhans M. *Hydraulic roughness, 2008*. URL: www.geog.uu.nl/fg/mkleinhans/teaching/rivmorrough.pdf.

[26] Righetti M. and Armanini A. *Flow resistance in open channel flows with sparsely distributed bushes*. 2002: Journal of Hydrology 269: 55-64.

[27] C. Manes, D. Pokrajac, V.I. Nikora, L. Ridolfi, and D. Poggi. *Turbulent friction in flows over permeable walls*. 2011: Geophysical Research Letters, Vol. 38, L03402.

[28] Gourlay MR. *Discussion of: Flow resistance in vegetated channels, by Kouwen N, Unny TE and Hill HM*. 1970: Journal of the Irrigation and Drainage Division of the American Society of Civil Engineers 96(IR3): 351-357.

[29] Fenzl R. N. *Hydraulic Resistance of Broad, Shallow Vegetated Channels*. 1962: thesis presented at the University of California, Davis, at Davis, California, in partial fulfillment of the requirements for the degree of Doctor of Philosophy.

[30] Kouwen Nicholas and Unny Tharakkal Eroman. *Flexible roughness in open channels*. 1973: Journal of the Hydraulics Division, 99(5), 713-728.

[31] Pitlo RH. and Dawson FH. *Flow resistance of aquatic weeds*. 1990: In Aquatic weeds: The Ecology and Management of Nuisance Aquatic Vegetation, Pieterse AH, Murphy KJ (eds). Oxford University Press. Oxford; 74-84.

[32] Petryk S. and Bosmanjian G. III. *Analysis of flow through vegetation*. 1975: J. Hydraul. Div., ASCE 101 (HY7), 871-884.

[33] Haslam SM. *River plants:The Macrophytic Vegetation of Watercources*. 1978: Cambridge University Press: Cambridge.

[34] Stephan U. and Gutknecht D. *Hydraulic resistance of submerged flexible vegetation*. 2002: Journal of Hydrology 269 (2002) 27-43.

[35] Nikora V, Lamed S, Nikora N, Debnath K, Cooper G, and Reid M. *Hydraulic resistance due to aquatic vegetation in small streams: field study*. 2008: J. Hydraul. Eng. ASCE, 134(9):1326-32.

[36] Nikora V.I., Goring D.G., McEwan I., and Griffiths G. *Spatially-averaged open-channel flow over a rough bed*. 2001: J. Hydraul. Eng. ASCE, 127(2), 123-133.

[37] Ree WO. and Palmer VJ. *Flow of water in channels protected by vegetative linings*. Feb. 1949: U.S. Dept. of Agriculture, 115 pp.